ELSEVIER

Coordination Chemistry Reviews 233–234 (2002) 1–39

COORDINATION CHEMISTRY REVIEWS

www.elsevier.com/locate/ccr

The chemistry of krypton

John F. Lehmann, Hélène P.A. Mercier, Gary J. Schrobilgen *

Department of Chemistry, McMaster University, Hamilton, Ont., Canada L8S 4M1

Received 4 February 2002; accepted 24 May 2002

Dedicated to Professor Neil Bartlett, our friend and colleague, on the occasions of his 70th birthday and the 40th anniversary of his discovery of noble-gas reactivity, and in recognition of his many other outstanding and exciting contributions to the field of inorganic fluorine chemistry.

Contents

Abstract

Krypton is the only noble gas other than xenon to give rise to isolable compounds in macroscopic amounts, although the chemistry of krypton is presently limited to the +2 oxidation state. The strong oxidant-fluorinator properties and thermal instabilities of krypton(II) compounds have posed considerable challenges to determining the extent to which the chemistries of krypton(II) and xenon(II) are analogous. Krypton(II) compounds possessing Kr–F, Kr–O and Kr–N bonds have been prepared

* Corresponding author. Tel.: +1-905-525-9140x23306; fax: +1-905-522-2509
E-mail address: schrobil@mcmaster.ca (G.J. Schrobilgen).

PII: S0010-8545(02)00202-3

and structurally characterized by X-ray crystallography, spectroscopic means (NMR, vibrational, Mössbauer), and electron structure calculations. The strong oxidative fluorinators, KrF_2 and KrF^+, have found application in the syntheses of new examples of fluorides and oxide fluorides of main-group, transition metal, lanthanide, and actinide elements in their highest oxidation states.

Keywords: Noble-gas chemistry; Krypton; Fluorine; Krypton compounds; Oxidative fluorinators; High-oxidation states

1. Introduction

Canadian contributions to noble-gas chemistry span the discovery of noble-gas reactivity to the present. The chain of events leading to the discovery of krypton reactivity and its chemistry, the subject of the present Review, was inaugurated at the University of British Columbia on March 23, 1962 when Neil Bartlett demonstrated that the reaction of xenon gas with PtF_6 vapor at ambient temperature instantaneously gave a stable yellow-red solid, then formulated as $Xe^+PtF_6^-$ [1]. The discovery of the first noble-gas compound made folklore of the preexisting dogma that the rare or noble gases should be referred to as 'inert' and served to rewrite chemistry textbooks by confronting the doctrine that held the valence electron octet to be inviolate [2].

Over the ensuing years since the discovery of noble-gas reactivity, a considerable body of the known chemistry of krypton has evolved at McMaster University in the laboratories of Ronald J. Gillespie and Gary J. Schrobilgen, where it presently remains a highly active research area and where the majority of known krypton compounds have been synthesized and characterized structurally. The present overview of krypton chemistry also seeks to represent the equally important and considerable contributions of non-Canadian laboratories to this challenging and fascinating field of chemistry and is the first comprehensive review of the subject since that of Bartlett and Sladky in 1973 [3]. Various aspects of krypton chemistry also appear in several general reviews of noble-gas chemistry [4–11].

2. Discovery of krypton reactivity

In 1924, A. von Antropoff published a paper in Zeitschrift für angewandte Chemie in which he eloquently argued for the placement of the noble gases in group VIIIb of the periodic table [12,13]. Accordingly, he pointed out that noble gases are potentially reactive and that such positioning would give them a maximum valence of eight, except in the case of helium where it is two. In his words he noted that 'one should not forget that as the valence number increases from one group to the next, the intensity of the valence forces decreases' and that 'placement in Group VIIIb leaves them the possibility to form bonds with the most negative elements, oxygen and fluorine'. Several years later he and his coworkers were motivated to validate these concepts by attempting the preparation of the first noble gas compounds, and krypton was chosen [14]. It may be speculated that the choice was determined because krypton was then the heaviest noble gas that was available in sufficient quantities and because it should have a greater tendency to react than the lighter noble gases. Moreover, an earlier attempt by Henri Moissan [15], the discoverer of elemental fluorine, to react fluorine gas and argon at room temperature and under the action of an induction spark had failed. Von Antropoff and his coworkers attempted to react krypton with chlorine and bromine under intense electric discharges while circulating the Kr/Cl_2 and Kr/Br_2 mixtures through a liquid air trap [14]. The observed pressure drops and formation of a dark red solid, in the case of the Kr/Cl_2 discharge experiment, in the cold trap were taken as evidence for compound formation. The red compound was noted to be volatile and stable in the gas phase, and heating with calcium was reported to give a violent reaction and only krypton was reported to remain. With the permission of von Antropoff, Otto Ruff and Walter Menzel [16] conducted similar experiments with argon/fluorine and krypton/fluorine mixtures, but without success. A year later in 1933, von Antropoff's group showed that the red solid they had originally isolated was not a krypton compound, but an already known compound of NO and HCl [17]. The retraction article, however, notes that they were not able to account for certain losses in krypton pressure. The next mention of the plausibility of forming krypton compounds was also in 1933. Based on a consideration of univalent radius ratios, Linus Pauling [18] reasoned that KrF_6, along with H_4XeO_6, Ag_4XeO_6, AgH_3XeO_6, XeF_6, and XeF_8 should be capable of existence, suggesting that XeF_8 might be unstable. It was also at about this time that Don Yost and Albert Kaye [19] reported on their failed attempts to synthesize xenon fluorides by means of electric discharges through xenon/fluorine mixtures.

Efforts to prepare krypton compounds lay dormant until Neil Bartlett revived interest in noble-gas chemistry with the synthesis of the first noble-gas compound, a xenon compound resulting from the reaction of xenon gas with the powerful oxidant and fluorinator, PtF_6. The resulting compound, then formulated as $Xe^+PtF_6^-$ [1], was subsequently shown to be a mixture of $XeF^+PtF_6^-$, $XeF^+Pt_2F_{11}^-$ and PtF_5 [20]. Bartlett also

attempted to react krypton with PtF_6 and RhF_6 at temperatures below 50 °C without success [21].

The first synthesis of a krypton compound was reported by Grosse et al. [22,23], who claimed to have prepared KrF_4 by use of a high voltage glow discharge through a mixture of krypton and fluorine at −78 °C. Subsequent independent attempts to repeat the glow discharge synthesis of KrF_4 verified the formation of a krypton fluoride [24], however, the vapor pressures and ^{19}F-NMR spectrum were very similar to those reported in the meantime for KrF_2 [25]. Other workers have since failed to synthesize KrF_4 by the method of Grosse et al. or by any other method, producing only KrF_2. Turner and Pimentel [26,27] prepared KrF_2 by irradiation of Kr/F_2 mixtures at 20 K in an argon matrix using focused light from a medium pressure mercury lamp, and were the first to correctly identify KrF_2 and characterize it by infrared spectroscopy. Bands were observed at 580 and 236 cm^{-1} and these were assigned to the $\nu_3(\Sigma_u^+)$ and $\nu_2(\Pi_u)$ vibrational modes of the linear centrosymmetric KrF_2 molecule.

Streng and Grosse [28] reported that hydrolysis of what they claimed was 'KrF_4' produced aqueous solutions having an oxidizing strength equivalent to a 2–3 mol% yield of 'KrO_3'. When the hydrolysis was carried out in a $Ba(OH)_2$ solution, 90% of the Kr was recovered and the precipitated BaF_2 contained an oxidizing strength equivalent to a 9 mol% yield of 'KrO_3', equivalent to the retention of 7% of the original krypton in the precipitate. The authors concluded that 'KrO_3' was present as the stable salt, 'barium kryptate ($BaKrO_4$)'. Like KrF_4, these findings have never been substantiated and cannot be considered as proof for the existence of aqueous krypton compounds or Kr–O bonded species. Attempts to observe KrO_3 by tracer and Mössbauer techniques after β-decay of ^{83}Br in BrO_3^- have been unsuccessful [29,30], suggesting that KrO_3 may be too unstable to be synthesized. Indeed, XeO_3 and XeO_4, which are expected to be more stable than their krypton analogues, are both highly endothermic and kinetically unstable.

The neutral fluorides of krypton are presently limited to KrF_2, which is isolable in gram quantities. The violet-colored $KrF^\bullet$ radical has been obtained by γ-irradiation of single crystals of KrF_2 with a ^{60}Co source at −196 °C [31]. The entrapped radical was detected in the KrF_2 host crystal by ESR spectroscopy and identified from the ^{19}F hyperfine interaction. The radical is stable indefinitely at −196 °C, but decomposes upon warming to −153 °C, and can otherwise be considered a transient species. Because of the transient nature of $KrF^\bullet$, its chemistry is not discussed at length in this Review, however, the role the excited state species, $KrF^{\bullet *}$ [32–34], plays in the synthesis of KrF_2 by UV photolysis will be briefly discussed. The formation of the KrF^- anion has been studied in the gas phase by using a Penning ion source with radical extraction [35]. The existence of KrF^- has been confirmed by observing the negative ion mass spectrum of KrF_2.

3. Krypton difluoride

Other than xenon, krypton is the only noble gas that forms isolable chemical compounds in macroscopic amounts, with the simplest of these compounds being KrF_2. The importance of KrF_2 is emphasized by the fact that all krypton chemistry is currently derived from KrF_2. Consistent with its thermodynamic instability, KrF_2 is a potent oxidative fluorinating agent that is capable of oxidizing xenon to XeF_6 [36] and gold metal to AuF_6^- [37,38] below room temperature and has consequently found use as a low-temperature oxidative fluorinating agent (see Section 8).

3.1. Synthesis of krypton difluoride

The preparation of KrF_2 in synthetically useful amounts is technically challenging and difficult to scale. Because the heat of formation of KrF_2 is endothermic ($\Delta H_f = 60.2$ kJ mol^{-1}, gas at 93 °C) [39,40], KrF_2 cannot be synthesized by the standard high-pressure, high-temperature methods used to prepare the thermodynamically stable xenon fluorides, XeF_2 [41], XeF_4 [42], and XeF_6 [43], which have standard enthalpies of formation of −162.8, −267.1 and −338.2 kJ mol^{-1} [44], respectively. In addition to the thermodynamic instability of KrF_2, its preparation is further complicated by the difficulty of atomizing fluorine at the low temperatures required to stabilize the product. Four methods, which overcome these obstacles, have been developed for the preparation of macroscopic quantities of KrF_2, and use high-energy particle beams (e^-, protons, α) [45,46], electric discharges [24,47,48], UV irradiation [27,49–52], and hot wires [52–54] as means to generate fluorine atoms at low temperatures (Eq. (1)). Of these methods, the latter two are currently the preferred methods of preparation based on reproducibility of yields and relative experimental simplicity. In each method, the highly reactive fluorine radicals react with krypton at low temperatures to form the metastable $KrF^\bullet$ radical (Eq. (2)). Although the process for the conversion of $KrF^\bullet$ to KrF_2 has not been thoroughly investigated, it is presumed that the reaction proceeds through Eq. (3) and/or Eq. (4) [55]. All of these methods are energetically demanding as a result of F_2

$$F_2 \rightarrow 2F^\bullet \quad (1)$$

$$F^\bullet + Kr \rightarrow KrF^\bullet \quad (2)$$

$$KrF^\bullet + KrF^\bullet \rightarrow KrF_2 + Kr \quad (3)$$

$$KrF^\bullet + F^\bullet \rightarrow KrF_2 \quad (4)$$

atomization, but vary considerably depending on the technique that is used. For example, the process of atomization using UV irradiation requires 1.1 to 2.5 eV per fluorine atom produced, but is significantly higher for the electron impact (5 eV/F$^{\bullet}$) and electric discharge (7.0±0.8 eV/F$^{\bullet}$) methods [55–57].

3.1.1. Small particle bombardment

The preparation of KrF_2 using a 1.5 MeV electron beam was reported by MacKenzie in 1963 [45]. This method uses an electron beam which is introduced into a nickel reaction vessel through a thin (0.013 cm) nickel window. Bombardment of an F_2 rich Kr/F_2 mixture at −150 °C produced visible amounts of KrF_2 (ca. 100 mg), however, optimization of the electron impact synthesis has not been pursued, and little data regarding product yields or production rates are available.

Proton beams, with energies of 10 MeV and currents of 5 μA, have also been utilized in the preparation of KrF_2 from gaseous mixtures of Kr and F_2 at temperatures ranging from −60 to −140 °C [46]. The rate of KrF_2 production can reach 1 g h^{-1} at the lower end of this temperature range. High-energy α-particles (40 MeV) from cyclotron sources also produce KrF_2 under similar reaction conditions [46]. Although proton and α-particle bombardments are capable of producing gram quantities of KrF_2 in relatively short time periods, the operating expenses and relative scarcity of cyclotron facilities strongly dissuade experimentalists from using these methods.

3.1.2. UV photolysis

The synthesis of bulk quantities of KrF_2 by UV irradiation was first reported in 1965 by Streng and Streng, who exposed Kr and F_2 (or OF_2) mixtures to sunlight for 5 weeks in a Pyrex vessel cooled to −78 °C [49]. The synthesis was later improved by the use of a medium pressure mercury discharge lamp as the UV source and by carrying the reaction out at −196 °C [50]. The effect of modifying the incident UV spectral range has also been investigated with the general consensus that harder UV radiation is detrimental to product yields [52,55,58]. Although there is considerable discrepancy with regards to the near UV absorption spectrum of KrF_2 [52,59], (see Section 3.3), the reduced yields observed when hard UV radiation is not filtered out has been attributed to these absorptions, which are suspected to initiate product dissociation. The strong, broad absorbance in the mid-UV region (158 nm) has been extensively characterized because it can be used to produce KrF$^{\bullet}$*, which emits UV laser lines at 222 and 248 nm upon relaxation to KrF$^{\bullet}$, and could also be a competing factor in the production of KrF_2 [34]. The effects of product photodissociation have been shown to be minimized if Pyrex (UV cutoff, 280 nm) apparatus or filters are used in the place of Vycor (UV cutoff, 210 nm) or quartz (UV cutoff, 170 nm) [52]. At high light intensities, the highest KrF_2 yields are obtained with irradiation in the 303–313 nm region [58].

The photochemical immersion wells currently used in this synthesis were primarily developed at the Jožef Stefan Institute, Ljubljana, Slovenia and are described by these researchers [50,51], with detailed descriptions also provided by Kinkead et al. [52]. A typical photochemical reactor is depicted in Fig. 1 and utilizes a medium pressure mercury arc lamp located in the center of the reactor to irradiate solid Kr/liquid F_2 mixtures contained in a quartz or Pyrex outer compartment cooled to −196 °C, which surrounds the UV source. The complexity of the reactor design is primarily the result of the large temperature gradient required between the cryogenic Kr/F_2 mixture and the UV source. The mercury arc lamp is not functional at these cryogenic temperatures, and is located in the center of the apparatus within a water-cooled Dewar jacket to prevent cooling of the lamp. Photolysis has been shown to be most efficient at −196 °C, at which temperature Kr is a solid and F_2 is a liquid. The lower yields obtained from the irradiation of gas-phase Kr/F_2 mixtures at 0, −78, and −183 °C have been attributed to the thermal instability of the KrF$^{\bullet}$ radical in the gas phase where translational energies are considerable [55,60]. Additional stabilization of the radical in the solid state has been postulated to occur by means of electron sharing, i.e. KrF$^{\bullet}$–Kr [55]. Although the KrF$^{\bullet}$ radical is unarguably unstable, the significance of a translational energy contribution to its dissociation should be regarded with some skepticism because it appears to contradict the high yields of KrF_2 obtained for proton and α-particle bombardments at −140 °C (see Section 3.1.3). Such a photochemical reactor is capable of producing in excess of 1.22 g h^{-1} of KrF_2 [52], making it one of the highest yielding methods reported to date. This method requires the handling of liquid fluorine in a quartz apparatus, and introduces the risk of over pressurization and F_2 release in the event of accidental warming of the apparatus above the boiling point of fluorine (−188.14 °C).

3.1.3. Hot wire reactor

The hot wire reactor was originally designed for the synthesis of highly thermally and kinetically unstable species such as O_2F_2 (ΔH_f°, 19.8(1.2) kJ mol^{-1}) [61] and KrF_2 (ΔH_f°, 60.2 kJ mol^{-1}) [39,40]. The preparation of KrF_2 by this method was first described by Bezmel'nitsyn et al. [53], and further commentary with regards to the optimization, design and operation of hot wire reactors has been provided by Kinkead et al. [52] (Fig. 2) and by Schrobilgen et al. [54]. The hot wire reactor technique relies on the thermal dissociation of F_2 upon contacting a resistively heated (ca. 700 °C) nickel filament, which extends down the axis of a cylindrical

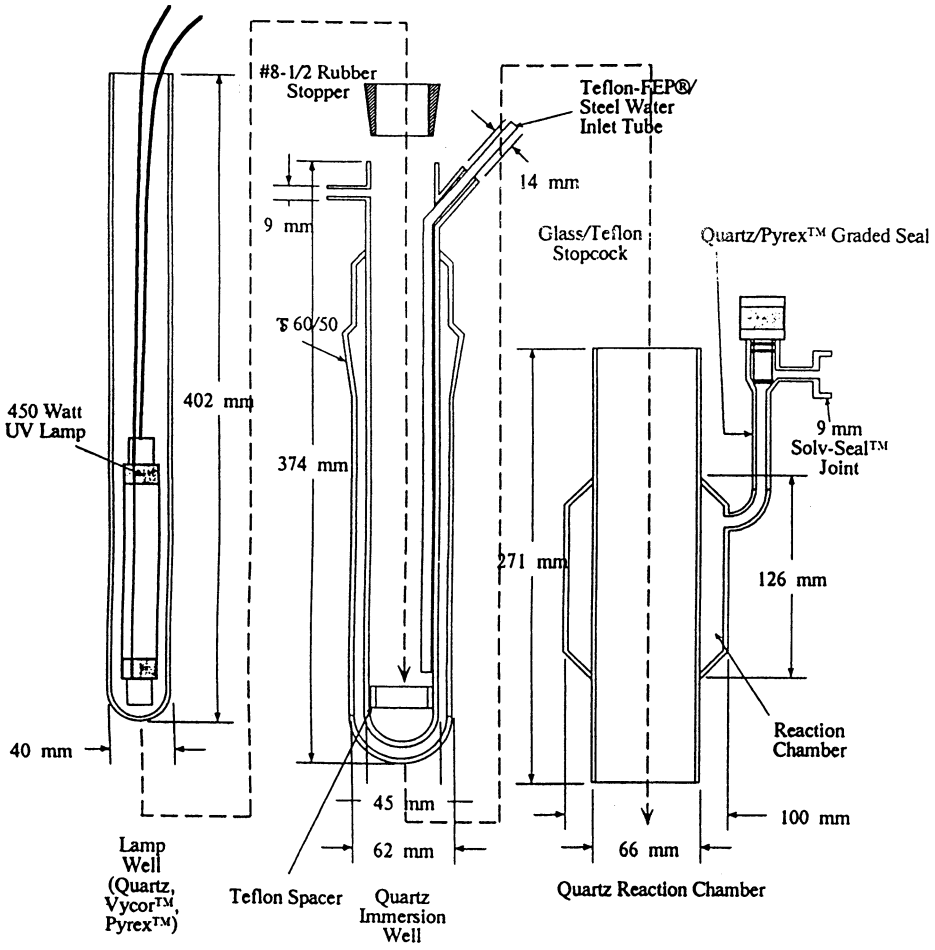

Fig. 1. Small photochemical immersion well for low-temperature KrF_2 synthesis. The immersion well and reaction chamber are of quartz; the lamp well is of quartz, Vycor, or Pyrex, as desired. The lamp well is sized for a 450 W or smaller medium pressure UV lamp (37 mm O.D.) Reproduced with permission from Ref. [52].

reaction chamber whose external walls are cooled to −196 °C. The rate of KrF_2 production is not only dependant on the rate of $F^{\bullet}$ production at the surface of the nickel filament, but also on the mean free path of the fluorine radicals through the residual gaseous F_2 reagent to the solidified krypton on the reactor walls. These factors have been addressed both theoretically [53] and experimentally [52] and optimized conditions have been reached for reactors with diameters of 2–4 cm operating with residual F_2 pressures of 40 Torr. Pretreatment of the nickel filament with O_2 at 800–900 °C has been reported to catalyze the dissociation of F_2 and increase KrF_2 yields by a factor of two, however, some experimentalists have failed to see significant increases in yield with this treatment [63]. Yields for hot wire reactors under these conditions can reach up to 6 g h^{-1} [53]. Most modern reactors are fabricated from 316 stainless steel (Fig. 2), however, KrF_2 produced using reactors fabricated from stainless steel is frequently discolored light pink because of small amounts of chromium-containing species [63], which likely include CrF_5, $CrOF_4$, and $KrF_2 \cdot CrOF_4$ (see Section 4.2). These contaminants can be easily removed by flash distillation of the crude product at 0 °C [54]. The low gas pressures and rugged stainless steel designs of these reactors substantially reduce the chemical hazards associated with the preparation of KrF_2 when compared with the liquid F_2-UV photolysis method. The high current (30 A at 6 VDC [53], 60 A at 16 VDC [54]) required to resistively heat the nickel filament is cautioned, and utmost care should be taken in the design and operation of the power supplies associated with these devices.

3.1.4. Electric glow discharge

The preparation of KrF_2 using electric discharge methods has also proven to be a viable, although generally less common, method for producing gram quantities of KrF_2. Despite the low vapor pressure of krypton at liquid nitrogen temperature (P (−196 °C) = 1.9 Torr), which is unfavorable for maintaining near stoichiometric 1:1 F_2:Kr ratios under ideal operating pressures, the optimized discharge conditions at this temperature have been established by Sessa [48].

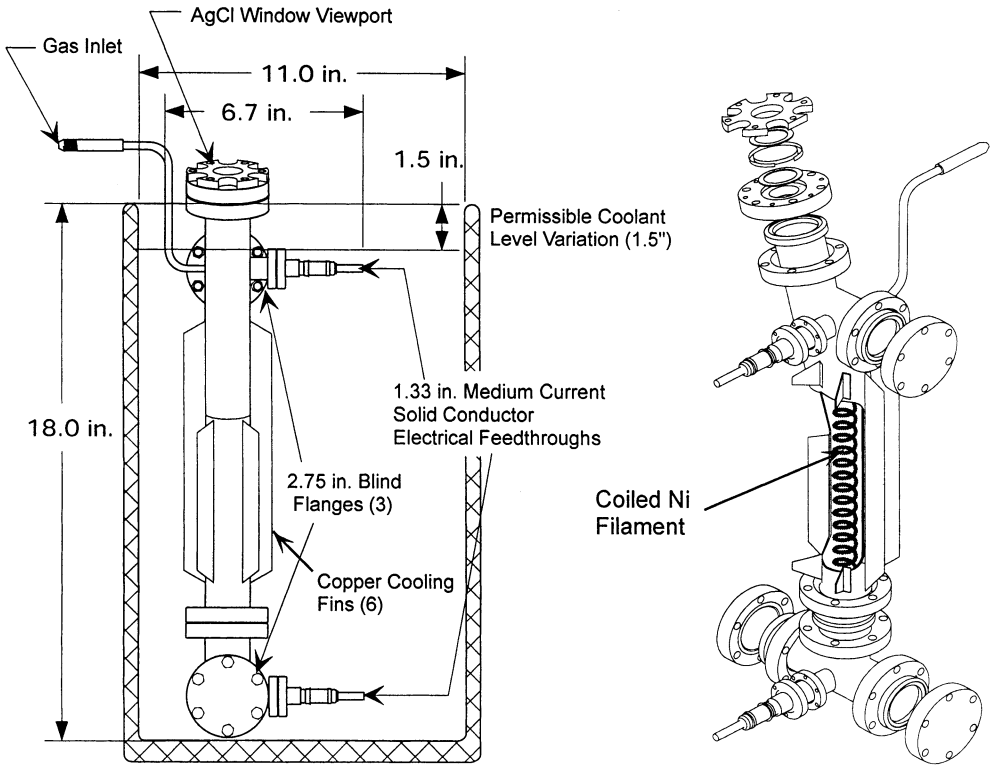

Fig. 2. Stainless steel hot-wire reactor used for the preparation of KrF_2; external view and dimensions of a hot wire reactor submerged in a liquid nitrogen coolant bath (cut-away view), and a perspective drawing of the hot wire reactor showing the flange assembly and nickel filament (cut-away region). Reproduced with permission from Ref. [62].

The low krypton pressure can be overcome by use of the more hazardous coolant, O_2(l), at which temperature (−183 °C), solid krypton has a vapor pressure of 20 Torr [24]. The electric discharge is generated between two copper electrodes, roughly 20 mm in diameter and 75 mm apart, with a current of 20 mA and a net potential of 3–4 kV (Fig. 3). The net pressure in the system is generally regulated between 40 and 60 Torr, corresponding to F_2:Kr ratios of ca. 1:1 to 2:1 in the gas phase at −183 °C. High-voltage electric glow discharges through mixtures of krypton and fluorine over a period of several hours results in product deposition on the cold walls of the discharge tube between the electrodes. The method is less reliable with respect to product yields on a routine basis than either the UV photolysis or the hot wire methods, however, rates of 0.05 [64] and 0.25 g h^{-1} (75% yield based on Kr) [24] have been reported. A method for producing KrF_2 by means of electric discharges through Kr and CF_2Cl_2 has also been patented, but has not found widespread use [65].

3.2. Physicochemical properties of KrF_2

Krypton difluoride is a colorless crystalline solid, which decomposes to its elements at ambient temperature over the course of several days [24], and melts (sublimes) with rapid decomposition at 77 °C [66]. The thermal decomposition of KrF_2 has been studied at 20–100 °C and 5–70 Torr initial pressure [67]. Between 50–100 °C, the decomposition of KrF_2 proceeds as a homogeneous monomolecular first-order reaction having $k = 2 \times 10^{12} \exp(-99580/RT)$ s^{-1} for $R = 8.314$ J mol^{-1} K^{-1}. At temperatures below 50 °C, the reaction is heterogeneous in nature and depends on the specific surface area of the reactor.

The thermodynamic properties of KrF_2 have already been discussed in the context of its synthesis (see Section 3.1) and are summarized in Table 1. The solid can be stored indefinitely at −78 °C at which temperature its vapor pressure is negligible [24]. Because of its strong oxidizing properties, thermal instability and significant vapor pressure at 0 °C (29±2 Torr) [39,47], the preferred method for transferring KrF_2 is by sublimation under static or dynamic vacuum. Although KrF_2 reacts explosively with water and organic materials, it can be handled and stored in vessels fabricated from fluoroplastics (FEP [54], Kel-F [64], PTFE [64], PFA [68]), metals (nickel [45], Monel [39,40], stainless steel [39,40], aluminum [67]), and Pyrex glass [24,49] or quartz [52] that have been well dried under dynamic vacuum and thoroughly passivated with fluorine.

The high solubilities of KrF_2 in anhydrous HF and BrF_5 (Table 1) and the resistance of these solvents to oxidation by KrF_2 have resulted in their wide spread use

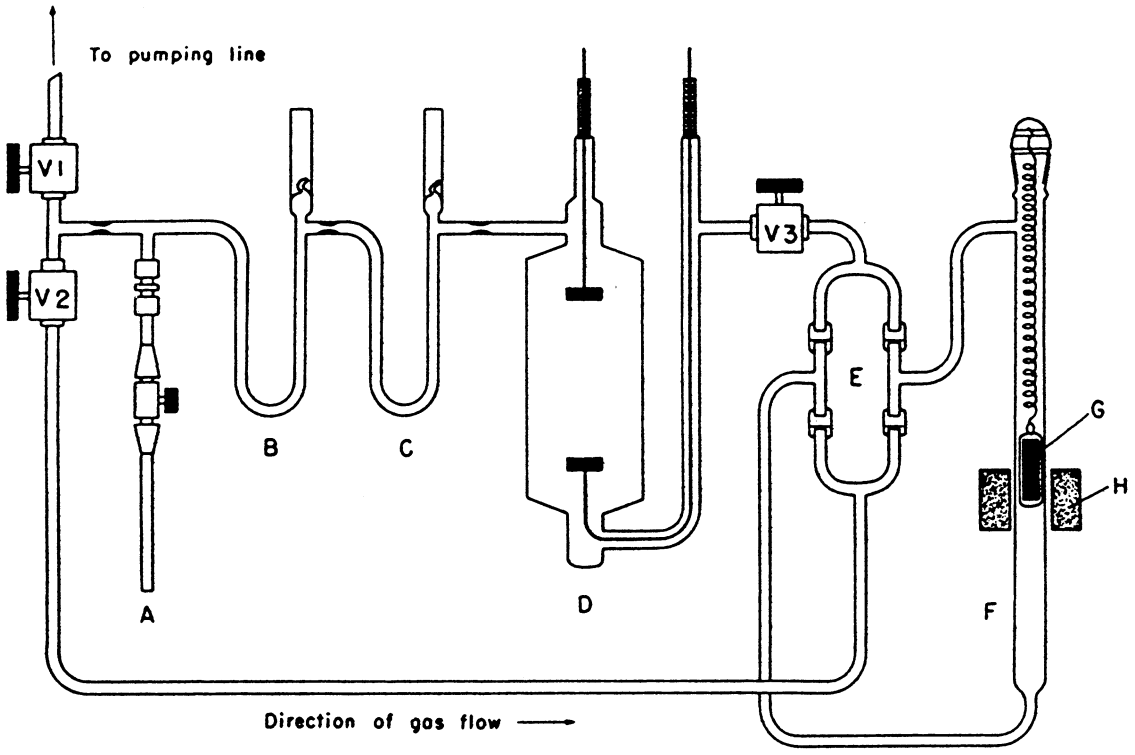

Fig. 3. Glow discharge apparatus for the preparation of KrF_2. (A) Kel-F container for the collection and storage of the compound, attached to the glass apparatus by compression fittings. (B, C) U-tubes of Pyrex glass with break-seals. (D) Electrical discharge reaction vessel made of Pyrex glass (diameter 60 mm; height of wide portion 200 mm) is immersed in liquid O_2 during the glow discharge. Two copper discs of 20 mm diameter and 5 mm thickness, spaced 75 mm apart, serve as electrodes. The leads to the electrodes are silver-soldered into Kovar to glass seals. (E) Valve manifold to convert push–pull operation of magnetic piston pump into unidirectional gas circulation as indicated. Each individual valve consisted of a 10-mm glass tube ground flat at the end, protruding into a wider tube and closed with a thin square piece of glass held in place by gravity. Application of a small pressure head from below (0.1 mm) permits gas to flow upward. Downward flow is inhibited by the closure of the ground end of the glass tube by the square piece of glass. Arrangement of four valves in the way indicated in the figure permits use of the pumping action of each half stroke of the piston. (F) Magnetic piston pump after Brenschede (Z. Physik. Chem. A178 (1936) 74). (G) Piston of pump suspended from stainless steel spring. (H) Solenoid. V1, V2, V3: Monel valves. With the reaction in progress valve 1 is kept closed while valves 2 and 3 are open. During the purification and sublimation of the product, first to tube C and then into tube B, valves 2 and 3 are closed to separate the pump from the rest of the system, and valve 1 is open to establish a connection to the vacuum line. Reproduced with permission from Ref. [24].

in synthetic applications involving KrF_2 (see Sections 4.1, 5.1, 8.2, 8.3 and 8.4). The $KrF_2{\cdot}BrF_5$ binary phase diagram has been studied [66]. The incongruently melting solvates $KrF_2{\cdot}9BrF_5$ and $KrF_2{\cdot}2BrF_5$ and the congruently melting solvate $KrF_2{\cdot}BrF_5$ (the distectic point is at -17 °C) are formed in the system. Sulfuryl-chlorofluoride (SO_2ClF) has also proven useful as a low temperature solvent medium for KrF_2 (see Sections 3.3, 4.2 and 6) [69].

Table 1
Physical properties of KrF_2

Thermodynamics	
ΔH_{sub} [a]	41(±4) kJ mol^{-1}
ΔH_f° [a]	60.2(±3.4) kJ mol^{-1}
$\Delta H_{atomization}$ [a]	97.9 kJ mol^{-1}
Mean Kr–F bond energy [a]	48.9 kJ mol^{-1}
Vapor pressure [b]	$\log(P) = 8.814 - (2000/T)$
Solubility	16 mol KrF_2 per kg of HF at 20 °C [c]
	16.5 mol KrF_2 per kg of BrF_5 [d]

[a] Refs. [39,40].
[b] P in Torr, T in Kelvin.
[c] Ref. [24].
[d] Ref. [66], temperature not specified.

3.3. Structure and spectroscopic properties of KrF_2

Despite its chemically aggressive nature, KrF_2 has been extensively studied using a wide variety of spectroscopic techniques to investigate its electronic (UV–vis [33,34,52,59], UV-PES [70], X-ray PES [71], XANES [72]), vibrational (IR [27,73], Raman [73–75]), rotational (high resolution IR) [76–78], and nuclear (^{19}F-NMR [24,79,80], Mössbauer [81,82]) properties. In addition to the structural information accumulated by these spectroscopic methods, the structure of KrF_2 has been determined in its two known crystallographic

Table 2
UV absorbance spectra of KrF_2

Absorption energy (nm)	Region (nm)	Ref.
115–190 (max at ca. 162)	120–200	[33]
120–200 (max at ca. 159)	120–200	[34]
220–320 [a] (max at ca. 220)	210–320	[59]
218, 188–190 (max at ca. 188–190)	185–218 [b]	[86]

[a] Broad absorption.
[b] The upper limit is not given but is >218 nm.

modifications by X-ray crystallography [54,83,84] and in the gas phase by electron diffraction [85]. The results of all of these studies are consistent with a linear triatomic molecule having $D_{\infty h}$ point group symmetry as predicted by VSEPR rules.

The electronic structure of KrF_2 has been studied using UV absorption, photon electron (PES) and X-ray absorption near edge (XANES) spectroscopies and theoretical methods. The UV absorption spectrum (Table 2) is well defined in the hard-UV region (120–200 nm) where KrF_2 exhibits a single intense absorption maximum at 158–162 nm [33,34]. This absorption results in the cleavage of a Kr–F bond and the formation of $KrF^{\bullet}$* in either its D or B excited states, which relax spontaneously to the ground state radical, $KrF^{\bullet}$, with the emission of 222 and 248 nm laser lines, respectively [34]. The soft UV region (185–320 nm) has been investigated by several researchers and the reported spectra exhibit considerable variation both with regards to absorption energies and optical densities. The PE spectrum of gaseous KrF_2 (Table 3), obtained by using He(I) and He(II) irradiation, was found to be analogous to that of XeF_2 [70]. Additional information regarding the orbital energies of KrF_2 has been obtained by means of PES shake-up experiments using Mg–K_α irradiation to probe transitions from lower lying energy levels, with predominantly Kr-3d and F-1s characters, to unoccupied molecular orbitals [71]. The structure of the unoccupied orbitals of KrF_2 has also been investigated using XANES, which monitored X-ray absorptions originating from Kr-1s orbital [72].

The vibrational selection rules for the centrosymmetric KrF_2 molecule predict that the symmetric KrF_2 stretching mode, $\nu_1(\Sigma_g^+)$, is Raman active, and those of the asymmetric stretching, $\nu_2(\Pi_u)$, and bending, $\nu_3(\Sigma_u^+)$, modes are infrared active [90]. The vibrational frequencies for KrF_2 have been determined experimentally in the gas phase [73,74], in an argon matrix [27], and in the solid state [73,75] and are compared with the values calculated at a number of levels of theory in Table 4. Factor-group analyses of the Raman spectra of KrF_2 have been used to distinguish between its two crystallographic modifications (vide infra) [75]. Although the vibrational frequencies are comparable to those of XeF_2 ($\nu_1(\Sigma_g^+)$, 514.5; $\nu_2(\Pi_u)$, 213.2; $\nu_3(\Sigma_u^+)$, 555 cm^{-1}) [93,94], the lower frequency of the symmetric stretch in KrF_2 is noteworthy because it reflects the weaker Kr–F bonding interaction. The stretching force constants, f_r, for KrF_2 (246 N m^{-1}) and XeF_2 (284 N m^{-1}) [73] confirm this trend (Table 4). A striking feature of the force constants for KrF_2 is the negative value of its bond–bond interaction constant, $f_{rr} = -20$ N m^{-1}. The negative value indicates that it is easier to lengthen or to shorten both bonds simultaneously than it is to lengthen one bond and shorten the other. The opposite is true for XeF_2 with $f_{rr} = 13$ N m^{-1}. The absence of a Fermi resonance splitting of $\nu_3(\Sigma_u^+)$ by the $\nu_2(\Pi_u)$ overtone has been justified by the small value of f_r and the negative value of f_{rr} [95]. This serves to reduce the magnitude of the Fermi resonance operator to 2.40 cm^{-1}, which is small when compared with the energy difference between $\nu_3(\Sigma_u^+)$ and $2\nu_2(\Pi_u)$ in the gas phase (15 cm^{-1}).

Table 3
Photoelectron spectrum of KrF_2

Orbital	Adiabatic I.P. [a]	Vertical I.P. [a]	Calculated			
			STO [b]	STO [c]	STO [d]	Xα-Sw [e]
$4\pi_u$	≤ 13.16	13.34, 13.47	10.5	14.44	15.43	13.56
$8\sigma_g$	13.75	13.90	7.9	12.72	14.71	14.57
$2\pi_g$	14.0	14.37	12.6	16.30	17.64	14.53
$3\pi_u$	16.25	16.92	15.0	18.40	19.36	16.11
$5\sigma_u$	–	17.7	16.1	19.88	20.85	18.80
$7\sigma_g$	22.0	23.0	29.0	33.08	33.77	28.56
$4\sigma_u$						33.51
$6\sigma_g$						33.94

[a] Ref. [70].
[b] Ref. [87].
[c] Ref. [88].
[d] Ref. [89].
[e] Ref. [71].

Table 4
Experimental and calculated vibrational frequencies and force constants for KrF_2

Experimental (cm^{-1})			Calculated (cm^{-1})				Assignment	Force constants [a]
KrF_2 (g)	KrF_2 (matrix)	KrF_2 (s)	HF/3-21G* [b]	MP2/SBK+(D) [d]	CCSD(T)/SBK+(D) [d]	LDFT [c]		
449 [e]		462.3 [e] 465.5 [f,g] 469.5, 468.6 [f,h]	558	448	400	504	ν_1, Σ_g^+ sym. stretch R	f_r, 246 [e]
588 [e], 590 [i]	580 [j]		649	626	589	623	ν_2, Π_u asym. stretch IR	f_{rr}, −20 [e]
232.6 [e] 1032 [e]	236 [j]		267	233	225	228	ν_3, Σ_u^+ bend IR $\nu_1+\nu_2$, comb. band IR	f_α, 21 [e]

[a] Stretching constants, N m^{-1}; deformation constants, N m rad^{-1}.
[b] Ref. [91].
[c] Ref. [54].
[d] Ref. [92].
[e] Ref. [73].
[f] Ref. [75].
[g] α-Phase; space group, *I4/mmm*.
[h] β-Phase; space group, $P4_2/mnm$.
[i] Ref. [74].
[j] Ref. [27].

Table 5
Experimental and calculated Kr–F bond lengths for KrF_2

State	Bond length (Å)	Method	Ref.
Gas	1.889(10)	Electron diffraction	[85]
	1.875(2)–1.867(2) [a]	High resolution IR	[77]
	1.882821(9) [a]	High resolution IR	[76]
	1.882766(8) [b]	High resolution IR	[76]
Solid	1.894(5) [c]	X-ray diffraction	[54]
	1.89(2) [d]	X-ray diffraction	[83]
	1.881(4)–1.887(4) [e]	X-ray diffraction	[54]
	1.868(4)–1.888(4) [f]	X-ray diffraction	[54]
Theory	1.822	Hartree–Fock	[54]
	1.826	Hartree–Fock	[91]
	1.910	LDFT	[54]
	1.919	MP2/SBK+(D)	[92]
	1.933	CCSD/SBK+(D)	[92]
	1.88	NDDO-2 (α,β)	[96]
	1.91	Xα-Sw	[71]

[a] Calculated from the rotational substructure of the ν_2 vibration of $^{84}KrF_2$.
[b] Calculated from the rotational substructure of the ν_3 vibration of $^{86}KrF_2$.
[c] α-Phase; space group, *I4/mmm*; −125 °C.
[d] β-Phase; space group, $P4_2/mnm$; −80 °C.
[e] $(Kr_2F_3^+SbF_6^-)_2\cdot KrF_2$.
[f] $Kr_2F_3^+SbF_6^-\cdot KrF_2$.

The Kr–F bond length was first estimated from rotational fine structure on the $\nu_3(\Sigma_u^+)$ vibration of the gas-phase infrared spectrum. Although distinct rotational transitions were not originally resolved, the energy gap between the P and R branches provided an initial value of 1.9(1) Å [73], which was later refined, yielding two possible solutions for $^{86}KrF_2$, 1.875(2) or 1.967(2) Å [77]. A more recent study of the $\nu_3(\Sigma_u^+)$ rotational structure of $^{84}KrF_2$ suggests that these values are in error and has provided a precise value of 1.882821(9) Å ($r_e = 1.876930(23)$ Å) [78] for the Kr–F bond length. This revised value is consistent with the value determined from the rotational fine structure of the $\nu_2(\Pi_u)$ bend (1.882766(8) Å) [76] (Table 5). The rotational constant, B_o, has been determined for $^A KrF_2$ ($A = 82$ [76], 83 [76], 84 [76], 86 [76,77]) by gas phase rotational spectroscopy and these values are summarized in Table 6.

Table 6
Rotational constants for $^M KrF_2$(g)

^{M}Kr	B_o (cm^{-1})
^{82}Kr [a]	0.125149(4)
^{83}Kr [a]	0.125143(4)
^{84}Kr [a]	0.1251493(10)
^{86}Kr [a]	0.125154(3)
^{86}Kr [b]	0.12626 or 0.12728

[a] Obtained from the rotational fine structure of the $\nu_2(\Pi_u)$ bending vibration in the high-resolution FT infrared spectrum, Ref. [76].
[b] Obtained from the rotational fine structure of the $\nu_3(\Sigma_u^+)$ asymmetric stretching vibration, Ref. [77].

The ^{19}F-NMR spectrum of KrF_2 has been obtained in HF, BrF_5 and SO_2ClF solvents [79] and the respective chemical shifts are given in Table 7 along with those of other krypton(II) compounds. The secondary krypton

Table 7
NMR chemical shifts and coupling constants for krypton containing compounds

Noble gas species	Solvent	T (°C)	$\delta(^{19}F)$ (ppm)	δ(L) (ppm)	$J(^{19}F–L)$ [a] (Hz)	Ref.
KrF_2	HF	26	55.6			[79]
KrF_2	BrF_5	27	77.7			[79]
KrF_2	BrF_5	−50	67.9			[79]
KrF_2	SO_2ClF	−10	82			[68]
KrF_2	SO_2ClF	−15.6	89.5			[63]
KrF_2	SO_2ClF	−118	63			[68]
KrF^+	HF	−40	−22.6			[79]
$Kr_2F_3^+(SbF_6^-)$	BrF_5	−65	73.4 (F_t) 18.8 (F_b)		$^2J/^{19}F$ 347	[79]
$Kr_2F_3^+(AsF_6^-)$	BrF_5	−65	73.8 (F_t) 19.0 (F_b)		$^2J/^{19}F$ 347	[79]
$Kr_2F_3^+(SbF_6^-)$	BrF_5	−66	73.6 (F_t) 19.0 (F_b)		$^2J/^{19}F$ 351	[79]
$Kr(OTeF_5)_2$	SO_2ClF	−90	−42.1 (F_{ax}) −47.2 (F_{eq})	^{17}O 95.2	$^2J/^{19}F$ 181	[69]
$HCNKrF^+$ [b]	BrF_5	−57	99.4	^{15}N −200.8 ^{13}C 98.5 ^1H 6.09	$^2J/^{15}N$ 26 $^3J/^{13}C$ 25.0 $^4J/^1H$ 4.2	[97]
$HCNKrF^+$	HF	−60	81.0			[97]
CF_3CNKrF^+	BrF_5	−58	93.1 (FKr) −53.9 (CF_3)			[98]
$C_2F_5CNKrF^+$	BrF_5	−58	91.1 (FKr) −83.8 (CF_3) −108.6 (CF_2)			[98]
$C_3F_7CNKrF^+$	BrF_5	−58	91.9 (FKr) −81.1 (CF_3) −105.7 (CF_2) −125.2 (CF_2CN)			[98]
$FKrFMoOF_4$ [c]	SO_2ClF	−121	70.4 (F_tKr) −12.4 (KrF_b) 148.6 (F_1Mo)		$^2J/^{19}F_b$ 296 $^2J/^{19}F_1$ 44	[99]
$FKrF(MoOF_4)_2$ [c]	SO_2ClF	−121	64.9 (F_tKr) −28.8 (KrF_b) 190.8 (F_1Mo_1) 208.5 ($F_1'Mo_1$) −34.8 ($Mo_1F_b'Mo_2$) 150.1 (F_2Mo_2)		$^2J/^{19}F_b$ 314 $^2J/^{19}F_b'$ 48 $^2J/^{19}F_1$ 44 $^2J/^{19}F_1'$ 52 $^2J/^{19}F_b'$ 92 $^2J/^{19}F_1'$ 100 $^2J/^{19}F_b'$ 110 $^2J/^{19}F_2$ 44	[99]
$FKrF(MoOF_4)_3$ [c]	SO_2ClF	−121	65.4 (F_tKr) −31.1 (KrF_b) 0.0 (F_1Mo_1) 0.0 (F_1Mo_1) 14.6 ($Mo_1F_b'Mo_2$) 10.8 ($Mo_2F_b''Mo_3$) 10.8 (F_3Mo_3)		$^2J/^{19}F_b$ 326	[99]
$FKrFWOF_4$ [c]	SO_2ClF	−121	67.7 (F_tKr) −26.1 (KrF_b) 67.9 (F_1W)		$^2J/^{19}F_b$ 311 $^2J/^{19}F_1$ 48	[99]

[a] Only the magnitude of the coupling constant is given.
[b] $^1J(^{13}C–^{15}N) = 312$ Hz, $^2J(^{15}N–^1H) = 12.2$ Hz.
[c] The numerical subscript, x, of the metal atom, M (M = Mo, W), and the fluorines, F_x, attached to MX in the compounds $FKrF(MOF_4)_n$ ($x = 1–n$) increases with distance from the krypton atom. In the case of M_1, where the fluorines *cis* to the oxygen atom are non-equivalent, these atoms are denoted F_1 and F_1', and are *cis* and *trans* to the $Kr–F_b–M_1$ fluorine bridge, respectively.

isotope effect on the ^{19}F chemical shift of KrF_2 has been resolved in SO_2ClF solvent at −15.8 °C for krypton isotopes having nuclear spins $I = 0$, the isotopically shifted components (Fig. 4) that have intensities are proportional to their natural abundances (given in parentheses), namely, ^{78}Kr (0.35%), ^{80}Kr (2.25%), ^{82}Kr (11.56%), ^{84}Kr (56.90%), and ^{86}Kr (17.37%) [80]. The ^{19}F resonance arising from $^{83}KrF_2$ is not detectable

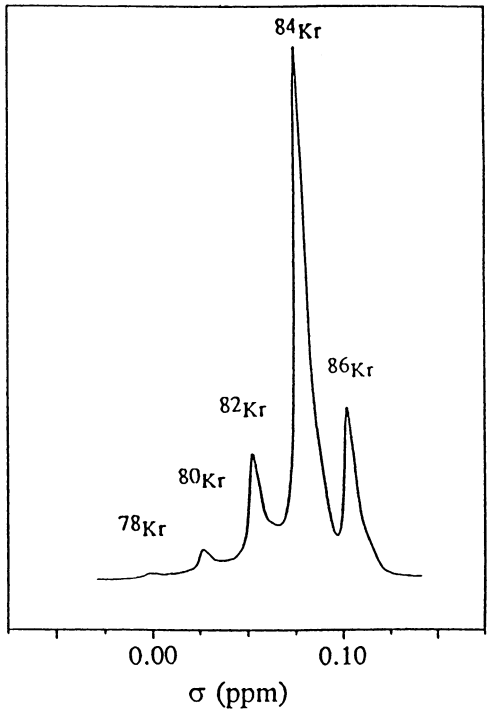

Fig. 4. High-resolution ^{19}F-NMR spectrum showing the secondary isotope effect of krypton on the ^{19}F-NMR spectrum (470.599 MHz, −15.8 °C) of KrF_2 dissolved in SO_2ClF. Lines assigned to individual krypton isotopes are denoted by the mass number of the isotope. Reproduced with permission from Ref. [80].

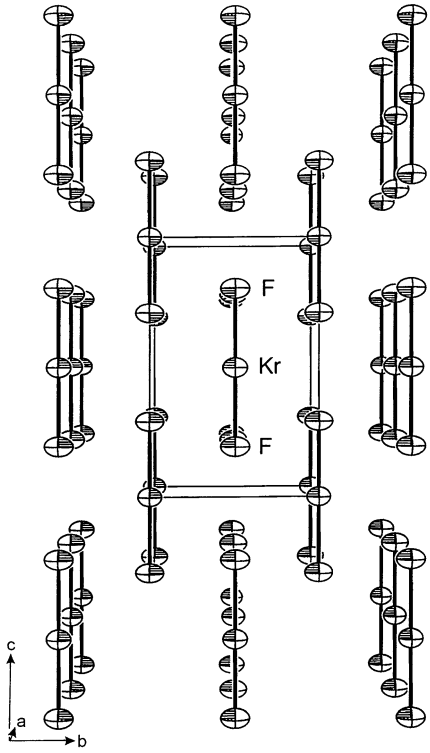

Fig. 5. Packing diagram of α-KrF_2 along the *a*-axis. Reproduced with permission from Ref. [54].

because the decet arising from spin–spin coupling of ^{19}F with the only NMR active krypton isotope, ^{83}Kr ($I = 9/2$, 11.55% natural abundance), is severely broadened and collapsed into the spectral baseline as a result of quadrupolar relaxation. Because krypton does not possess an NMR-active nuclide that is observable in a chemically bound state or that gives rise to observable spin–spin coupling to ^{19}F in the ^{19}F-NMR spectrum, the observation of the secondary krypton isotope shift is an important tool in verifying the existence of a Kr–F bond (see Section 3.3).

The structure of KrF_2 has been determined for both of its known crystallographic morphologies. An early single crystal study by Siegel and Gerbert [84] at an unspecified temperature indicated a primitive tetragonal cell with $a = 6.533$ Å and $c = 5.831$ Å, however, the quality of the diffraction pattern was noted to be poor and prevented the determination of the space group and the metric parameters of KrF_2. Subsequent studies have shown that the β-phase of KrF_2 crystallizes at temperatures above ca. −80 °C in the space group $P4_2/mnm$ (D_{4h} unit cell point symmetry) with $a = 4.585$ Å, $c = 5.827$ Å and $Z = 2$ [83], while at lower temperatures the α-phase with the space group $I4/mmm$ (D_{4h} unit cell point symmetry) with $a = 4.1790(6)$ Å and $c = 6.489(1)$ Å (−125 °C) and $Z = 2$ (Fig. 5) is more stable [54]. The Raman-active $\nu_1(\Sigma_g^+)$ vibrational band of the $D_{\infty h}$ molecule appears as a single band in the low temperature α-phase of KrF_2, but is factor-group split into two broad bands ($A_{1g} + B_{2g}$) in the β-phase [75]. The change in crystallographic morphology appears to be reversible and can occur without loss of the crystallinity of KrF_2. The Kr–F bond lengths in the low-temperature α-phase and high-temperature β-phase are 1.894(5) and 1.89(2) Å, respectively, and are in excellent agreement with the bond lengths derived from rotational spectroscopy [76–78], gas-phase electron diffraction [85], and those estimated by theory [54,71,91,92,96] (Table 5).

3.4. Bonding in KrF_2

The bonding in KrF_2 has been interpreted in terms of a three-center four-electron model in which the primary interaction between the Kr and F atoms is through the valence Kr-4p and F-2p orbitals (Fig. 6), similar to that described for the Xe-5p and F-2p overlap in XeF_2 [100]. This gives rise to σ–p type bonding with formal Kr–F bond orders of one-half and is consistent with the valence bond description of KrF_2 (structures **I** and **III**). Detailed descriptions of the valence

$$\underset{\mathbf{I}}{F-Kr^+F^-} \leftrightarrow \underset{\mathbf{II}}{F^{t\ +}Kr-F}$$

molecular orbitals of KrF_2 have been determined computationally by Collins et al., confirming the strong

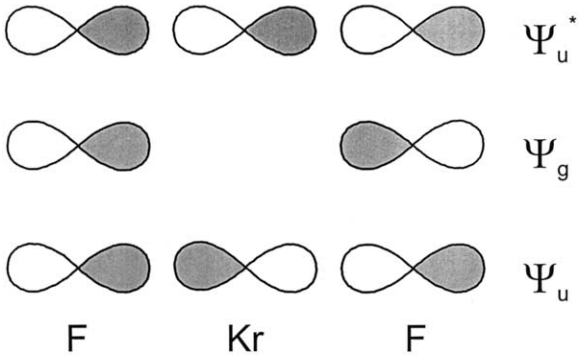

Fig. 6. Molecular orbital diagram of KrF_2.

3c–4e σ-interactions between the Kr-4p orbitals and the F-2p orbitals, and minimal contributions from π-type orbitals [88]. The degree of negative charge localization on the terminal fluorine atoms is expected to be related to the electronegativity of the central noble gas atom ($\chi_{Kr} = 2.58$ [101], 2.99 [24], $\chi_{Xe} = 2.24$ [101], 2.65 [24]) and by this rationalization KrF_2 is anticipated to have more covalent character than XeF_2. The charge distribution in KrF_2 and XeF_2 has been investigated using ^{19}F-NMR and Mössbauer spectroscopies.

On the basis of the ^{19}F-NMR chemical shifts of KrF_2 (55.6 ppm) [79] and XeF_2 (−199.6 ppm) [102] in anhydrous HF, the fluorine nuclei are considerably more deshielded in KrF_2. The charges on the fluorine atoms in KrF_2 and XeF_2 have been estimated to be −0.445 and −0.73 e [24], respectively, based on the assumption that the chemical shifts are dominated by the paramagnetic term.

The nuclear quadrupole interaction energy determined for KrF_2 (960 [82], 978 [81] MHz) by Mössbauer spectroscopy has been compared with that of the $^3P_2$ excited state ($4p^5 5s^1$) of krypton (452.2 MHz) determined by atomic beam magnetic resonance [103]. The interaction energies in these species are the result of non-zero electric field gradients arising from non-spherical electron densities around their krypton nuclei. The ratio of the interaction energies of these species has been interpreted, to a first approximation, to represent the transfer of −0.94 e from krypton to fluorine in KrF_2, predicting a charge distribution of −0.47 e per fluorine atom [82]. The smaller electronegativity of xenon is reflected by the larger charge transfer in XeF_2 (−0.71 e per fluorine atom) [104] and is in good agreement with the trends observed by ^{19}F-NMR spectroscopy (vide supra). Although the difference in charge distribution is already compelling, it has been speculated that it may be necessary to take into account the Kr-4d contribution in order to determine the charge distribution in KrF_2 more precisely from the Mössbauer spectroscopy data [3].

At the local density functional level of theory, the charge on each fluorine atom has been calculated to be −0.36 e [54], which is significantly smaller than the estimates provided by ^{19}F-NMR and Mössbauer spectroscopies, but consistent with a more covalent model of bonding for KrF_2. By comparison, this level of theory predicts a charge of −0.53 e on the fluorine atoms of XeF_2 [105]. Local density functional theory predicts a formal Kr–F bond order of 0.67, which is slightly larger than the value of 0.5 arrived at using the valence bond model, but also identifies a significant F–F interaction with a bond order of 0.22 [54].

The covalent 3c–4e bonding of KrF_2 is also consistent with the ability of KrF_2 to act as a source of fluorine atoms, because cleavage of a Kr–F bond results in the formation of $KrF^\bullet$ and $F^\bullet$. Homolytic cleavage in this fashion suggests that $KrF^\bullet$ and $F^\bullet$ have similar electron affinities, and contrasts with the ionic model, which would require $F^\bullet$ and Kr^{2+} to be produced as a result of dissociation of the more strongly bound species KrF^+ (Eq. (5)). The isolation of $KrF^\bullet$ upon γ-irradiation of

$$KrF_2 \rightarrow KrF^+ + F^- \rightarrow {}^\bullet Kr^+ + F^\bullet + F^- \quad (5)$$

crystalline KrF_2 [31] and the production of $F^\bullet$ under jet conditions from KrF_2 at 170–310 °C [106] were both detected by ESR spectroscopy and provide further evidence that dissociation of KrF_2 to form $F^\bullet$ proceeds by the former mechanism.

4. Fluoride ion donor properties of KrF_2

4.1. Krypton(II) fluorocations, KrF^+ and $Kr_2F_3^+$

4.1.1. Syntheses of KrF^+ and $Kr_2F_3^+$ salts

Krypton difluoride exhibits fluoride ion donor properties that are analogous to those established for XeF_2. Xenon difluoride reacts with pentafluorides of strong and moderate fluoride ion acceptor strengths to form adducts having the general formulations $XeF_2 \cdot 2MF_5$, $XeF_2 \cdot MF_5$, and $2XeF_2 \cdot MF_5$, which are best formulated as salts of the XeF^+ and $Xe_2F_3^+$ cations; i.e. $XeF^+M_2F_{11}^-$ (M = Nb [107–114], Ta [107,109–116], Ru [107,117], Pt [20,107], Ir [117,118], Sb [102,110–112,115,119–127], Bi [128]), $XeF_2 \cdot VF_5$ [129,130], $XeF^+MF_6^-$ (M = Nb [107–113], Ta [107–113,122], Ru [107,117,131,132], Os [107,117], Pt [20,117], Ir [117,118], Au [38], As [102,114,117,118,133–135], Sb [102,109–112,114,123,125–127], Bi [122,128]), and $Xe_2F_3^+MF_6^-$ (M = Ta [109–111], Ru [117,131], Os [117,131], Pt [117,136], Ir [117,118], Au [37,38], As [102,114,117,118,122,135,137–139], Sb [102,109–111,114,126,127], Bi [122,128]). The pentafluorides of the group 5 and 15 elements and those of platinum and gold form KrF^+ and/or $Kr_2F_3^+$ salts: $KrF^+M_2F_{11}^-$ (M = Nb [36,64], Ta [36,64], Ru [140], Pt [140], As [75], Sb [64,66,79,75,141–143]), $KrF_2 \cdot VF_5$ [144], $KrF^+MF_6^-$ (M = Ta [36,64], Ru [140], Rh [140], Pt

[79,142], Au [37,38,145], As [54,75,79,142,146], Sb [54,64,79,142,147,148], Bi [54,128]), $Kr_2F_3^+MF_6^-$ (M = Ta [64], Au [38], As [79,142,146], Sb [64,75,79,142,146,147]).

The corresponding KrF^+ and $Kr_2F_3^+$ salts are formed by low-temperature reaction between KrF_2 and the fluoride ion acceptor either neat (Schemes 1 and 2) or in the oxidatively resistant solvent media, HF and BrF_5 (Schemes 3 and 4). Salts of the KrF^+ and $Kr_2F_3^+$ cations are extremely potent oxidizers [79,146] when compared with their xenon analogues. The use of fluorine passivated apparatus constructed from FEP or sapphire tubing and equipped with stainless steel valves is essential. Apparatus fabricated from Kel–F is to be avoided because KrF^+ and $Kr_2F_3^+$ salts aggressively attack this polymer by oxidatively fluorinating the C–Cl bonds, instantaneously causing the material to crack and possibly rupture at the point of contact with solid salts or their solutions [63].

Unlike their xenon(II) analogues, all krypton(II) compounds are thermodynamically unstable with respect to redox decomposition. The salts of KrF^+ and $Kr_2F_3^+$ display a range of thermal stabilities. Solutions of $KrF^+SbF_6^-$ and $KrF^+PtF_6^-$ in anhydrous HF, KrF_2 in liquid SbF_5 ($KrF^+Sb_nF_{5n+1}^-$), and $Kr_2F_3^+MF_6^-$ and $KrF^+MF_6^-$ (M = As, Sb) in BrF_5 are unstable and decompose rapidly at room temperature according to Eqs. (6) and (7) [79]. In the case of

$$Kr_2F_3^+MF_6^- \rightarrow KrF^+MF_6^- + Kr + F_2 \quad (6)$$

$$KrF^+MF_6^- \rightarrow MF_5 + Kr + 1/2F_2 \quad (7)$$

BrF_5 solvent, some BrF_5 is oxidized to the BrF_6^+ cation at room temperature by $KrF^+MF_6^-$ (As [142,146], Sb [142,146], Au [38]; also see Section 7). It is possible that the instability of KrF^+ in anhydrous HF is caused by reduction of the cation by $(HF)_nF^-$ according to Eqs. (8) and (9) [140].

$$(n+2)HF \rightleftharpoons H_2F^+ + (HF)_nF^- \quad (8)$$

$$KrF^+ + (HF)_nF^- \rightarrow nHF + F_2 + Kr \quad (9)$$

In contrast, $KrF^+AuF_6^-$, which has a very low solubility in HF and is stable either as the dry compound or under HF, room temperature for indefinite periods of time [149].

The relative kinetic stabilities of KrF^+ and $Kr_2F_3^+$ salts show considerable variance, with the majority of

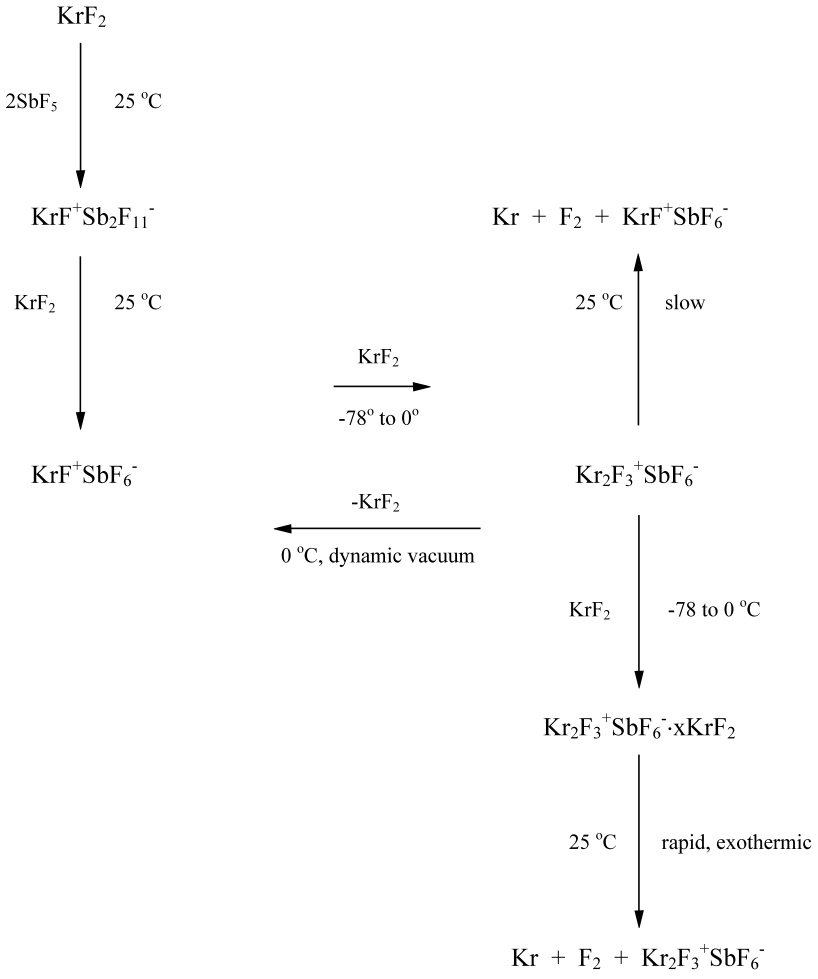

Scheme 1. The formation of KrF^+ and $Kr_2F_3^+$ salts derived from the reaction of KrF_2 with SbF_5. Reproduced with permission from Ref. [79].

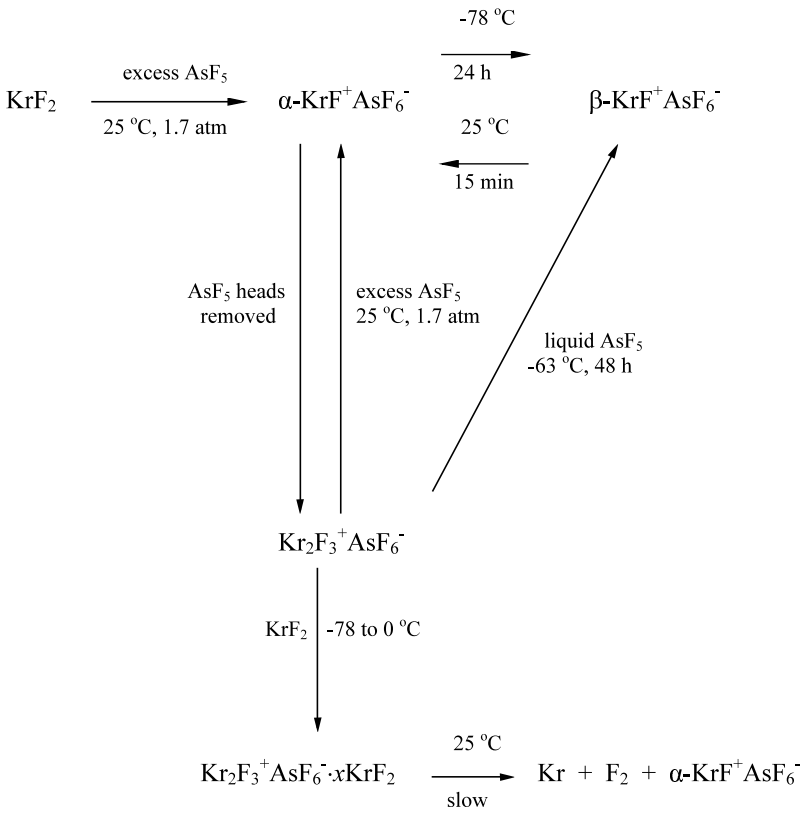

Scheme 2. The formation of KrF^+ and $Kr_2F_3^+$ salts derived from the reaction of KrF_2 with AsF_5. Reproduced with permission from Ref. [79].

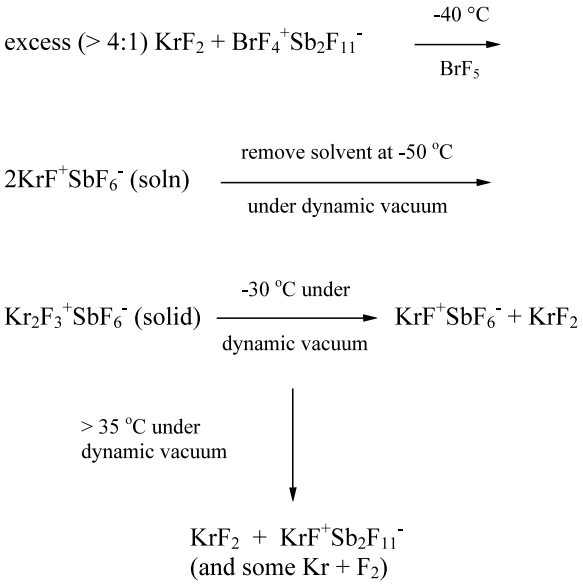

Scheme 3. The formation of KrF^+ and $Kr_2F_3^+$ salts derived from the reaction of KrF_2 with SbF_5 in BrF_5 solvent. Reproduced with permission from Ref. [64].

the solid salts decomposing below room temperature. The solid $KrF^+MF_6^-$ (M = Sb [64,79,142,147], Bi [128], Pt [79,142] and Au [37,38]) and $KrF^+Sb_2F_{11}^-$ [64,79,142,147] salts can be handled and stored at room temperature for appreciable periods of time without significant decomposition. The $KrF^+SbF_6^-$ salt undergoes slow redox decomposition at 35 °C to $KrF^+Sb_2F_{11}^-$, Kr and F_2, [64] with the latter salt being stable to dynamic pumping at room temperature (Scheme 3). In a related study [150], the thermal decomposition of $KrF^+Sb_2F_{11}^-$ was studied in connection with the development of a technique for fixing radioactive krypton emitted during the nuclear fission process. The decomposition rate of the complex was also shown to be slow, but detectable at 30 °C and increased markedly with increasing temperature. In contrast, $KrF^+AsF_6^-$ is rapidly converted to $Kr_2F_3^+AsF_6^-$ upon removal of static heads of AsF_5 at 25 °C (Scheme 2), whereas $Kr_2F_3^+SbF_6^-$ slowly decomposes to $KrF^+SbF_6^-$, Kr and F_2 when pumped on dynamically at 25 °C (Scheme 1). The KrF_2 adducts of weak fluoride ion acceptors, TaF_5 and NbF_5, have been isolated from BrF_5 solvent and have correspondingly much lower thermal stabilities with respect to dissociation under dynamic vacuum (Scheme 4). When compared with $KrF^+SbF_6^-$ and $KrF^+Sb_2F_{11}^-$, the observed trend in thermal stability is $KrF^+Sb_2F_{11}^- > KrF^+SbF_6^- > KrF^+Ta_2F_{11}^- > Kr_2F_3^+SbF_6^- > KrF^+TaF_6^- > KrF^+Nb_2F_{11}^-$ [64]. No $KrF^+NbF_6^-$ or $Kr_2F_3^+$ salts of TaF_6^- and NbF_6^- could be isolated and characterized as solids, although tentative Raman

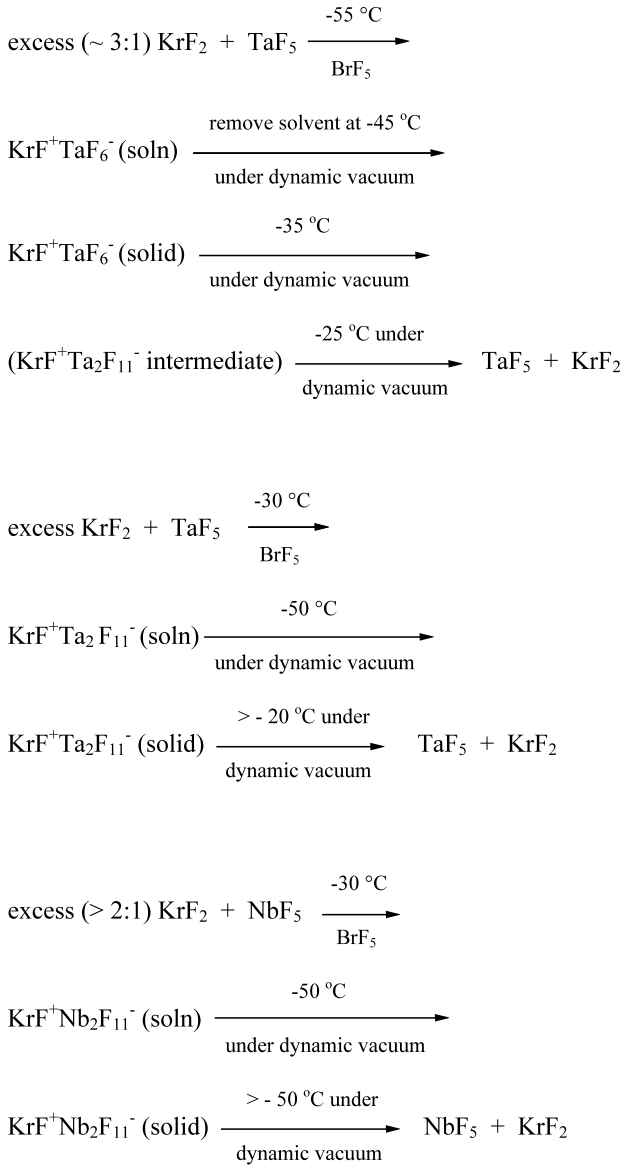

Scheme 4. The formation of KrF^+ and $Kr_2F_3^+$ salts derived from the reaction of KrF_2 with TaF_5 or NbF_5 in BrF_5 solvent. Reproduced with permission from Ref. [64].

spectroscopic evidence has been obtained for $Kr_2F_3^+TaF_6^-$ in frozen BrF_5 solutions [36,64]. Thermal decomposition of KrF_2 mixtures of TaF_5 and NbF_5 derived from dynamic pumping of their BrF_5 solutions at −55 and −50 °C, respectively, have produced evidence for intermediate adducts which have been tentatively formulated as $KrF^+Ta_2F_{11}^-\cdot nKrF_2$ and $KrF^+Nb_2F_{11}^-\cdot nKrF_2$ [64]. Attempts to prepare $KrF^+CrF_6^-$ from KrF_2 and the weak fluoride ion acceptor CrF_5 in either the presence or absence of HF as a solvent have proven unsuccessful [151].

The $KrF^+PtF_6^-$ and $KrF^+AuF_6^-$ salts have been synthesized by direct reaction of KrF_2 with PtF_5 [140], AuF_5 [38], and PtF_6 (Eq. (10)) [79,142], or excess KrF_2 with gold powder (Eq. (11), also see Section 8.3) [37,38,149] in anhydrous HF. The solid salts are both stable indefinitely at room temperature.

$$KrF_2 + PtF_6 \rightarrow KrF^+PtF_6^- + 1/2F_2 \quad (10)$$

$$7KrF_2 + 2Au \rightarrow 2KrF^+AuF_6^- + 5Kr \quad (11)$$

In the absence of HF, KrF_2 ignites Au powder, causing it to burn with a bright white flame [63], demonstrating the necessity of providing an adequate heat sink when reacting this potent oxidative fluorinator with metal powders. Evolution of F_2 in Eq. (10) indicates that the electron affinity of PtF_6 is greater than that of the KrF^+ cation [79,142] and contrasts with a claim that $KrF^+PtF_6^-$ decomposes at 0 °C according to Eq. (12) [140]. Recent attempts to prepare KrF^+ by reaction

$$2KrF^+PtF_6^- \rightarrow KrF_2 + Kr + 1/2F_2 + PtF_6 \quad (12)$$

of krypton with the highly reactive and thermally unstable NiF_3^+ cation in anhydrous HF (prepared from the reaction of the NiF_6^{2-} anion with AsF_5 in HF) failed, although the NiF_3^+ has proven capable of oxidizing ClF_5 and BrF_5 to the previously known ClF_6^+ and BrF_6^+ cations [152] (see Sections 8.1 and 8.2).

The low-temperature X-ray structures of $KrF^+MF_6^-$ (M = As [54], Sb [54], Bi [54], Au [149]) have been recently determined (see Section 4.1.3). The X-ray structure of the double salt, $Kr_2F_3^+AsF_6^-\cdot KrF^+AsF_6^-$ has also been obtained [54]. Several $Kr_2F_3^+$ salts have also been synthesized which have been ascertained by Raman spectroscopy to contain undetermined amounts of weakly associated KrF_2, namely, $Kr_2F_3^+MF_6^-\cdot nKrF_2$ (M = P [54], As [79,142], Sb [79,142]) and $Kr_2F_3^+BF_4^-\cdot nKrF_2$ [153]. The X-ray crystal structures of two of these salts, $Kr_2F_3^+SbF_6^-\cdot KrF_2$ and $(Kr_2F_3^+SbF_6^-)_2\cdot KrF_2$, have recently been determined [54] and confirm that KrF_2 is weakly associated in these structures (see Section 4.1.3). Thus far, no X-ray structure of a simple $Kr_2F_3^+$ salt has been determined. Anhydrous HF was used as the synthetic and crystallization medium in the aforementioned cases.

There are several KrF_2 adducts which remain structurally ill-defined. The adduct, $KrF_2\cdot VF_5$, is reported to form at low temperatures in liquid VF_5 and melts at 5.0 ± 0.5 °C [144]. The adduct was identified by infrared spectroscopy and the stoichiometry was established by determining the melting points as a function of KrF_2:VF_5 ratio. Infrared spectra of a mixture having a KrF_2:VF_5 ratio of 1:2 at −196 °C consisted of the spectra of $KrF_2\cdot VF_5$ and VF_5, with no evidence for $KrF_2\cdot 2VF_5$. Unlike the KrF^+ salts discussed above, and like its xenon analogue [129,130,144], the $KrF_2\cdot VF_5$ adduct appears to be predominantly covalent in character. This assessment is based on the differences in the frequency separations between $\nu_{as}(KrF_2)$ and $\nu_s(KrF_2)$ of adducted KrF_2, which can be used to assess relative degree of covalency (see Section 4.2). The adducts, $KrF_2\cdot MnF_4$ and $KrF_2\cdot 2MnF_4$, have been prepared by reaction of

MnF_2 with KrF_2 in anhydrous HF and their stoichiometries inferred from their weight loss versus time pumping curves, but no spectroscopic data is available for either adduct [154]. The 2:1 adduct decomposes at −45 °C yielding the 1:1 adduct, which is stable to −25 °C (see Section 8.3). The adduct, $KrF_2 \cdot XeF_6$ has been prepared by dissolution of KrF_2 (2:1 excess) and XeF_6 in BrF_5 or anhydrous HF followed by removal of the solvent and excess KrF_2 under vacuum at −25 °C [155]. The adduct is reported to have a vapor pressure of ca. 1 Torr at −10 °C and 11 Torr at 20 °C, subliming under vacuum in a molar ratio of 1:1. The formation of $KrF^+XeF_7^-$ has been excluded on the basis of a comparative study of the infrared spectra of $KrF_2 \cdot XeF_6$, KrF_2, XeF_6, and $CsF \cdot XeF_6$ ($Cs^+XeF_7^-$). Rather, weak association of KrF_2 and XeF_6 in the form of a molecular compound is suggested.

4.1.2. *Vibrational, Mössbauer and ^{19}F-NMR spectroscopic studies*

Structural characterization of the KrF^+ and $Kr_2F_3^+$ salts in the solid state using Raman spectroscopy has been most extensive (KrF^+ [36–38,64,75,79,128,140,142,147], $Kr_2F_3^+$ [36,38,54,64,75,79,142,153]) whereas studies using infrared spectroscopy have been limited (KrF^+ [64,141]). Because of difficulties in sample preparation arising from the strong oxidant properties of both cations (see Sections 8.1 and 8.2), as exemplified by the oxidation of chloride in AgCl windows to ClF_3 and ClF_5 [73]. Raman spectra of the salts are generally readily obtained in a variety of sample vessel materials such as FEP, Pyrex glass, and quartz.

The Raman spectra of KrF^+ salts and the crystal structures of $KrF^+MF_6^-$ (M = As [54], Sb [54], Bi [54], Au [149]) indicate that the KrF^+ cation strongly interacts with the anion by formation of a fluorine bridge between krypton and a fluorine of the anion, as is the case for XeF^+ in the crystal structures of $XeF^+MF_6^-$ (M = Ru [132], As [134,156], Sb [156], Bi [156]), $XeF^+Sb_2F_{11}^-$ [120,121,156] and $XeF^+Bi_2F_{11}^-$ [156]. Consequently, fluorine bridge modes and vibrational modes resulting from symmetry lowering of the octahedral anion have been reported and tentatively assigned [64,79,128]. Most recently, the Raman spectra of the fluorine bridged $KrF^+MF_6^-$ (M = As, Sb, Bi) ion pairs have been reassigned by comparison with vibrational spectra calculated for the gas-phase ion pairs [54]. The Kr–F stretch in KrF^+ salts uniformly occur at higher frequency (597–627 cm^{-1}, Table 8) than the symmetric stretch of KrF_2 (Table 4). The Raman spectroscopic studies indicate that the fluorine bridge interactions between the NgF^+ cations and anions derived from pentafluorides are weakest for the $Sb_2F_{11}^-$ anion. The NgF^+ cations in the $Sb_2F_{11}^-$ salts exhibit the highest Ng–F stretching frequencies (KrF^+ 619, 627 [64] and 624 [79] cm^{-1}; XeF^+, 619 cm^{-1} [114]) and therefore most closely approximate free NgF^+ cations.

The Raman spectra of $Kr_2F_3^+$ salts have been assigned on the basis of an essentially V-shaped fluorine bridged geometry (C_{2v} point symmetry) for the cation [54,64,79,142,147] (Table 9), consistent with that determined by X-ray crystallography for the $Kr_2F_3^+$ [54] and $Xe_2F_3^+$ [137,139] cations. Recently, calculated vibrational frequencies of $Kr_2F_3^+$ [54] have allowed the differentiation of the terminal symmetric and asymmetric Kr–F_t and bridging symmetric and asymmetric Kr···F_b stretching modes, which were not explicitly assigned previously. The analogous assignment has also been made recently for $Xe_2F_3^+$ in light of theoretical calculations [139]. In contrast with the KrF^+ salts, the cation–anion interactions in the $Kr_2F_3^+MF_6^-$ salts appear to be weak, as indicated by retention of octahedral symmetry by the anion in the Raman spectrum and by insensitivity of the cation frequencies to the nature of the anion [54,64,79,142,147]. A Raman spectroscopic study of the KrF_2/PF_5 system at −78 °C in the presence of excess PF_5 indicates that the only species present is $Kr_2F_3^+PF_6^- \cdot nKrF_2$ [54]. The Raman spectrum of this compound is characteristic of other $Kr_2F_3^+MF_6^- \cdot nKrF_2$ (M = As, Sb) adduct-salts [79,142], which exhibit vibrational modes that are consistent with weakly bound KrF_2 molecules in their crystal lattices. Failure to synthesize $KrF^+PF_6^-$ in the presence of excess PF_5 at −78 °C reflects the lower fluoride ion affinity of PF_5 (397 kJ mol^{-1}) [157] and conforms with the theoretical results, which predict an adduct in which PF_5 is weakly fluorine bridged to KrF_2 and the KrF_2 bond lengths exhibit little distortion from the bond lengths of free KrF_2 [54].

The Kr–F_t stretching frequencies of the $Kr_2F_3^+$ cation are intermediate with respect to those of KrF_2 and KrF^+ salts. The order of terminal Kr–F symmetric stretching frequencies for $KrF_2 < Kr_2F_3^+ < KrF^+$ (Tables 4, 8 and 9) correlates well with the terminal Kr–F_t bond length order $KrF_2 > Kr_2F_3^+ > KrF^+$ obtained from the crystal structure determinations and from theory (Tables 5 and 10) [54]. The Kr···F_b bonds of $Kr_2F_3^+$ are significantly shorter than their counterparts in KrF^+ salts, but appear to exhibit symmetric and asymmetric Kr···F_b stretching frequencies that are lower than the Kr···F_b stretching frequencies of KrF^+ salts. The discrepancy presumably arises because the Kr···F_b modes of the KrF^+ salts couple with the Kr–F_t stretching mode and/or the stretching modes of the MF_5 moiety in F_t–Kr···F_b–MF_5 (M = As, Sb, Bi) [54].

The Mössbauer spectra of KrF_2 [81,82], α- and β-$KrF^+AsF_6^-$, and $KrF^+SbF_6^-$ [82] have been measured using the 9.4 keV transition of ^{83}Kr produced in the decay of an ^{83}RbF source. The values of the quadrupole constant strengths and isomer shifts indicate that the Kr–F bonding in the compounds studied is very similar.

Table 8
Vibrational frequencies (cm^{-1}) of the fluorine-bridged F–Kr···F moieties in KrF^+ salts [a]

		ν(Kr–F)	ν(Kr···F)	δ(F–Kr···F)	Ref.
$KrF^+Nb_2F_{11}^-$	R [b]	613 (56) 606 (66) 597 (100)	372 (6)	194 (100) 189 (27) 181 (17.3) 167 (9.4)	[64]
$KrF^+Ta_2F_{11}^-$	R [b]	609 (100) 600 (100) 594 (27)	337 (12)	not obsd.	[64]
$KrF^+Sb_2F_{11}^-$	R [c]	627 (100) 619 (20)	298 (6)? 270 (5) 260 (5)	150 (3)	[64]
	I.R. [c]	616 m			[64]
	R [d]	624 (100)	262 (6)	145 (4)	[79]
$KrF^+TaF_6^-$	R [b]	603.5 (100) 599 (97)	343.5 (10) 339 (9) 325 (8.1)	192 (18) 179 (12)	[64]
$KrF^+PtF_6^-$	R [d]	606 (50) 599 (60)	338 (3)	169 (3) 139 (8)	[79]
$KrF^+AuF_6^-$	R [e]	597 (82)	346 (2)	163 (2)	[37]
α-$KrF^+AsF_6^-$	R [d]	607 (100) 596 (100)	328 (12)	173 (8)	[79]
β-$KrF^+AsF_6^-$	R [d]	619 (72) 615 (100)	338 (16)	173 (10) 162 (11)	[79]
$KrF^+SbF_6^-$	R [c]	621 (85) 618 (100)	348 (2.7) 344 (2.7)	174 (3.5) 166 (4.8) 149 (2.7)	[64]
	I.R. [c]	607 s			[64]
	R [d]	619 (74) 615 (100)	338 (4)	169 (5) 162 (7) 145 (3)	[79]
$KrF^+BiF_6^-$	R [b]	610 (100) 604 (11) 600 (25)	316 (6)	173 (7)	[128]

[a] Abbreviations denote Raman (R), infrared (I.R.), medium (m), strong (s). Numbers in parentheses are relative intensities.
[b] Spectra recorded at −196 °C.
[c] Spectra recorded at room temperature.
[d] Spectra recorded at −90 °C.
[e] Spectra recorded at −80 °C.

A slight increase of the quadrupole coupling in going from KrF_2 to $FKr\cdots FMF_5$ can be interpreted in terms of a shortening of the terminal Kr–F bond length and an elongation of the bridge bond length which lead to an increase in the electric field gradient at the ^{83}Kr nucleus. The trend is in the correct direction, the experimental error is too large to attach significance to the difference between quadrupole splittings observed for $KrF^+AsF_6^-$ and $KrF^+SbF_6^-$. In retrospect, it is not surprising that the quadrupole splittings of $KrF^+AsF_6^-$ and $KrF^+SbF_6^-$ are similar because the $Kr–F_t$ and $Kr\cdots F_b$ bond lengths have been found to be identical with $\pm 3\sigma$ (Table 3) in both salts.

Fluorine-19 NMR spectroscopy has also been used to study the KrF^+ cation in HF solution and the $Kr_2F_3^+$ cation in BrF_5 solution (Table 7). The ^{19}F-NMR spectrum of $KrF^+SbF_6^-$ in HF at −40 °C comprises a singlet at −22.6 ppm assigned to KrF^+, which is shifted to lower frequency with respect to its parent compound, KrF_2 (55.6 ppm; HF solvent, 26 °C) [79,142]; a similar but more pronounced shift is observed for XeF^+ (−289.8 ppm; SbF_5 solvent, 26 °C) relative to XeF_2 (−199.6 ppm; HF solvent, −68 °C) [102,142]. Bromine pentafluoride solutions of $Kr_2F_3^+AsF_6^-$ and $Kr_2F_3^+SbF_6^-$ give AX_2 spectra at low temperatures [79,142] (Fig. 7), and have provided the first unambiguous characterization of the structure of the fluorine bridged $Kr_2F_3^+$ cation (Fig. 7), which is similar to that previously established for $Xe_2F_3^+$ in BrF_5 solution by ^{19}F [102] and ^{129}Xe [158]-NMR spectroscopy and in the solid state by X-ray crystallography [137,139]. Unlike $Xe_2F_3^+$ (F_t, −252.0 ppm; F_b, −184.7 ppm in BrF_5 solvent at −62 °C) [102], the ^{19}F terminal (F_t) resonance of $Kr_2F_3^+$ occurs at higher frequency than that of the bridging fluorine (F_b). The $^2J(^{19}F_t–^{19}F_b)$ coupling in $Kr_2F_3^+$ (347–351 Hz) is significantly larger than those

Table 9
Experimental Raman and calculated vibrational frequencies, assignments and mode descriptions for $Kr_2F_3^+$

$[Kr_2F_3][AsF_6]$ [a,b]	$[Kr_2F_3][SbF_6]$ [a,b]	$[Kr_2F_3][PF_6]\cdot n\,KrF_2$ [b,c,d]	$[Kr_2F_3][AsF_6]\cdot n\,KrF_2$ [a,b]	$[Kr_2F_3][SbF_6]\cdot n\,KrF_2$ [a,b]	LDFT [d,e]	Assignments for $Kr_2F_3^+$ in C_{2v} point group [d,f]	
610(43), 600(80), 594(100)	603(100), 594(89)	605(100)	602(100)	599(100)	628(12)	$\nu_1(A_1)$	$\nu(KrF_t+KrF_t)$
570(4), 567(31)	555(34)	555(52)	575(23), 553(50)	557(50)	608(273)	$\nu_6(B_1)$	$\nu(KrF_t-KrF_t)$
437(5)	456(4)	462(11)	462	466(60)	441(212)	$\nu_7(B_1)$	$\nu_{as}(KrF_b)$
347(sh), 336(17)	330(18)	358(19)	355(19)	340(14)	313(11)	$\nu_2(A_1)$	$\nu_s(KrF_b)$
183(15)	186(16)	191(11)	190(10)	200(2)	196(14)	$\nu_9(B_2)$	$\delta(F_t-Kr\cdots F_b)$ oop antisym comb
174(13)	180(sh)	185(7)	184(sh)	188(10)	168(1)	$\nu_3(A_1)$	$\delta_s(F_t-Kr\cdots F_b)$ ip sym comb
158(2)	176(sh)	176(5)	177(sh)	122(46)	159(0)	$\nu_5(A_2)$	$\delta(F_t-Kr\cdots F_b)$ oop sym comb
					155(0)	$\nu_8(B_1)$	$\delta(F_t-Kr\cdots F_b)$ ip antisym comb
					41(0)	$\nu_4(A_1)$	$\delta(Kr\cdots F_b\cdots Kr)$ bend

[a] From Ref. [79]; anion modes are also given in this reference. The abbreviation, sh, denotes a shoulder.
[b] Values in parentheses denote relative Raman intensities.
[c] Frequencies observed for PF_6^-: 748(7) $\nu_1(A_{1g})$; 581(7) and 572(13), $\nu_2(A_{1g})$; 475(12), 469(35) and 464(11), $\nu_5(T_{2g})$. Spectrum recorded on a powder in a 1/4-in. FEP sample tube at -80 °C using 514.5 nm excitation. Values in parentheses denote relative Raman intensities. Additional weak bands were observed at 1859(0.20) and 1863(0.15) cm^{-1} that were associated to O_2^+.
[d] From Ref. [54].
[e] Infrared intensities, in km mol^{-1}, are given in parentheses.
[f] The abbreviations oop and ip denote out of plane and in plane, respectively.

Table 10
Metric parameters derived from X-ray structures and theoretical calculations for NgF^+ and $Ng_2F_3^+$ (Ng = Kr, Xe)

	Ng–F_t (Å)	Ng···F_b (Å)	∠ F_t–Ng···F_b (°)	∠ Ng···F_b···M (°) [a]	T (°C)	Ref.
β-$KrF^+AsF_6^-$	1.765(2)	2.131(2)	176.8(1)	133.7(1)	−120	[54]
LDFT	1.867	1.998	177.7	120.0		
HF	1.746	2.002	178.3	128.3		
$Kr_2F_3^+AsF_6^- \cdot KrF^+AsF_6^-$	1.783(6)	2.106(6)	177.3(3)	124.6(3)	−120	[54]
$KrF^+SbF_6^-$	1.765(3)	2.140(3)	177.9(2)	139.2(2)	−113	[54]
LDFT	1.857	2.017	177.4	114.1		
HF	1.739	2.038	178.6	124.9		
$KrF^+BiF_6^-$	1.774(6)	2.090(6)	177.0(4)	138.3(3)	−130	[54]
LDFT	1.859	2.012	177.2	113.8		
HF	1.745	2.003	178.7	131.2		
$KrF^+AuF_6^-$	1.76(1)	2.15(1)	175.4(7)	125.3(7)	−130	[149]
$XeF^+AsF_6^-$	1.888(3)	2.208(3)	179.1(2)	133.6(2)	−173	[156]
$XeF^+AsF_6^-$	1.873(6)	2.212(5)	178.9(7)	134.8(2)	24	[134]
$XeF^+SbF_6^-$	1.885(2)	2.278(2)	177.94(9)	136.9(1)	−173	[156]
$XeF^+BiF_6^-$	1.913(7)	2.204(7)	178.4(3)	156.1(4)	−173	[156]
$XeF^+Sb_2F_{11}^-$	1.884(4)	2.343(4)	179.3(2)	148.1(2)	−173	[156]
$XeF^+Sb_2F_{11}^-$	1.82(3)	2.34(3)	176.0(1)	149.0(2)	– [b]	[16,121]
$XeF^+RuF_6^-$	1.87(2)	2.18(2)	177.0(1)	137.2(5)	– [b]	[132]
$Kr_2F_3^+AsF_6^- \cdot KrF^+AsF_6^-$	1.780(7)–1.803(6)	2.049(6)–2.061(6)	178.2(3)–178.6(3)	127.5(3)	−120	[54]
$Kr_2F_3^+SbF_6^- \cdot KrF_2$	1.790(5)–1.800(5)	2.027(5)–2.046(5)	175.1(2)–176.8(2)	142.5(3)	−113	[54]
$[Kr_2F_3^+]_2[SbF_6^-]_2 \cdot KrF_2$	1.787(4)–1805(5)	2.041(4)–2.065(4)	177.8(2)–178.7(2)	126.0(2)–128.0(2)	−125	[54]
$Kr_2F_3^+$ LDFT	1.826	2.081	177.4	135.2		[54]
$Kr_2F_3^+$ HF	1.730	2.082	180.0	180.0		
$Xe_2F_3^+AsF_6^-$ (monoclinic)	1.908(6)–1.929(6)	2.142(7)–2.157(3)	177.3(4)–177.7(3)	148.6(4)–149.5(4)	−127	[139]
$Xe_2F_3^+AsF_6^-$ (trigonal) [c]	1.907(11)	2.09(2)–2.26(2)	167.7(6)	139.8(8)	−116	[139]
$Xe_2F_3^+AsF_6^-$						[137]
$Xe_2F_3^+SbF_6^-$	1.918(9)–1.922(9)	2.141(8)–2.146(8)	176.9(3)–178.6(4)	160.3(3)	−125	[139]
$Xe_2F_3^+$ LDFT	1.963	2.217	177.7	149.0		[139]

[a] M = As, Sb, Bi, Au or Kr.
[b] Ambient temperature.
[c] The $Xe_2F_3^+$ cation is positionally disordered in the trigonal case.

observed for xenon fluoride cations such as $Xe_2F_3^+$ (308 Hz) [102], XeF_3^+ (174 Hz) [159], XeF_5^+ (176 Hz) [160], and $XeOF_3^+$ (103 Hz) [159]. In the $Ng_2F_3^+$ cations, the F_t–Ng···F_b angle is ∼180°, whereas the bond angles in the other cations are ∼90°.

4.1.3. X-ray crystal structures and electron structure calculations of KrF^+ and $Kr_2F_3^+$ salts

While the strong oxidant characters of KrF_2, KrF^+ and $Kr_2F_3^+$ provide clean, low-temperature synthetic routes to a number of novel high-oxidation state species (see Sections 8.2, 8.3 and 8.4), they have served as a significant impediment to their detailed structural characterization by single crystal X-ray diffraction, and until recently, only KrF_2 (see Section 3.3) had been structurally characterized in detail by diffraction techniques. The low-temperature X-ray crystal structures of several KrF^+ (Figs. 8 and 9) and $Kr_2F_3^+$ (Figs. 9–11) salts show bond length and bond angle trends among $[NgF^+][MF_6^-]$ ion pairs, NgF_2 and $Ng_2F_3^+$ salts that are analogous for krypton and xenon.

Single crystal X-ray structure determinations of KrF^+ salts [54] and theoretical calculations show (Table 10) that the solid state and gas-phase $[KrF^+][MF_6^-]$ ion pairs are strongly fluorine bridged as originally proposed on the basis of their vibrational spectra. With the exception of theoretically predicted $KrF_2 \cdot PF_5$ adduct, the Kr–F_t bond length is essentially unaffected by the MF_6^- anion. Although the fluoride ion affinities of AsF_5 (443.1 kJ mol^{-1}) and SbF_5 (503.3 kJ mol^{-1}) differ by significant amounts, no significant difference in the Kr···F_b bond length is observed in the low-temperature structures of the AsF_6^- and SbF_6^- salts, although this bond length is found to be significantly shorter in the BiF_6^- salt, in accord with the higher covalent character associated with the weaker fluoride ion acceptor strength of BiF_5. An interesting feature not previously noted in the X-ray structures of XeF^+ salts is the small, but significant, deviation in the F_t–Kr···F_b angle from linearity (Table 10). The angle ranges from 175.4(7) to 177.9(2)° in the crystal structures that have been determined. Although there are longer weak contacts between krypton and fluorines in the lattice, ranging from 2.980 to 3.480 Å compared with the sum of the krypton (2.02 Å) [161] and fluorine (1.47 Å [161], 1.35 Å [162]) van der Waals radii, which may be responsible for these distortions, density functional theory (DFT) calculations reproduce these small angle distortions for

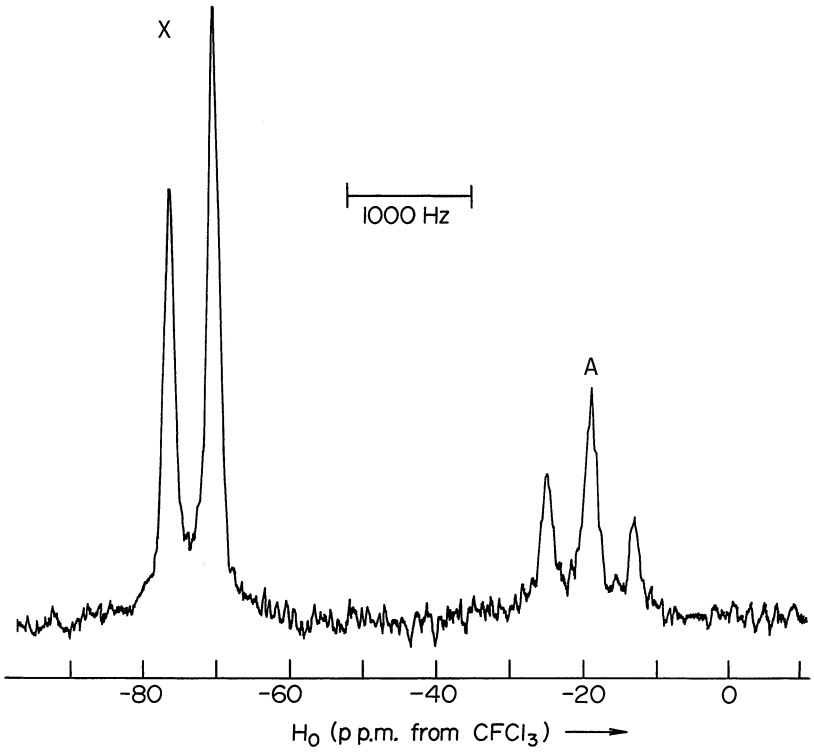

Fig. 7. ^{19}F-NMR spectrum (58.3 MHz, −66 °C) of the $Kr_2F_3^+$ cation (~0.5 M $Kr_2F_3^+SbF_6^-$ in BrF_5 solvent): (A) bridging fluorine; (X) terminal fluorines. The chemical shift scale must be multiplied by −1 to conform with the present IUPAC convention. Reproduced with permission from Ref. [79].

the gas-phase ion pairs (Table 10). Recent reinvestigations of the low-temperature crystal structures of several XeF^+ salts [156] have provided more precise metric parameters than obtained for the previously published ambient temperature structures and reveal similar F_t–Xe···F_b angle distortions (Table 10).

The covalency of the Kr···F_b bonds in $Kr_2F_3^+$ is reflected in the Kr···F_b···Kr bridge angle, which is significantly bent in all crystal structures of its salts [54] (Table 10). The bent angles are consistent with AX_2E_2 VSEPR arrangements at their respective fluorine bridge atoms, but are more open than the ideal tetrahedral angle. The $Kr_2F_3^+$ cation is highly deformable in the solid state with regards to the Kr···F_b bond distances and the Kr···F_b···Kr bridge bond angle. These deformations have been attributed to long contacts between the krypton atoms in the cation and fluorine atoms of the anion. Moreover, the solid state Kr···F_b···Kr angles differ significantly from that arrived at by DFT calculations of the gas-phase $Kr_2F_3^+$ cation geometry (Table 10). The upper limit of the Kr···F_b···Kr bond angle (range, 126.0(2)–142.4(3)°) is in good agreement with the Xe···F_b···Xe bond angles observed in the monoclinic (148.6(4)°) and trigonal (139.8(8)°) phases of $Xe_2F_3^+AsF_6^-$, but is considerably smaller than the angle observed in $Xe_2F_3^+SbF_6^-$ (160.3(3)°) [137,139]. In all of the crystal structures of $Kr_2F_3^+$ salts that have been determined thus far, the F_t–Kr···F_b angles are nonlinear and range from 175.1(2) to 178.7(2)°. Both angles lie in the cation plane and are bent away from the C_2-axis of the cation, giving rise to a shallow W-shaped cation. Recent low-temperature crystal structures of $Xe_2F_3^+$ salts reveal very similar F_t–Xe···F_b angle distortions [139]. The optimized gas-phase geometries of $Kr_2F_3^+$ and $Xe_2F_3^+$ reproduce the F_t–Ng···F_b angle distortions from linearity at the DFT level of theory ($Kr_2F_3^+$: expt. 3.2(1)–2.1(2)°, theor., 2.6° [54]; $Xe_2F_3^+$: expt., 2.4(3)° [As] and 1.4(4)° [Sb]; theor., 2.3° [139]). The importance of high level calculations in accurately reproducing the angles in these cations is illustrated by the linear geometries predicted at the HF level [54,139].

The Kr–F_t bond exhibits a considerable variation in length among the solid state krypton fluoride structures that are now known and increases in length in the order $KrF^+ < Kr_2F_3^+ < KrF_2$ [54]. This trend is consistent with the valence bond (structures **I** and **II**) and 3c–4e descriptions of KrF_2 (see Section 3.4), which predict a formal Kr–F bond order of one-half for KrF_2 and one for the free KrF^+ cation. The Kr–F_t bond length in $Kr_2F_3^+$ which is intermediate with respect to those of KrF_2 and KrF^+, consistent with the dominant roles KrF^+ and KrF_2 play in the resonance description of $Kr_2F_3^+$ (structures **III**–**V**) and with a description that invokes a significant

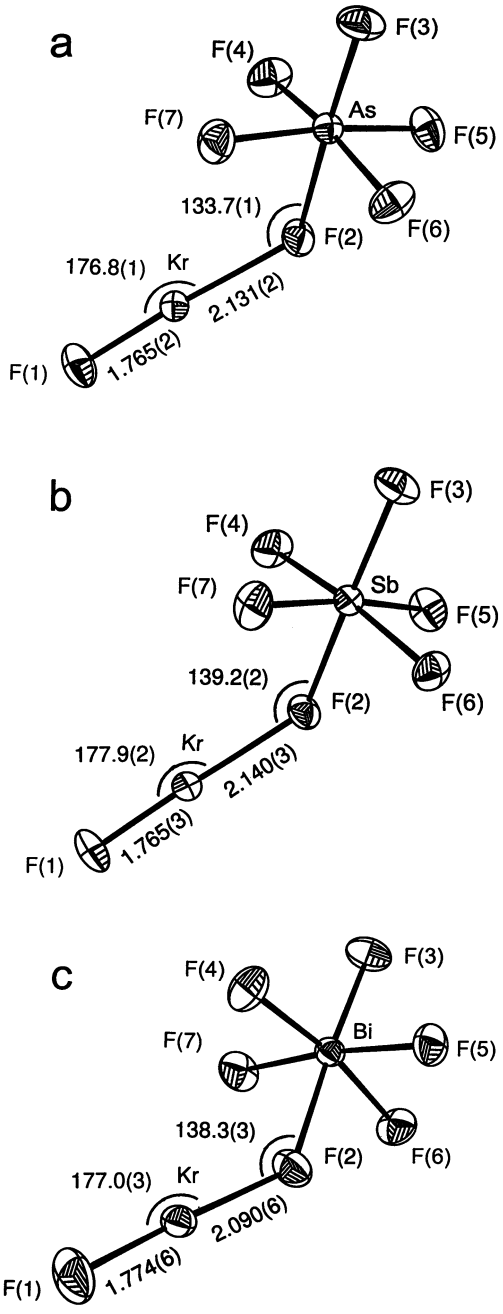

Fig. 8. Structures of (a) $[KrF][AsF_6]$, (b) $[KrF][SbF_6]$, (c) $[KrF][BiF_6]$; thermal ellipsoids are shown at the 50% probability level. Reproduced with permission from Ref. [54].

$$\underset{\mathbf{III}}{F-Kr-F^{+}}Kr-F \leftrightarrow F-\underset{\mathbf{IV}}{Kr^{+}F^{-}}\ {}^{+}Kr-F$$
$$\leftrightarrow F-Kr^{+}\underset{\mathbf{V}}{F}-Kr-F$$

contribution from the fully ionic resonance structure **IV**. Although the $Kr\cdots F_b$ bond (2.027(5)–2.065(4) Å) of $Kr_2F_3^+$ is significantly longer than that of KrF_2, it also has substantial covalent character and is ca. 1.4 Å shorter than the sum of the krypton [161] and fluorine [161,162] van der Waals radii.

The Mayer bond orders, Mayer valencies and atomic charges for KrF_2, KrF^+, $Kr_2F_3^+$, and the $[KrF^+][MF_6^-]$ ion pairs have been estimated using the electronic structures derived from LDFT calculations [54]. The calculated values for KrF_2, KrF^+, and $Kr_2F_3^+$ are in semiquantitative agreement with the simple valence bond descriptions of NgF^+, NgF_2 (structures **I** and **II**) and $Ng_2F_3^+$ (structures **III**–**V**). The atomic charges of KrF_2 were calculated to be 0.72 on krypton and −0.36 on each of the fluorine centers. For KrF^+, the full positive charge resides on krypton with zero charge on the fluorine atom. The Mayer bond order for uncoordinated KrF^+ is 1.09 and the valence at Kr is 1.09 compared with the Kr–F bond order of KrF_2, which is reduced to 0.67 with a Kr valence of 1.35 in KrF_2. There is a considerable residual bond order of 0.22 between the terminal fluorine atoms which may be interpreted in terms of the 3c–4e bond that may be used to describe the bonding in KrF_2 (Fig. 6). This bonding model leads to build up of electron density on the terminal fluorine atoms that are linked through the 3c–4e bond. The bond orders are similar for both $Ng_2F_3^+$ cations [54,139], however, the charges and valencies ($Xe_2F_3^+$ values taken from ref. [139] are given in square brackets), show some noteworthy variations. The $Kr\cdots F_b$ bridge bond order of $Kr_2F_3^+$ is 0.38 [0.40] while the $Kr–F_t$ bond order of 0.86 [0.92] is intermediate with respect to that of free KrF^+ and KrF_2. The valence at the krypton atoms in $Kr_2F_3^+$ is 1.28 [1.37], and is slightly reduced with respect to that of KrF_2. The valencies for F_t, 1.04 [1.03], and F_b, 1.03 [0.94], are also similar, but the fluorine charges; F_t, –0.37 [−0.24] and F_b, −0.16 [−0.46]; and Ng atom charges, 0.85 [0.96], indicate that, relative to $Xe_2F_3^+$, a significant amount of charge has shifted from the bridge fluorine onto the $Kr–F_t$ groups. The calculated bond orders, charges and valencies suggest that the bonds in $Xe_2F_3^+$ are more covalent that those in $Kr_2F_3^+$. The charge on F_t (−0.37) of $Kr_2F_3^+$ is very similar to those on the fluorines of KrF_2 and that of F_b (−0.16) is intermediate with respect to that of KrF^+ (0.00) and KrF_2 (−0.36). The charge distributions indicate that the bridge fluorine of $Kr_2F_3^+$ is, next to the fluorine of KrF^+, the most electrophilic fluorine in the series under discussion. There is, again, a significant bond order for $F_t\cdots F_b$ (0.14) in the $Kr_2F_3^+$ cation, which is reduced with respect to that of KrF_2 (0.22), but significantly greater than that in $Xe_2F_3^+$ (0.08) [163]. The 5c–6e bond can be used to qualitatively describe the bonding in $Kr_2F_3^+$ and accounts for the interaction between F_b and F_t atoms. Furthermore, the smaller number of electrons involved in the 5c–6e bond when compared with the 3c–4e bond in KrF_2 is consistent with a decrease in the Mayer bond order between F_b and F_t in $Kr_2F_3^+$. This is consistent with the 5c–6e model superimposed on an ionic model of $Kr_2F_3^+$

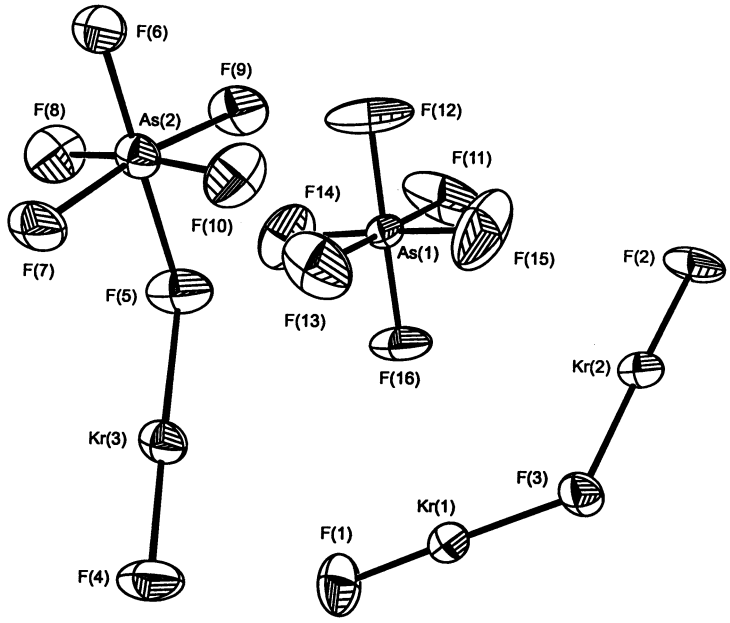

Fig. 9. Structure of $[Kr_2F_3][AsF_6]\cdot[KrF][AsF_6]$; thermal ellipsoids are shown at the 50% probability level. Reproduced with permission from Ref. [54].

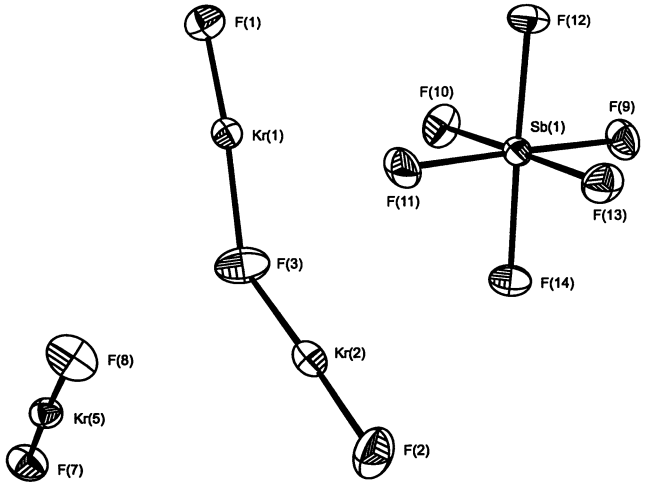

Fig. 10. Structure of $[Kr_2F_3][SbF_6]\cdot KrF_2$; thermal ellipsoids are shown at the 50% probability level. Reproduced with permission from Ref. [54].

in which F^- interacts with two KrF^+ cations. A similar set of results is found for XeF_2 and $Xe_2F_3^+$ [163].

The $Kr–F_t$ bond orders for the optimized $[KrF^+][MF_6^-]$ ion pairs show little dependence on the MF_6^- anion despite the strong fluorine bridge between the two ions, and are in agreement with the constancy of the $Kr–F_t$ bond lengths observed among the crystal structures of $KrF^+MF_6^-$ (M = As, Sb, Bi) and their calculated values [54] (Table 10). Little variation and no clear pattern are apparent among the atomic charges of the $F_t–Kr\cdots F_b$ groups of the $[KrF^+][MF_6^-]$ ion pairs. The negative charges on the axial and equatorial fluorine atoms of the MF_5 groups increase on descending group 15, a trend that is consistent with a corresponding increase in fluoride ion acceptor strength. Thus, the $[KrF^+][MF_6^-]$ ion pairs containing the heavier pnicogens are shown to be more ionic from their $M\cdots F_b$ bond orders [0.23 (P), 0.37 (As), 0.42 (Sb), 0.18 (Bi)], their valencies at M [5.36 (P), 5.60 (As), 5.14 (Sb), 3.15 (Bi)] and their $Kr\cdots F_b$ bond orders [0.54 (P), 0.50 (As), 0.47 (Sb), 0.48 (Bi)]. The valencies at Kr remain nearly constant at 1.31–1.32 over the series. The $Kr–F_t$ bond orders [0.74 (P), 0.76 (As), 0.79 (Sb), 0.79 (Bi)] and $F_t\cdots F_b$ bond orders [0.19 (P), 0.18 (As), 0.17 (Sb), 0.18 (Bi)] are intermediate with respect to those of $Kr_2F_3^+$ (0.86 and 0.14, respectively) and KrF_2 (0.67 and 0.22, respectively). The most significant increase in $M\cdots F_b$ bond order and in pnicogen valence occurs on going from P to As with a smaller decrease in the $Kr\cdots F_b$ bond order. Similar changes are noted for the transition from As to Sb, but no significant changes in the aforementioned parameters occur in going from Sb to Bi except that the $Bi\cdots F_b$ bond order is smaller by 0.24. The anomaly seen for bismuth likely arises from the core potential used in the calculations [54]. These results show that the degree of F^- complexation increases as the size of the central atom increases and the coordination sphere around the pnicogen atom becomes less crowded, allowing MF_5 to more effectively compete with the KrF^+ cation for the bridge fluorine. This is consistent with the gas phase fluoride ion affinities of PF_5, AsF_5, and SbF_5 [157] and failure to prepare $KrF^+PF_6^-$ [54] (see Section 4.1.3). A comparison of the $P\cdots F_b$ bond order in the $[KrF^+][PF_6^-]$ ion pair with the $Kr\cdots F_b$ bond order in $Kr_2F_3^+$ indicates that KrF^+

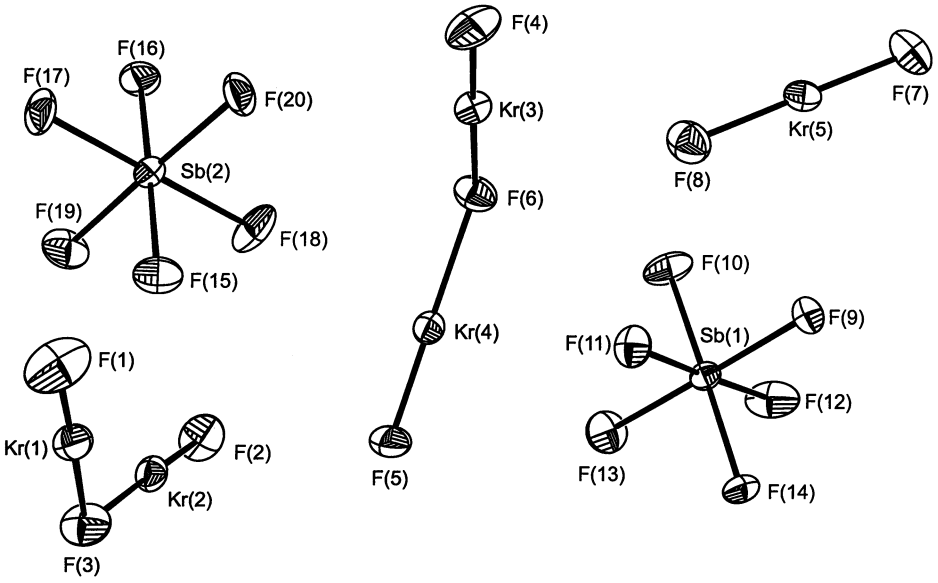

Fig. 11. Structure of $[Kr_2F_3]_2[SbF_6]_2 \cdot KrF_2$; thermal ellipsoids are shown at the 50% probablility level. Reproduced with permission from Ref. [54].

has a greater F^- affinity than PF_5 and accounts for the inability to synthesize $KrF^+PF_6^-$.

4.2. Molecular adducts of KrF_2 with MOF_4 ($M = Cr, Mo, W$)

Adducts with the weak fluoride ion acceptors $CrOF_4$ [68], $MoOF_4$ [99], and WOF_4 [99] are known in which KrF_2 interacts with the metal center by formation of asymmetric Kr–F···M bridges (M = Cr, Mo, W). In the case of molybdenum and tungsten [99], the KrF_2-metal oxide fluoride adducts have been prepared by reaction of KrF_2 with MOF_4 (M = Mo, W) in SO_2ClF solution at −100 to −80 °C (Eq. (13)). Solutions of KrF_2 and WOF_4 in SO_2ClF are highly unstable above −100 °C, and Kr and O_2 gases are rapidly evolved according to Eq. (14). These decompositions are

$$KrF_2 + nMOF_4 \rightarrow F\text{–}Kr\text{–}F\cdots MOF_4(MOF_4)_{n-1} \quad (13)$$

M = Mo ($n = 1-3$); W ($n = 1$)

$$KrF_2 + WOF_4 \rightarrow Kr + 1/2O_2 + WF_6 \quad (14)$$

particularly vigorous when a stoichiometric excess of WOF_4 is used, and go to completion within a few seconds at −80 °C. In marked contrast, SO_2ClF solutions of the $F\text{–}Kr\text{–}F\cdots MoOF_4(MoOF_4)_{n-1}$ adducts could be briefly warmed to room temperature in SO_2ClF. The ^{19}F-NMR spectra of $KrF_2 \cdot nMoOF_4$ (n = 1–3) and $KrF_2 \cdot WOF_4$ at −121 °C in SO_2ClF show that they are best formulated as essentially covalent structures containing Kr–F···M bridges and mononuclear or polynuclear molybdenum oxide fluoride moieties in which the Kr–F bonds are little perturbed with respect to the free KrF_2 molecule (Table 7). The KrF_2 molecules in $KrF_2 \cdot 2MoOF_4$ and $KrF_2 \cdot 3MoOF_4$ coordinate cis to the oxygen and bridging fluorine of a terminal MOF_4 group. Unlike the xenon(II) system [164,165], polynuclear metal oxide fluoride ligands are not observed for WOF_4 in the krypton(II) system [99]. Whereas isomerization leads to stable Xe–O–W linkages when $n \geq 2$ [164,165], the analogous isomerization from the Kr–F···W bridged species to the Kr–O–W species for $n \geq 2$ does not yield stable $KrF_2 \cdot nWOF_4$ ($n \geq 1$) adducts, but likely initiates the rapid decomposition at low temperatures [99]. The decomposition behavior is consistent with the formation of kinetically unstable Kr–O bonded intermediates (see Section 6). Raman spectra of the solid $KrF_2 \cdot MOF_4$ (M = Mo, W) adducts isolated from SO_2ClF at −48 °C are similar to those of the xenon(II) analogues [99] and are also interpreted in terms of F-bridged structures in which KrF_2 is weakly coordinated to the metal center. These structures are analogous to that determined by single crystal X-ray diffraction for $F\text{–}Xe\text{–}F\cdots WOF_4$, in which the bridging fluorine coordinates trans to oxygen [166]. Isolation of solid $F\text{–}Kr\text{–}F\cdots WOF_4$ could only be accomplished by reaction of a 25% molar excess of KrF_2 with WOF_4 at −80 °C followed by warming to −48 °C and removal under vacuum of SO_2ClF solvent as well as O_2, WF_6, and Kr, resulting from the competing decomposition reaction (Eq. (13)) [99]. An excess amount of KrF_2 apparently suppresses the formation of highly unstable Kr–O–W species that are present in equilibrium with Kr–F···W bridged species when $n \geq 2$ for $KrF_2 \cdot nWOF_4$.

The reaction of CrO_2F_2 with KrF_2 in anhydrous HF solution at room temperature provides a high-purity synthesis of $CrOF_4$ (see Section 8.3). Chromium oxide

tetrafluoride forms a 1:1 adduct with KrF_2 in HF solution at −78 °C which decomposes upon warming to Kr, F_2 and $CrOF_4$. The adduct, formulated as $KrF_2 \cdot CrOF_4$, is predominantly covalent containing a Kr–F···Cr bridge [68] that is analogous to those of F–Kr–F···$MoOF_4$ and F–Kr–F···WOF_4. The stretching frequencies associated with the KrF_2 part of the $KrF_2 \cdot MOF_4$ (M = Cr, Mo, W) adducts serve as a qualitative measure of the relative ionic characters of the adducts [68,99]. The frequency separations between $\nu_{as}(KrF_2)$ or $\nu(KrF_t)$ and $\nu_s(KrF_2)$ or $\nu(Kr\cdots F_b)$ can be used to assess relative degrees of covalency and decrease with increasing covalency. The frequency separations for $KrF_2 \cdot MOF_4$ increase in the order Cr < Mo < W, indicating that the covalency of $KrF_2 \cdot MOF_4$ increases in the order W < Mo < Cr. Unlike the molybdenum and tungsten analogues, the chromium adduct has been shown to be completely dissociated in SO_2ClF solution between −118 and −10 °C [68]. The finding is consistent with the increased covalency of the chromium analogue relative to its molybdenum and tungsten analogues, which show unequivocal ^{19}F-NMR evidence for fluorine bridged adducts in SO_2ClF solution at low temperatures [99] (vide supra).

5. Krypton–nitrogen bonded compounds

5.1. Syntheses of $RCNKrF^+AsF_6^-$ ($R = H$, CF_3, C_2F_5, n-C_3F_7)

The Lewis acid properties of KrF^+ that lead to fluorine bridging in KrF^+ salts (see Section 4.1.1) are further manifested by the formation of donor–acceptor bonds between KrF^+ and the nitrogen electron lone pairs of oxidatively resistant nitriles [97,98]. Numerous examples of the XeF^+ cation coordinated to organic nitrogen base centers have also been synthesized and structurally characterized [7] in which the XeF^+ cation coordinates to HCN [167–169], a variety of alkyl- [167] and perfluoroalkylnitriles [98], perfluoropyridines [164], perfluorodiazenes [170] and *s*-trifluorotriazene [98]. Despite the strong oxidizing properties of the KrF^+ cation, a limited number of nitriles having first adiabatic ionization potentials that are comparable with or exceed the estimated electron affinity of the KrF^+ cation (13.2 eV), are resistant to oxidation by the KrF^+ cation at low temperatures. These KrF^+ adduct-cations are currently limited to $HCNKrF^+$ [97], CF_3CNKrF^+, $C_2F_5CNKrF^+$, and n-$C_3F_7CNKrF^+$ [98]. All are thermally and kinetically unstable above ca. −40 °C and are currently the only examples of krypton bonded to nitrogen. The synthetic strategies that lead to HCN and perfluoroalkylnitrile adduct-cations are largely determined by the strong oxidant properties of the KrF^+ cation. Unlike XeF^+, the reaction of HCN with the more potent oxidizer, KrF^+, in HF has not been attempted. Rather, reaction of $HCNH^+AsF_6^-$ with KrF_2 in HF has been employed (Eq. (15)) [97], resulting in the deposition of solid white $HCNKrF^+AsF_6^-$ at −60 °C.

$$KrF_2 + HCNH^+AsF_6^- \rightarrow HCNKrF^+AsF_6^- + HF \quad (15)$$

Warming the compound above −50 °C results in rapid evolution of Kr, NF_3 and CF_4 gases which may be accompanied by violent detonation. The detonation problem is overcome by carrying the reaction out in BrF_5 solvent at −58 °C where both reactants and products are soluble, thus avoiding the establishment of radical chain reactions in the solid that lead to explosion. The $HCNKrF^+$ cation is stable in BrF_5 to at least −55 °C for several hours with only minor decomposition. The syntheses of the R_FCNKrF^+ cations ($R_F = CF_3$, C_2F_5, n-C_3F_7) have also been undertaken at low temperatures in BrF_5 solvent using the general synthetic approach given in Eq. (16) [98]. All three fluoro(perfluoroalkylnitrile)krypton(II) cations

$$KrF_2 + R_FCNAsF_5 \rightarrow R_FCNKrF^+AsF_6^- \quad (16)$$

are thermally less stable with respect to redox decomposition than $HCNKrF^+$ or their xenon(II) analogs, preventing their isolation and characterization in the solid state. Decompositions have been monitored by ^{19}F-NMR spectroscopy and occur over ca. 1–2 h at −57 to −61 °C. The major decomposition products consist of Kr, CF_4, C_2F_6, and NF_4^+ for all three R_FCNKrF^+ cations, as well as n-C_3F_8 for $C_2F_5CNKrF^+$ and n-C_3F_8 and n-C_4F_{10} for n-$C_3F_7CNKrF^+$.

5.2. Multi-NMR studies of the solution structures of the $RCNKrF^+$ cations

The solution structure of the $HCNKrF^+$ cation has been unambiguously established by low-temperature ^{1}H-, ^{19}F- and ^{15}N-NMR studies of 99.5% ^{15}N enriched $HCNKrF^+AsF_6^-$ in BrF_5 solvent [97] (Table 7). The ^{19}F and ^{1}H resonances exhibit doublet splittings attributed to ^{15}N coupling (Fig. 12a,b). The two-bond spin-spin coupling, $^2J(^{19}F-^{15}N) = 26$ Hz, compares favorably in magnitude with values for $FXeN(SO_2F)_2$ ($^2J(^{19}F-^{15}N) = 39.2$ Hz) and CH_3CNXeF^+ ($^2J(^{19}F-^{15}N) = 25$ Hz; calculated from $^2J(^{19}F-^{14}N) = 18$ Hz). Krypton isotopic shifts arising from ^{82}Kr (11.56%), ^{84}Kr (56.90%) and ^{86}Kr (17.37%) have been resolved on the ^{19}F resonance (0.0138 ppm amu^{-1}) (Fig. 12a) and serve as an added confirmation that the fluorine resonance arises from fluorine directly bonded to krypton. The doublet fine structure (12.2 Hz) on the ^{1}H resonance of the ^{15}N enriched cation (Fig. 12b) is assigned to $^2J(^{15}N-^1H)$ (cf. $^2J(^{15}N-^1H) = 19.0$ Hz for $HCNH^+$ in HF solvent). The ^{15}N-NMR spectrum

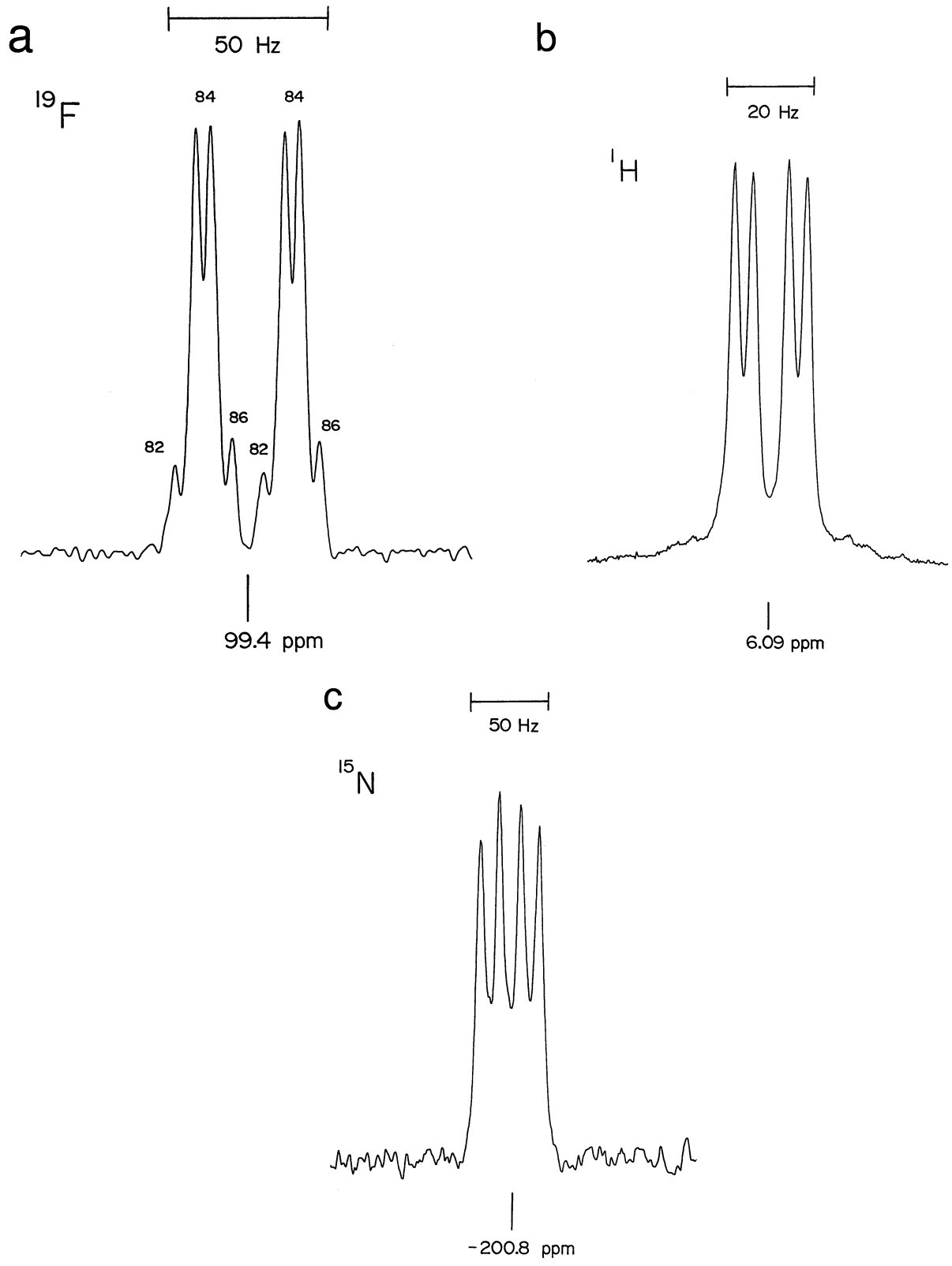

Fig. 12. NMR spectra of the $HCNKrF^+$ cation enriched to 99.5% ^{15}N, recorded in BrF_5 solvent at −57 °C. (a) ^{19}F-NMR spectrum (235.36 MHz) depicting $^2J(^{19}F-^{15}N)$ and $^4J(^{19}F-^1H)$ and krypton isotope shifts. Lines assigned to fluorine bonded to ^{82}Kr (11.56%), ^{84}Kr (56.90%), and ^{86}Kr (17.37%) are denoted by the krypton mass number. The innermost lines of the ^{87}Kr and ^{86}Kr doublets overlap their corresponding ^{84}Kr doublets. The isotopic shift arising from ^{83}Kr (11.53%) is not observed because of quadrupole collapse of the $^1J(^{83}Kr-^{19}F)$ coupling; those of ^{78}Kr (0.35%) and ^{80}Kr (2.27%) are too weak to be observed. (b) ^1H-NMR spectrum (80.02 MHz) depicting $^2J(^{15}N-^1H)$ and $^4J(^{19}F-^1H)$. (c) ^{15}N-NMR spectrum (50.70 MHz) depicting $^2J(^{19}F-^{15}N)$ and $^2J(^{15}N-^1H)$. Reproduced with permission from Ref. [97].

Table 11
Calculated and experimental vibrational frequencies (cm^{-1}) and IR intensities (km mol^{-1}) for $HCNKrF^+$

Vibrational assignment	Symmetry	$\nu_{(calc)}$ HF [a]	$\nu_{(scaled)}$ HF [a]	$\nu_{(calc)}$ HF [b]	$\nu_{(calc)}$ MP2d [b]	$\nu_{(calc)}$ MP2 [c]	$\nu_{(calc)}$ MP2/DZV+ [d]	$\nu_{(expt)}$ [e]	$I_{(calc)}$ [a]
ν(C–H)	Σ	3556	3253	3588	3467	3446	3424		133
ν(CN)	Σ	2446	2128	2461	2130	2100	2121	2158	221
δ(H–CN)	Π	935	760	940	762	752	751		43
ν(Kr–F)	Σ	782	620	782	644	562	589	560	66
δ(CN–Kr–F)	Π	253	228	256	271	244	282		63
ν(Kr–N)	Σ	217	195	222	287	267	256		72
δ(CN–Kr–F)	Π	115	104	120	116	117	111		28

[a] Ref. [175].
[b] Ref. [172].
[c] Ref. [171].
[d] Ref. [173].
[e] Ref. [97].

comprises a doublet of doublets (Fig. 12c) arising from $^2J(^{19}F-^{15}N)$ and $^2J(^{15}N-^1H)$, which simplifies to a doublet (26 Hz) upon broad-band ^1H decoupling, confirming the aforementioned coupling.

The R_FCNKrF^+ cations have been characterized in BrF_5 by low-temperature (−57 to −61 °C) ^{19}F-NMR spectroscopy [98] (Table 7). The spectra consist of two sets of signals: a singlet in the F–on-Kr(II) regions, and resonances in the F-on-C region with characteristic $^3J(^{19}F-^{19}F)$ and $^1J(^{19}F-^{13}C)$ couplings having chemical shifts to high frequency of the parent base molecules. The F-on-Kr(II) resonance of CF_3CNKrF^+ displays the ^{82}Kr, ^{84}Kr and ^{86}Kr isotopic shifts (0.0105 ppm amu^{-1}), which compare favorably with values for $HCNKrF^+$ (0.0138 ppm amu^{-1}) and KrF_2 (0.0104 ppm amu^{-1}) [80]. The ^{19}F-on-Kr(II) resonances of the R_FCNKrF^+ and $HCN–KrF^+$ cations occur to higher frequencies of KrF_2 and KrF^+ while the ^{19}F-on-Xe(II) resonances of the xenon analogues [98] occur to lower frequency of XeF_2 and to higher frequency of XeF^+.

5.3. Theoretical studies of the $HCNKrF^+$ cation

The discovery of the first example of a Kr–N bond has generated considerable interest in the nature of bonding in $HCNKrF^+$, resulting in several theoretical studies on the $HCNKrF^+$ and its neon, argon, and xenon analogues [171–175]. The results of each theoretical study are consistent with an ionic and a covalent component in the bonding of KrF^+ with HCN, i.e. the fragments are σ-bonded with a high degree of ionic character. The Kr–N bond is the result of a donor–acceptor interaction between the sp-lone pair on N and the empty σ* orbital on KrF^+.

Theoretical investigations of $HCNKrF^+$ and $HCNXeF^+$ at the SCF level using the theory of atoms in molecules (AIM) [174], which circumvents the use of orbitals to describe chemical bonding, indicates that the ability of KrF^+ and XeF^+ cations to act as Lewis acids is related to the presence of holes in the valence shell charge concentrations of the noble-gas atoms which expose their cores. The mechanism of formation of the Ng–N bonds in the adducts of KrF^+ and XeF^+ with HCN is similar to the formation of a hydrogen bond, i.e. the mutual penetration of the outer diffuse non-bonded densities of the Ng and N atoms is facilitated by their dipolar and quadrupolar polarizations, which remove density along their axis of approach, to yield a final density in the interatomic surface that is only slightly greater than the sum of the unperturbed densities. Thus, the KrF^+ and XeF^+ cations are best described as hard acids. The energies of formation of these adducts are dominated by the large stabilizations of the Ng atoms that result from the increase in the concentration of charge in their inner quantum shells. The Ng–N bonds that result from the interaction of the closed-shell reactants KrF^+/XeF^+ and HCN lie closer to the closed shell limit than do bonds formed in the reaction of KrF^+/XeF^+ with F^-. The calculated gas-phase energies of the reaction between the closed-shell species are −136.0 and −144.3 kJ mol^{-1} for Ng = Kr and Xe, respectively, for Eq. (17) in the gas phase and −874.5 and −886.6 kJ mol^{-1} respectively, for Eq. (18).

$$NgF^+ + HCN \rightarrow HCNNgF^+ \quad (17)$$

$$NgF^+ + F^- \rightarrow NgF_2 \quad (18)$$

The molecular structure and force field of $HCNKrF^+$ have also been calculated at higher levels of theory (Table 11) [171–173,175] and the cation is predicted to be linear. The incorporation of electron correlation is necessary to describe satisfactorily the structures, stabilities and vibrational frequencies. Reasonable agreement with the two observed vibrational Raman bands in the solid has been found at the HF and MP2 levels of theory [171–173,175]. The Kr-N stretching mode leading to dissociation into KrF^+ and HCN was calculated to occur at 217 [175], 267 [171] and 287 [175] cm^{-1}. Despite the greater mass of the XeF group, the calculated Kr–N stretching frequency is notably lower than the experimental Xe–N stretching frequency of

Table 12
Bond distances (Å) and atomic charges (e) for the optimized geometries of KrF^+, HCN and $HCNKrF^+$

Species	r(C–H)	r(CN)	r(Kr–F)	r(KrN)		Level of theory	Ref.
KrF^+	1.697					MP2	[175]
			1.725			MP2	[172]
			1.752				[176]
			1.778			$MP2/DZV^+$	[173]
			1.727			HF/DZV*	[173]
HCN	1.057	1.126				MP2	[175]
	1.064	1.156					[177]
$HCNKrF^+$	1.065	1.122	1.709	2.320		MP2	[175]
	1.068	1.128	1.748	2.307		SCF	[174]
	1.067	1.168	1.707	2.313		HF	[172]
	1.073	1.129	1.772	2.183		MP2	[172]
	1.076	1.175	1.831	2.281		MP2	[171]
	1.082	1.169	1.823	2.231		$MP2/DZV^+$	[173]
	1.066	1.129	1.733	2.335		HF/DZV*	[173]
	H	C	N	Kr	F		
KrF^+				+1.15	−0.15	MP2	[175]
				+1.10	−0.10	HF/DZV*	[173]
				+1.00	0.00	LDFT	[54]
HCN	+0.24	−0.04	−0.20			MP2	[175]
	+0.31	+0.07	−0.38			HF/DZV*	[173]
$HCNKrF^+$	+0.31	+0.21	−0.23	+1.00	−0.29	MP2	[175]
	+0.38	+0.33	−0.53	+1.06	−0.24	MP2	[172]
	+0.42	+0.27	−0.53	+1.09	−0.25	HF/DZV*	[173]

$HCNXeF^+$ (328, 335 cm^{-1}) [168], suggesting that the Kr–N bond is significantly weaker than the Xe–N bond of the xenon analogue. A normal coordinate analysis would be required to confirm this supposition. The KrF and HCN fragments in the complex have geometries similar to those of KrF^+ and HCN (Table 12) and, in accord with its low Kr–N stretching frequency, the Kr–N bond distance is predicted to be 2.18–2.32 Å, which is considerably longer than the highly polar single-bonds between fluorine and third-row atoms, e.g. 1.894 Å in KrF_2 [54], 1.756 Å in BrF [177], 1.712 Å in AsF_3 [177], and 1.689 Å in GeF_4 [178], and is comparable with that of the Xe-N bond (2.235(3) Å) in $HCNXeF^+$ [179]. The Kr–F distance in the adduct is predicted to increase by only 0.0–0.13 Å relative to that of KrF^+. The $HCNKrF^+$ cation is predicted to be more stable by 130.1–176.1 kJ mol^{-1} [172,173,175] with respect to KrF^+ and HCN at higher levels of theory (cf. 126.4 [175] and 136.1 [174] kJ mol^{-1} at the SCF level) with zero-point energy corrections.

The charge distributions reported for $HCNKrF^+$ in all theoretical studies (Table 12) show some transfer of electronic charge from the carbon to the KrF^+ region, consistent with a contribution from the resonance structure **VI**.

$$H-{}^{+}C=\underset{\mathbf{VI}}{N}-Kr-F$$

The shift of ligand charge towards krypton is also evident from a determination of the centroids of charge for the localized molecular orbitals [175]. The lone pair centroid on nitrogen is 1.22 au from the nitrogen atom as compared with the lone pair in HCN, which is only 0.70 au from the nitrogen atom. Whereas the nitrogen lone pair is essentially localized on the N atom of HCN, the lone pair is delocalized by 0.24 e onto the Kr atom in $HCNKrF^+$. This is reflected in the hybridization of the lone pair on N in HCN ($sp^{0.79}$) [175]. The nitrogen p character in $HCNKrF^+$ increases to give a hybridization of $sp^{0.88}$ and is also consistent with charge delocalization onto the Kr atom.

The molecular orbitals for KrF^+, HCN, and $HCNKrF^+$ have been derived by Dixon and Arduengo [175]. The bonding in $HCNKrF^+$ has been analyzed in terms of three-center and four-center hypervalent bonds. The analysis indicates that the bonding between Kr and N is not a simple covalent σ-bond between two centers. Both three center (F–Kr–N based) and four center (F–Kr–N–C based) hypervalent bonds best describe the covalent σ-bonding in $HCNKrF^+$.

High-level ab initio calculations [173] predict that the argon-nitrogen bonded $HCNArF^+$ cation is also stable with a gas-phase heat of association (Eq. (17)) of −160 kJ mol^{-1}, which, as noted above, is comparable with that calculated for the krypton analogue. These results, together with another recent high-level theoretical calculation, which estimates the electron affinity for ArF^+ to be 13.66 eV [180], suggest that HCN, with its high first ionization potential (13.80 eV) [181], may be

oxidatively resistant enough to withstand the formidable electron affinity of the ArF^+ cation. At the correlated level, the $HCNNeF^+$ cation is predicted to be unstable towards dissociation to $HCNNe^+$ and F, where the $HCNNe^+$ fragment is itself a weakly bound species having a binding energy of only 6 kJ mol^{-1} with respect to loss of neon and the formation of HCN^+ [173].

6. Krypton–oxygen bonded compounds

The compound, $Kr(OTeF_5)_2$, provides the only verified example of a species in which krypton is bonded to oxygen. The formation and decomposition of $Kr(OTeF_5)_2$ has been carefully monitored and characterized by low temperature ^{19}F and ^{17}O-NMR spectroscopy [69] (Table 7). The compound has been prepared by the reaction of KrF_2 with natural abundance and ^{17}O enriched $B(OTeF_5)_3$ at −90 to −112 °C in SO_2ClF solvent (Eq. (19)) and is analogous to

$$3KrF_2 + 2B(OTeF_5)_3 \rightarrow 3Kr(OTeF_5)_2 + 2BF_3 \quad (19)$$

the method used to prepare $Xe(OTeF_5)_2$ [182], but reaction occurs at much lower temperatures. The thermolysis of $Kr(OTeF_5)_2$ is analogous to that of $Xe(OTeF_5)_2$ at 160 °C, but proceeds rapidly at −78 °C according to Eq. (20). An earlier published attempt to form Kr–O bonds reports the reaction of KrF_2

$$Kr(OTeF_5)_2 \rightarrow Kr + F_5TeOOTeF_5 \quad (20)$$

with $B(OTeF_5)_3$ in ClO_3F at −100 °C for 16 h followed by a further 3 h at −78 °C yielded only $F_5TeOOTeF_5$ and Kr gas [183]. The reactions of KrF_2 with $HOTeF_5$ and $HOSeF_5$ have been studied in $ClOF_3$ solvent at low temperatures forming the crystalline adducts, $KrF_2 \cdot HOTeF_5$ (m.p. −30 °C) and $KrF_2 \cdot HOSeF_5$ (m.p. −64 °C). The adducts have not been structurally characterized and decompose at −10 and −40 °C, respectively, to Kr, HF, $F_5TeOOTeF_5$ and $F_5SeOOSeF_5$.

The interaction of KrF_2 and $(IO_2F_3)_2$ in SO_2ClF solvent has also been reported to lead to peroxide formation at −45 °C by the route proposed in Eqs. (21) and (22), where $Kr(OF_4I{=}O)_2$ is proposed as an unstable

$$(IO_2F_3)_2 + KrF_2 \rightarrow Kr(OF_4I{=}O)_2 \quad (21)$$

$$Kr(OF_4I{=}O)_2 \rightarrow Kr + O{=}IF_4O{-}OF_4I{=}O \quad (22)$$

intermediate [69]. The series of adducts $XeF_2 \cdot nWOF_4$ ($n \geq 2$) undergo bond isomerization to give equilibrium mixtures of $F{-}Xe{-}F\cdots WOF_4(WOF_4)_{n-1}$ and $F{-}Xe{-}O{-}WF_5(WOF_4)_{n-1}$ in SO_2ClF solvent [164,165] while the $MoOF_4$ adducts and their KrF_2 analogues only exist as the $F{-}Kr{-}F\cdots MoOF_4(MoOF_4)_{n-1}$ structures [99]. While it was thought that the reaction between KrF_2 and WOF_4 might lead to Kr–O bonded species, these systems, unlike their fluorine bridged molybdenum analogues, are remarkably unstable when $n > 1$, decomposing upon warming above −100 °C in SO_2ClF to Kr, O_2, WF_6 and WOF_4. It was proposed that $F{-}Kr{-}F\cdots W \rightarrow F{-}Kr{-}O{-}W$ bond isomerization occurs above −100 °C and that the resulting thermodynamically unstable Kr–O bonded species are also kinetically unstable.

7. Compounds in which krypton is bonded to elements other than nitrogen, oxygen or fluorine

The existence of the CH_3Kr^+ cation has been established in the gas phase by ion cyclotron resonance trapped ion techniques [184]. The method has been used to investigate ion–molecule reactions in CH_3F/Kr mixtures. Protonated CH_3F, formed by the reaction of CH_3F^+ with CH_3F, reacts with krypton by transferring CH_3^+ to yield CH_3Kr^+. The Kr–C bond energy of the CH_3Kr^+ cation has been estimated to be 199.6 ± 10.5 kJ mol^{-1}, and is somewhat weaker than that estimated for the gas phase CH_3Xe^+ cation (231.0 ± 10.5 kJ mol^{-1}), but considerably stronger than the Kr–F bond of KrF_2 (48.9 kJ mol^{-1}).

The krypton-containing hydrides, HKrL (L = Cl or CN) have been prepared in low-temperature matrices by photodissociation of HL or DL followed by thermal mobilization of the photodetached hydrogen atoms at ca. 30–40 K [185]. The neutral HKrL and DKrL molecules are apparently formed in concerted reactions of the type

$$H + Kr + L \rightarrow HKrL \quad (23)$$

Experimental evidence for the formation of these species is essentially based on strong infrared bands that appear after annealing of the photolyzed matrices and are assigned to the H–Kr and D–Kr stretches of HKrCl, DKrCl (1476, 1106 cm^{-1}) and HKrCN, DKrCN (1497, 1109 cm^{-1}) with H–Kr–Cl and H–Kr–C bends at 544 and 618 cm^{-1}, respectively. The calculated (MP2 level of theory) H–Kr bond lengths are 1.466 (HKrCN) and 1.435 (HKrCl) Å and the Kr–L bond lengths are 2.349 (HKrCN) and 2.666 (HKrCl) Å. A similar experimental approach has recently been used to generate and characterize HArF and DArF in matrices.

The $KrCl^+$ (and KrF^+) cation has been produced in a steady-state low-pressure hollow cathode discharge and detected by quadrupole mass spectrometry [186]. The $KrCl^-$ and $KrBr^-$ have been studied by zero electron kinetic energy spectroscopy [187].

8. Applications of KrF_2 and KrF^+ to the syntheses of high-valent inorganic species

8.1. Oxidant properties of KrF_2 and KrF^+

The mean thermochemical bond energy for KrF_2 derived from calorimetric data is 48.9 kJ mol^{-1} [39,40], which is the lowest bond energy of any known fluoride. The energy of atomization for KrF_2 (97.9 kJ mol^{-1}) [39,40] is lower than that of F_2 (157.7 ± 0.4 kJ mol^{-1}) [188], causing it to be a better low-temperature source of fluorine atoms than elemental fluorine and an aggressive fluorinating agent even at low temperatures. In contrast, the dissociation of F_2 requires high temperature or photolytic conditions or other high-energy processes as illustrated by the syntheses of the thermodynamically stable xenon fluorides (XeF_2 [41,189,190], XeF_4 [42], and XeF_6 [43]) from xenon and elemental fluorine. Thus, KrF_2 has found wide application for the low-temperature syntheses of high-oxidation state species, which are otherwise unattainable by more conventional thermal and photosynthetic methods.

It has long been recognized that the oxidizing/fluorinating strengths of noble gas fluorides increase in the order $XeF_2 < XeF_4 < XeF_6 < KrF_2$, and the relative oxidative fluorination strengths of the xenon fluorides has recently been discussed by Liebman [191]. That Kr(II) is more strongly oxidizing than Xe(II) may be accounted for on the basis of the ionization potentials of krypton ($Kr \rightarrow Kr^+$, 13.999 eV; $Kr^+ \rightarrow Kr^{2+}$, 24.359 eV), which are significantly higher than those of xenon ($Xe \rightarrow Xe^+$, 12.130 eV; $Xe^+ \rightarrow Xe^{2+}$, 21.21 eV) [191]. The fact that KrF_2 has proven to be a better oxidative fluorinating agent than any of the xenon fluorides or fluorine rests on the thermodynamic stabilities of xenon fluorides and the thermodynamic instability of KrF_2 with respect to its elements. This is dramatically underscored by the rapid room temperature oxidative fluorination of xenon gas to XeF_6 and I_2 to IF_7 using KrF_2 as the fluorine source (Eqs. (24) and (25)) [36].

$$Xe + 3KrF_2 \rightarrow XeF_6 + 3Kr \quad (24)$$

$$I_2 + 7KrF_2 \rightarrow 2IF_7 + 7Kr \quad (25)$$

It is well known that the cations derived from the binary xenon fluorides and oxide fluorides, XeF^+, $Xe_2F_3^+$, XeF_3^+, XeF_5^+, $Xe_2F_{11}^+$, $XeOF_3^+$, and XeO_2F^+ are stronger oxidative fluorinators than their parent fluorides [5]. Correspondingly, the $Kr_2F_3^+$ and KrF^+ cations are more potent oxidants than either KrF_2 or the fluorocations of xenon. A quantitative scale of relative oxidizer strengths for cationic oxidative fluorinators has been developed which includes the KrF^+ cation [192]. The scale is based on relative F^+ detachment energies, which were obtained by local density functional theory calculations, and is anchored to its F^+ zero-point by an experimental value for KrF^+. The scale is actually defined as the positive F^+ detachment energy as illustrated by the KrF^+ cation in Eq. (26). The oxidizing strengths of 36 oxidizers were thus determined and shown

$$KrF^+ \rightarrow Kr + F^+ \quad (26)$$

to be consistent with all of the previously available qualitative experiments. The scale confirms that KrF^+ is unique in its oxidizer strength and is the strongest chemical oxidant presently known with an oxidizer strength value of 484.9 kJ mol^{-1}. The next strongest known oxidative fluorinators on this scale are N_2F^+ (582.8 kJ mol^{-1}) and BrF_6^+ (589.1 kJ mol^{-1}; see Section 8.2). The scale confirms that the known xenon cations are considerably weaker oxidative fluorinating agents, displaying higher detachment energies (XeF_3^+, 637.6 kJ mol^{-1}, XeF_5^+, 664.8 kJ mol^{-1}, XeF^+, 689.5 kJ mol^{-1}, $XeOF_3^+$, 724.2 kJ mol^{-1}, XeO_2F^+, 817.1 kJ mol^{-1}). Interestingly, it has not proven possible to synthesize the XeF_7^+ cation by direct oxidative fluorination of XeF_6 with KrF^+ [63,193]. The predicted F^+ detachment energy of XeF_7^+ (488.3 kJ mol^{-1}) is only marginally greater than that of KrF^+. Failure to form the XeF_7^+ cation by either direct reaction with neat XeF_6 or in HF solution may be attributed to the near thermoneutrality of the F^+ transfer and/or to the fluoride ion donor properties of XeF_6 towards KrF^+. Partial or full fluoride ion transfer to KrF^+ would render it a less potent oxidant, and the development of a partial or full positive charge on xenon as XeF_5^+ would render xenon more difficult to oxidize.

Should it prove possible to synthesize salts of the ArF^+ cation, it will be an oxidizer of unprecedented strength with an F^+ detachment energy of 352.7 kJ mol^{-1}. The predicted F^+ detachment energies of the ground state ($^3\pi$) species NeF^+ and HeF^+ are predicted to have values of 2.5 and −6.7 kJ mol^{-1} and indicates that the feasibility of producing these cations in the solid or gaseous states is unlikely [192]. Failed attempts to detect these cations in the gas phase using mass spectrometry support this hypothesis [194].

There are numerous main-group and metal fluoride and oxide fluoride species that have been synthesized by the use of KrF_2, KrF^+, or $Kr_2F_3^+$ as the oxidative fluorinating agent and which qualitatively affirm their strong oxidant properties. Although many of the species that are discussed in the following sections had been previously synthesized by more classical high-temperature and photolytic procedures, the facility with which a broad range of high-oxidation state species are achieved in high purities and at low temperatures using krypton(II) fluoride reagents is significant for appreciating the likely scope of their future synthetic applications. The following subsections provide such an overview. In a number of instances, the use of KrF_2 or KrF^+ as the fluorinator has provided the initial or sole synthetic

route to species which are, in themselves, interesting new high-oxidation state precursors or are species that were previously unaccounted for. In these instances, the novel chemistries these discoveries have spawned are also briefly surveyed. These vignettes serve to convey the broader impacts KrF_2 and KrF^+ have had as oxidative fluorinators in chemical syntheses.

8.2. Main-group chemistry

The KrF^+ cation is a powerful oxidative fluorinating agent with respect to O_2 and Xe, oxidizing both gases at room temperature to O_2^+ and XeF^+ [79] according to Eqs. (27) and (28).

$$KrF^+MF_6^- + Xe \rightarrow XeF^+MF_6^- + Kr \quad (27)$$

$$KrF^+MF_6^- + O_2 \rightarrow O_2^+MF_6^- + Kr + 1/2F_2 \quad (28)$$

The reaction of $KrF^+SbF_6^-$ with excess $XeOF_4$ has been investigated with the view to forming the xenon(VIII) cation, $XeOF_5^+$, according to Eq. (29). Instead, the reaction gives $XeOF_4{\cdot}XeF_5^+SbF_6^-$ and $O_2^+SbF_6^-$ salts (Eq. (28)) [37], but not $XeOF_5^+SbF_6^-$ as previously reported [143]. The reactivity of KrF^+ towards $XeOF_4$ contrasts with that towards isoelectronic IF_5, where a nucleophilic displacement reaction on the fluorine of KrF^+ by the electron lone pair on iodine results in the formation of the IF_6^+ cation (Eq. (29)) [195]. The corresponding reaction with $XeOF_4$ does not lead to $XeOF_5^+$ (Eq. (30)), but is predicted to form the hypofluorite, XeF_4OF^+, as an intermediate (Eq. (31)). Subsequent substitution and elimination reactions of the hypofluorite and oxofluorite intermediates (Eq. (32)) are speculated to lead to O_2^+ (Eq. (28)) and XeF_5^+ (Eq. (33)).

$$IF_5 + KrF^+ \rightarrow [Kr{-}F{-}IF_5] \rightarrow Kr + IF_6^+ \quad (29)$$

$$XeOF_4 + KrF^+AsF_6^- \rightarrow XeOF_5^+AsF_6^- + Kr \quad (30)$$

$$XeOF_4 + KrF^+AsF_6^- \rightarrow [F_4XeOF^+AsF_6^-] + Kr \quad (31)$$

$$[F_4XeOF^+AsF_6^-] + XeOF_4 \rightarrow [F_4XeOOF^+AsF_6^-] + XeF_4 \rightarrow XeF_4 + O_2 + XeF_5^+ \quad (32)$$

$$XeF_4 + KrF^+ \rightarrow XeF_5^+ + Kr \quad (33)$$

The development of bromine(VII) chemistry is a classic illustration of the reluctance of fourth-row nonmetals to exhibit maximum valence [196]. Prior to the application of KrF_2 and KrF^+ as oxidative fluorinators, the chemistry of bromine(VII) was limited to $HBrO_4$, BrO_4^- salts [197] and BrO_3F [198]. Although the ClF_6^+ [199–201] and IF_6^+ [202,203] cations were known and structurally characterized, the BrF_6^+ cation remained unaccounted for. The ClF_6^+ cation had been synthesized by reaction of ClF_5 with PtF_6, yielding a mixture of $ClF_6^+PtF_6^-$ and $ClF_4^+PtF_6^-$, while IF_6^+ had been synthesized by reaction of the only known halogen heptafluoride, IF_7, with strong fluoride ion acceptors such as AsF_5 to give $IF_6^+AsF_6^-$. Gillespie and Schrobilgen [142,146] showed that the BrF_6^+ cation could be synthesized in moderate yield by oxidation of BrF_5 using the KrF^+ or $Kr_2F_3^+$ cations as oxidative fluorinators. They also showed that, unlike ClF_5, BrF_5 was inert to oxidation by PtF_6. The reactions of the krypton(II) fluoro-cations with BrF_5 proceed according to Eqs. (34) and (35) at room temperature, and yield $BrF_6^+AsF_6^-$ and $BrF_4^+AsF_6^-$ when $KrF^+AsF_6^-$ or $Kr_2F_3^+AsF_6^-$ is used and $BrF_4^+Sb_2F_{11}^-$ and $BrF_6^+Sb_2F_{11}^-$ when $KrF^+Sb_2F_{11}^-$ are used. The oxidations compete with the decomposition reactions (Eq. (35)), giving

$$KrF^+ + BrF_5 \rightarrow BrF_6^+ + Kr \quad (34)$$

$$Kr_2F_3^+ + BrF_5 \rightarrow BrF_6^+ + Kr + KrF_2 \quad (35)$$

$$KrF^+ + MF_6^-[Sb_2F_{11}^-] \rightarrow Kr + F_2 + MF_5[2SbF_5] \quad (M = As, Sb) \quad (36)$$

rise to excess AsF_5 and SbF_5, which form BrF_4^+ salts. In the case of $BrF_4^+AsF_6^-$, the salt dissociates to BrF_5 and AsF_5 when the BrF_5 solution is pumped to dryness at room temperature, leaving high purity $BrF_6^+AsF_6^-$ as the sole product. Solutions of $Kr_2F_3^+AsF_6^-$ in BrF_5 are stable at -60 °C, providing the first evidence for the $Kr_2F_3^+$ cation in solution [79,142] (see Section 4.1.2 and Table 7). The BrF_6^+ cation was unambiguously characterized by ^{19}F-NMR spectroscopy in HF and BrF_5 solvents and by Raman spectroscopy in the solid state and in HF solution [142,146]. The O_h point symmetry of BrF_6^+ results in a zero electric field gradient at the ^{79}Br (50.54% natural abundance; $I = 3/2$) and ^{81}Br (49.46% natural abundance; $I = 3/2$) and slow quadrupolar relaxation of the ^{79}Br and ^{81}Br nuclides in HF at room temperature. This permitted the observation of the one bond ^{79}Br–^{19}F (1575 Hz) and ^{81}Br–^{19}F (1697 Hz) spin–spin couplings, which are manifested as two overlapping 1:1:1:1 quartets. The BrF_6^+ cation has since been characterized by infrared spectroscopy [204], normal coordinate analysis [204], single crystal X-ray diffraction of the $Sb_2F_{11}^-$ salt (Br–F bond length 1.657(8)–1.684(4) Å at -130 °C) [205] and by ^{79}Br and ^{81}Br-NMR spectroscopy ($\delta(^{79,81}Br)$, 2079.6 ppm with respect to aqueous Br^- at infinite dilution) [205]. The BrF_6^+ cation has also been prepared as the AuF_6^- salt by oxidation of BrF_5 with $KrF^+AuF_6^-$ [38].

Attempts to prepare BrF_7 by direct oxidative fluorination of BrF_5 with KrF_2 produced no reaction, whereas the attempted fluoride ion displacement of BrF_7 from $BrF_6^+AsF_6^-$ using NOF at -78 °C resulted in F_2 evolution and BrF_5 (Eq. (37)) [146].

$$BrF_6^+AsF_6^- + NOF \rightarrow BrF_5 + NO^+AsF_6^- + F_2 \quad (37)$$

The inability to synthesize BrF_7 appears to be a consequence of steric congestion of seven bonding electron pairs in the bromine valence shell and/or

F···F atom repulsions and places BrF_6^+, along with ClF_6^+ and NF_4^+, in a small group of coordinately saturated fluorocations. It was subsequently shown that the ClF_6^+ cation can be synthesized by an analogous route [206]. The reaction of KrF_2 with ClF_5 and AsF_5 in either ClF_5 or anhydrous HF solution produces $ClF_6^+AsF_6^-$ that is contaminated with significant amounts of ClF_4^+. Fortunately, $ClF_4^+AsF_6^-$ also dissociates under dynamic vacuum at room temperature to ClF_5 and AsF_5, leaving behind high purity $ClF_6^+AsF_6^-$. The reaction of KrF_2 with ClF_5 and SbF_5 produces $ClF_6^+SbF_6^-$; however, this salt cannot be isolated in pure form unless SbF_5 is used to displace AsF_5 from $ClF_6^+AsF_6^-$.

In an effort to prepare BrO_2F_3, the reaction of BrO_2F with KrF_2 does not proceed according to Eq. (38), but rather according to Eq. (39) [207]. The reaction of BrO_3F with KrF_2 has been attempted by analogy with Eq. (38) with the goal of preparing BrO_2F_3 according to Eq. (40), but BrO_3F and KrF_2 fail to react in HF solvent even after 15 min at room temperature [208]. When the more powerful fluorinating agent, $KrF^+AsF_6^-$, was used a reaction occurred, but only $O_2^+AsF_6^-$, BrF_5 and Br_2 could be detected [208]. The reaction of $BrOF_3$ with KrF_2 has also been attempted in an effort to prepare $BrOF_5$, but yielded BrF_5 as the only bromine-containing product (Eq. (41)) [207].

$$BrO_2F + KrF_2 \rightarrow BrO_2F_3 + Kr \quad (38)$$

$$BrO_2F + KrF_2 \rightarrow BrOF_3 + Kr + 1/2O_2 \quad (39)$$

$$BrO_3F + KrF_2 \rightarrow BrO_2F_3 + Kr + 1/2O_2 \quad (40)$$

$$BrOF_3 + KrF_2 \rightarrow BrF_5 + Kr + 1/2O_2 \quad (41)$$

The oxidative fluorination of NF_3 to NF_4^+ salts by KrF^+ salts has been extensively investigated [153]. In an early study [209], reactions were carried out at room temperature either with solid $KrF^+SbF_6^-$ and 1 atm of NF_3 or in HF solution with stoichiometric amounts of KrF_2, NF_3, and one of the Lewis acids SbF_5, NbF_5, PF_5, TiF_4, and BF_3. Although the products were assigned to NF_4^+ salts of the SbF_6^-, NbF_6^-, PF_6^-, TiF_6^{2-}, and BF_4^- anions on the basis of elemental analyses and vibrational spectra, a subsequent study [153] notes that for the alleged $NF_4^+SbF_6^-$ and $(NF_4^+)_2TiF_6^{2-}$ salts, the spectra correspond to polyanions salts. Consequently, the syntheses of $NF_4^+SbF_6^-$, $NF_4^+BF_4^-$, and $(NF_4^+)_2Ti_{n+1}F_{4n+2}^{2-}$ from KrF_2-Lewis acid adducts and NF_3 have been reinvestigated along with that of $NF_4^+AsF_6^-$ under differing and more carefully controlled reaction conditions [153]. The reactions of 7:2:1 molar ratios of NF_3:KrF_2:AsF_5/BF_3 yielded 97% $NF_4^+AsF_6^-$ and 31% $NF_4^+BF_4^-$, respectively, under autogenous pressures of 75 atm for 2 days at 50 °C. The fluorination of NF_3 by $KrF^+SbF_6^-$ to form $NF_4^+SbF_6^-$ was studied in HF solution at −31 °C, and in the presence of excess NF_3 (1000 Torr) and a 1:1 molar ratio of $KrF^+SbF_6^-$: NF_3, and gave respective $NF_4^+SbF_6^-$ yields of 100% after 1 h and 37% after 3 h (Eq. (42)). The reaction did not occur to a noticeable extent after 3 h at −78 °C when a 1:1

$$NF_3 + KrF^+SbF_6^- \rightarrow NF_4^+SbF_6^- + Kr \quad (42)$$

$KrF^+SbF_6^-$:NF_3 molar ratio was used and only a 23% yield was obtained under the same conditions when the reaction was carried out at −45 °C. When this reaction was carried out in HF solution at ambient temperature using a 1:1 $KrF^+SbF_6^-$:NF_3 ratio, the reaction was complete in less than 3 h, but the solid product was 91% $NF_4^+Sb_2F_{11}^-$, indicating that an appreciable amount of $KrF^+SbF_6^-$ had decomposed to Kr, F_2 and SbF_5 during the course of the reaction. The reaction of NF_3, KrF_2, and TiF_4 in a 2:2:1 mole ratio in HF at room temperature for 3 h yields only polytitanate ($Ti_{n+1}F_{4n+2}^{2-}$) salts of the NF_4^+ cation and no TiF_6^{2-} salt as previously claimed under identical reaction conditions. Attempts to fluorinate OF_2, CF_3NF_2, and $ClOF_4^-$ with KrF^+ salts to give OF_3^+, $CF_3NF_3^+$, and $ClOF_5$ have been unsuccessful [153]. Failure to form OF_3^+ appears to be inconsistent with the higher F^+ detachment energy of OF_3^+ (511.3 kJ mol^{-1}) [192] and is likely attributable to kinetic factors.

Whereas KrF^+ is capable of oxidizing NF_3, ClF_5, and BrF_5 to the corresponding complex fluoro cations, PtF_6 is capable of oxidizing only NF_3 and ClF_5 [153]. The experimental evidence presently available for the formation mechanisms of coordinately saturated fluorocations indicates reaction of a powerful one electron oxidizer (PtF_6, Eq. (43)) or two-electron (KrF^+, Eq. (45)) oxidizer with the substrate (NF_3, ClF_5, or BrF_5) results in electron transfer from the substrate to the oxidant, with subsequent (PtF_6, Eq. (44)) or simultaneous (KrF^+, Eq. (46)) fluorination of the intermediate radical cation ($^\bullet NF_3^+$, $^\bullet ClF_5^+$, $^\bullet BrF_5^+$) to give the final product (NF_4^+, ClF_6^+, BrF_6^+). Thus, the neutral oxidizer, PtF_6, participates in a radical mechanism [153]:

$$EF_n + PtF_6 \rightarrow {}^\bullet EF_n^+PtF_6^- \quad (43)$$

$$^\bullet EF_n^+PtF_6^- + PtF_6 \rightarrow EF_{n+1}^+PtF_6^-{\cdot}PtF_5 \quad (44)$$

where E = N ($n = 3$); Cl ($n = 5$) and the ionic oxidizer, KrF^+, participates in an ionic mechanism [153]:

$$EF_n + KrF^+MF_6^- \rightarrow [KrF\cdots EF_n]^+MF_6^- \quad (45)$$

$$[KrF\cdots EF_n]^+MF_6^- \rightarrow EF_{n+1}^+MF_6^- + Kr \quad (46)$$

where E = N ($n = 3$); Cl, Br ($n = 5$).

Mass spectroscopy of the product of [60]fullerene fluorination by KrF_2 in HF has shown that the most abundant species present are $C_{60}F_{44}$ and $C_{60}F_{46}$ [210]. Cage-opened compounds with molecular formulae up to $C_{60}F_{78}$ are also present. The electron impact mass spectrum differs from that obtained with F_2-fluorinated [60]fullerene, showing a greater concentration of frag-

mentation ions, including species of even mass, which may arise from cage-opened species. The ^{19}F-NMR spectrum of the product in dry THF solution is similar to that found with F_2-fluorinated material, and showed a sharp singlet at ca. 151 ppm that was previously attributed to a symmetric species such as $C_{60}F_{60}$.

8.3. Transition metal fluoride and oxide fluoride chemistry

Chromium pentafluoride is formed in high yield by reaction of KrF_2 with Cr metal in anhydrous HF solvent [211]. Chromium oxide tetrafluoride, $CrOF_4$, has been prepared in high yield and purity from CrO_2F_2 and KrF_2 in HF solution [68], contrasting with the high-temperature synthesis from CrO_3 and F_2, which can be contaminated with CrF_5 [212,213]. The vibrational spectra of gaseous, solid, and matrix-isolated $CrOF_4$ and its solution in BrF_5 and HF have been reported, as well as the ^{19}F-NMR spectra of the BrF_5 and SO_2ClF solutions [68]. The data confirm for gaseous, matrix-isolated, and dissolved $CrOF_4$ a monomeric, square-pyramidal molecule (C_{4v} point symmetry) in the gas phase, matrix and in solution and in the solid, $CrOF_4$ is a fluorine-bridged polymeric structure in which the Cr atom is six coordinate. Chromium oxide tetrafluoride also forms an unstable 1:1 adduct with KrF_2, which is discussed in Section 4.2.

Manganese difluoride is oxidatively fluorinated in HF to the adducts $2KrF_2\cdot MnF_4$ and $KrF_2\cdot MnF_4$ [154]. The $2KrF_2\cdot MnF_4$ adduct is unstable under dynamic vacuum at −45 °C, losing KrF_2 to form $KrF_2\cdot MnF_4$, which undergoes further decomposition at room temperature to form KrF_2 and high purity MnF_4 (see Section 4.1.1).

The last member of Tc(VII) oxide fluorides, $TcOF_5$, has been prepared by oxidative fluorination of TcO_2F_3 [214,215], a fluorine bridged *cis*-dioxo polymer, with KrF_2 in anhydrous HF (Eq. (47)). Interestingly, a noble-gas fluoride also provides the only known route to TcO_2F_3 by fluorination of TcO_3F with XeF_6 in HF solvent [216]. The pseudooctahedral (C_{4v}) structure of $TcOF_5$ was determined by ^{19}F- and ^{99}Tc-NMR, Raman, and IR spectroscopies and by single-crystal X-ray diffraction [214,215]. Technetium oxide pentafluoride was allowed to react with $KrF^+AsF_6^-$ in an attempt to form TcF_6^+ according to Eq. (48), but instead yielded $Tc_2O_2F_9^+AsF_6^-$ according to Eq. (49) [215]. In separate experiments, $TcOF_5$ was shown to behave as a F^- ion

$$TcO_2F_3 + KrF_2 \rightarrow TcOF_5 + Kr + 1/2O_2 \quad (47)$$

$$2TcOF_5 + 3KrF^+AsF_6^- \rightarrow 2TcF_6^+AsF_6^- + 3Kr + O_2^+AsF_6^- + 1/2F_2 \quad (48)$$

$$2TcOF_5 + KrF^+AsF_6^- \rightarrow Tc_2O_2F_9^+AsF_6^- + KrF_2 \quad (49)$$

$$2TcOF_5 + AsF_5\ (2SbF_5) \rightarrow Tc_2O_2F_9^+AsF_6^-\ (Tc_2O_2F_9^+Sb_2F_{11}^-) \quad (50)$$

donor toward AsF_5 and SbF_5 in HF solvent (Eq. (50)), also giving AsF_6^- and $Sb_2F_{11}^-$ salts of the fluorine bridged $Tc_2O_2F_9^+$ cation [215], which was characterized as the AsF_6^- and $Sb_2F_{11}^-$ salts by Raman spectroscopy and as $Tc_2O_2F_9^+Sb_2F_{11}^-$ by single-crystal X-ray diffraction. The $Tc_2O_2F_9^+$ cation consists of two F-bridged square pyramidal $TcOF_4$ groups in which the F bridge is trans to the oxygens and is structurally analogous to its rhenium analogue, $Re_2O_2F_9^+$ [217].

Several ReF_6^+ salts and ReF_7 have been prepared by oxidation of ReF_6 with KrF^+ and $Kr_2F_3^+$ salts [218]. Interaction of ReF_6 dissolved in WF_6 with $KrF^+Sb_2F_{11}^-$ gave orthorhombic ReF_6^+ ReF_7 $SbF_6^-SbF_5$. The rhombohedral form of this compound was prepared at ca. 20 °C by direct interaction of excess ReF_6 with $KrF^+SbF_6^-$ or $KrF^+Sb_2F_{11}^-$ or from a mixture of SbF_5 with a molar excess of ReF_6 and F_2 that had been photolyzed with a xenon lamp. The analogous gold(V) compound, ReF_6^+ ReF_7 $AuF_6^-AuF_5$, was prepared by interaction of $Kr_2F_3^+AuF_6^-$ with excess ReF_7 in HF solution at 0 °C to room temperature followed by removal of HF under dynamic vacuum at −78 °C. The solid mixture was then rapidly warmed to ca. 60 °C to melt ReF_7 and to decompose $Kr_2F_3^+AuF_6^-$, whereupon rapid Kr and F_2 evolution ensued. The X-ray powder pattern that was obtained for the resulting solid was not indexed. The formulations of all three compounds are based on their Raman spectra. In contrast, attempts to generate the TcF_6^+ cation by reaction of TcF_6 with solid KrF^+ salts and in HF solutions at ambient temperature (Eq. (51)) have failed [219], in accord with the expected ordering of electron affinities, i.e. $TcF_6 > ReF_6$.

$$TcF_6 + KrF^+AsF_6^-\ (KrF^+Sb_2F_{11}^-) \rightarrow TcF_6^+AsF_6^-\ (TcF_6^+Sb_2F_{11}^-) + Kr + 1/2F_2 \quad (51)$$

An Os(VIII) oxide fluoride obtained from the reaction of KrF_2 and OsO_4 in anhydrous HF solution was originally identified as $OsOF_6$ [220]. It was subsequently shown by material balance [221], electron diffraction, ^{19}F-NMR, ^{19}F{^{187}Os} inverse correlation NMR, vibrational spectroscopy, density functional theory calculations [222], and a disordered crystal structure [223] to be *cis*-OsO_2F_4 (C_{2v} point symmetry) which is formed according to Eq. (52).

$$2KrF_2 + OsO_4 \rightarrow \textit{cis}\text{-}OsO_2F_4 + 2Kr + O_2 \quad (52)$$

The clean synthesis of *cis*-OsO_2F_4 using KrF_2 as an oxidative fluorinator has provided a means to further explore the little studied chemistry of osmium(VIII), and in particular, the fluoride ion donor-acceptor properties of *cis*-OsO_2F_4. Osmium tetrafluoride dioxide reacts with the strong fluoride ion acceptors AsF_5 and SbF_5 in anhydrous HF and SbF_5 solutions to form orange salts [224]. The crystal structure of one of these salts, F(*cis*-$OsO_2F_3)_2^+Sb_2F_{11}^-$, consists of discrete F-bridged F(*cis*-

$OsO_2F_3)_2^+$ and $Sb_2F_{11}^-$ ions in which the fluorine bridge of the $F(cis\text{-}OsO_2F_3)_2^+$ cation is trans to an O atom of each OsO_2F_3 group. The $OsO_2F_3^+$ cation has been characterized by ^{19}F-NMR and by Raman spectroscopies in neat SbF_5 solution but was not isolable in the solid state [224]. The NMR and Raman spectroscopic findings are consistent with a trigonal bipyramidal cation in which the O atoms and an F atom occupy the equatorial plane and two F atoms are in axial positions. Attempts to prepare the $OsOF_5^+$ cation by oxidative fluorination of *cis*-OsO_2F_4 with $KrF^+AsF_6^-$ (KrF_2/AsF_5) in anhydrous HF have proven unsuccessful, generating instead, $F(cis\text{-}OsO_2F_3)_2^+AsF_6^-$ [224]. The $OsO_2F_5^-$ anion is formed by the interaction of *cis*-OsO_2F_4 with NOF and by the reaction of anhydrous $N(CH_3)_4^+F^-$ with *cis*-OsO_2F_4 in liquid NOF at −78 °C (Eq. (53)) [225]. The anion geometry has been

$$cis\text{-}OsO_2F_4 + N(CH_3)_4^+F^- \rightarrow N(CH_3)_4^+F^-OsO_2F_5^- \quad (53)$$

determined by ^{19}F-NMR spectroscopy and displays a novel *cis*-dioxo geometry based on a monocapped trigonal prismatic arrangement of ligand atoms (structure **VIII**).

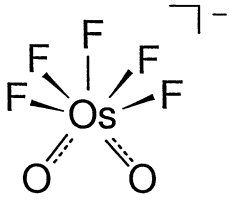

VIII

The fluorination of RuO_4 has been attempted using F_2 or KrF_2 in HF solution. Of the two fluorinating agents, only KrF_2 reacts with RuO_4 to form $RuOF_4$ according to Eqs. (54) and (55) [226].

$$RuO_4 + 2KrF_2 \rightarrow RuO_2F_4 + 2Kr + O_2 \quad (54)$$

$$RuO_2F_4 \rightarrow RuOF_4 + 1/2O_2 \quad (55)$$

The reaction of RuO_2 with KrF_2 in HF solution leads to the Ru(V) dioxygenyl salt, $O_2^+RuF_6^-$, and that of OsO_2 to $OsOF_5$ [227]. A large excess of either KrF_2 or KrF^+ in HF solution does not react further with $OsOF_5$. The formation of $O_2^+RuF_6^-$ has been explained by the following reaction sequence:

$$RuO_2 + 3KrF_2 \rightarrow RuF_6 + O_2 + 3Kr \quad (56)$$

$$RuF_6 + O_2 \rightarrow O_2^+RuF_6^- \quad (57)$$

The fluorination of RuO_4 by KrF_2 may go through RuO_2F_4 as an intermediate (Eq. (54)) by analogy with the reaction between KrF_2 and OsO_4 [221,222]. Unlike *cis*-OsO_2F_4, the Ru(VIII) analogue appears to be unstable, decomposing to O_2 and $RuOF_4$ (Eq. (55)). The difference is attributed to the smaller bond energy of the Ru–O bond when compared with that of the Os–O bond. The remaining oxygen in $RuOF_4$ is also weakly bound, as indicated by its low stretching frequency (900 cm^{-1}) [226] when compared with that of $OsOF_4$ (1009 cm^{-1}) [228], and results in the decomposition of $RuOF_4$ to RuF_4 at 65–75 °C. The fluorination of OsO_2 does not proceed beyond $OsOF_5$ whereas that of RuO_2 proceeds through to RuF_6, which may again be attributed to the weakness of the Ru–O bond in the hypothetical $RuOF_5$ molecule [227].

Platinum metals react with KrF_2 in HF and BrF_5 solvents to give $KrF^+MF_6^-$ (M = Pt, Ru, Rh) and $KrF^+M_2F_{11}^-$ (M = Pt, Ru) [140]. These salts have been discussed in Section 4.1.1. Palladium metal reacts readily with KrF_2 in BrF_5 and HF solvents. Dark red solutions were observed when excess KrF_2 was used, and it was hypothesized that PdF_5 was formed. It was not possible to isolate PdF_5 with PdF_4 crystallizing from solution as the concentration of KrF_2 decreased upon standing. Reaction of KrF_2 with PdF_4 in the presence of NaF or O_2 resulted in $Na^+PdF_6^-$ and $O_2^+PdF_6^-$, respectively. The salt, $(Xe_2F_{11}^+)_2NiF_6^{2-}$, has been prepared by reaction of NiF_2, KrF_2, and XeF_6 in anhydrous HF [229].

Salts of the diamagnetic AgF_4^- anion were first described by Hoppe [230] and shown to be isomorphous with their AuF_4^- analogues. More recently, $KAgF_4$, has been prepared by reaction of a stoichiometric excess of KrF_2 with equimolar amounts of AgF_2 and KF at room temperature in anhydrous HF solvent (Eq. (58)) [231]. The method yielded $KAgF_4$ in the form of crystals suitable

$$KrF_2 + 2KF + 2AgF_2 \rightarrow 2KAgF_4 + Kr \quad (58)$$

for X-ray structure determination, but failed to find evidence for oxidation beyond Ag(III) despite the relative ease of oxidation of AuF_3 to AuF_5 and AuF_4^- to AuF_6^- by KrF_2. The more demanding synthesis of AgF_3 was first claimed by Bougon and Lance [232], who described a red–brown, highly reactive solid made by the reaction of Ag, AgF or AgF_2 in anhydrous HF with KrF_2 at room temperature. The X-ray powder data showed that the red–brown solid was not structurally related to AuF_3. Moreover, the solid was weakly paramagnetic, raising the possibility that some of the Ag(III) was in the triplet state. Bright red, diamagnetic AgF_3 was subsequently prepared by precipitation from anhydrous HF solutions of AgF_4^- by addition of fluoroacids according to Eq. (59) (L = BF_3 or AsF_5) [233]. With additional AsF_5, Ag(III) is reduced,

$$AgF_4^- + L \rightarrow AgF_3 + LF^- \quad (59)$$

while such reduction does not occur with BF_3 and is therefore preferred for the preparation of AgF_3. Silver trifluoride is isostructural with AuF_3. The Ag and Au atoms lie at the center of an elongated octahedron. The main difference in the structures of AgF_3 and AuF_3 is

the interaction distance along the z-axis (Ag–F = 2.540(4) and Au–F = 2.756(8) Å). The latter is in accord with the stronger binding of the Ag(III) d-orbital electrons and is the main reason why Au(III) is readily oxidized by KrF_2 to Au(V) while the corresponding oxidation of Ag(III) to Ag(V) does not take place. The tighter binding of the Ag(III) d-electrons is also evident in the strong oxidizing properties of AgF_3 compared with AuF_3. The reaction between AgF_2 and an excess of XeF_6 and KrF_2 in anhydrous HF yields a light yellow diamagnetic solid, $XeF_6 \cdot AgF_3$ [234]. On the basis of the vibrational data, this compound has been formulated as $XeF_5^+ AgF_4^-$ and is thermally stable under dynamic vacuum up to 70 °C where it begins to lose XeF_6, yielding AgF_3. The formulation of the compound originally reported by Bougon and Lance [232] has been reinvestigated and shown to be a mixed-valence compound, $Ag^{II}Ag_2^{III}F_8$, which may have the formulation $Ag^{2+}(AgF_4^-)_2$ [233].

Gold metal reacts vigorously with KrF_2 in anhydrous HF to give $KrF^+AuF_6^-$ [37] (Eq. (60)). Pyrolysis of freshly prepared $KrF^+AuF_6^-$ at 60 to 65 °C over a period of 8 h gives AuF_5 (Eq. (61)), which reacts with an excess of XeF_2 in HF or BrF_5 to give $Xe_2F_3^+AuF_6^-$ and with NOF in HF

$$7KrF_2 + 2Au \rightarrow 2KrF^+AuF_6^- + 5Kr \quad (60)$$

$$KrF^+AuF_6^- \rightarrow Kr + AuF_5 + 1/2F_2 \quad (61)$$

to give $NO^+AuF_6^-$. The salt, $KrF^+AuF_6^-$, is a powerful oxidative fluorinating agent, oxidizing O_2 to O_2^+ and Xe to XeF_5^+ with the evolution of Kr. A subsequent report [38] repeating elements of the original work [37] also notes that $KrF^+AuF_6^-$ oxidizes BrF_3 and BrF_5 to $BrF_6^+AuF_6^-$ (also see Section 4.1.1), XeF^+ to XeF_5^+, and $Xe_2F_3^+$ to $Xe_2F_{11}^+$. The AuF_4^- anion of $XeF_5^+AuF_4^-$ is oxidatively fluorinated by KrF_2 in anhydrous HF at temperatures below 0 °C to yield $XeF_5^+AuF_6^-$ [234].

8.4. Lanthanide and actinide fluoride and oxide fluoride chemistry

The use of KrF_2 as a fluorination agent has afforded a means to access the +4 oxidation state of cerium, praseodymium, and terbium at low temperatures. Fluorination of PrF_3 by KrF_2 in anhydrous HF [235] is slow yielding only 30% PrF_4 after four days, and an even lower yield (10%) in the solid phase reaction after three days. Fluorination of PrF_3 by KrF_2 in the presence of CeF_3 and in the absence of solvent sharply increases the yield to 56% PrF_4 after only two days. The reaction of KrF_2 with Pr_6O_{11} at 20 °C in anhydrous HF gives quantitative yields of PrF_4 after three days. Krypton difluoride reacts with MO_2 (M = Ce, Pr, Tb) in 2:1 and 3:1 molar ratios in HF solvent to give MF_4. With the exception of terbium, which required 1.5 weeks to react, the reactions were complete after one day. At a 1:1 molar ratio, compounds were formed having compositions close to MOF_2. Krypton difluoride is also reported to react with CeO_2 and the nonstoichiometric oxides Pr_6O_{11} and Tb_4O_7 at room temperature in the absence of a solvent to give LnF_4 (Ln = Ce, Pr, Tb) in 99.9–99.99% purity [236].

The xenon(VI) fluorometalates of praseodymium and terbium in their +4 oxidation states, $XeF_6 \cdot 4PrF_4$ and $XeF_6 \cdot 2TbF_4$, have been prepared by reaction of Pr_6O_{11} and Tb_4O_7 with a large excess of XeF_6 in anhydrous HF followed by addition and reaction with a large excess of KrF_2 [237]. The vibrational spectra are in accord with the formulation of these compounds ($XeF_6 \cdot 4PrF_4$ and $XeF_6 \cdot 2TbF_4$) as salts of XeF_5^+ having polymeric anions. Reaction of Nd_2O_3 with XeF_6 and KrF_2 under similar conditions yielded NdF_3.

In contrast with the formation of the actinide hexafluorides, which appear to occur in a single step in the high-temperature fluorinations of actinide tetrafluorides with elemental fluorine [238], no intermediate fluorides, in particular pentafluorides, are formed. The controlled fluorinations of the uranium [238] and neptunium [238,239] tetrafluorides to the pentafluorides by KrF_2 in anhydrous HF occur in the temperature ranges: $UF_4 \rightarrow UF_5$, −30 to 10 °C and $NpF_4 \rightarrow NpF_5$, −15 to 5 °C [238]. Although NpF_5 had been previously prepared by reduction of NpF_6 with IF_5, it was contaminated with NpF_4 [240]. Low-temperature fluorination of NpF_4 with KrF_2, as well as the reduction of NpF_6 with PF_3 [241] and I_2 [242], provides a high-purity synthetic route to NpF_5. At higher temperatures, both UF_5 and NpF_5 disproportionate to their respective tetrafluorides and hexafluorides [239]. In an attempt to prepare the unknown pentafluoride, PuF_5, KrF_2 oxidation of PuF_3 in anhydrous HF at room temperature has yielded PuF_4 instead [242]. While there is no mention of PuF_6 formation in reference [242], gaseous KrF_2 has been shown to fluorinate solid PuF_4 to PuF_6 [243]. Gaseous KrF_2 is only the second known low-temperature fluorinating agent for the generation of PuF_6 from PuF_4 (the other agent is O_2F_2 [244]). Uranium hexafluoride has also been formed by reaction of gaseous KrF_2 with UF_4 at ambient temperatures [243]. The fluorination of UF_4 by KrF_2 has also been briefly mentioned in reference [245]. Treatment of nickel and Monel surfaces, that have been contaminated with the lower fluorides and oxide fluorides of neptunium and plutonium, with gaseous KrF_2 at ambient temperatures liberates volatile NpF_6 and PuF_6 at room temperature [243]. Volatilization of uranium as UF_6 from stainless steel surfaces contaminated with lower valent uranium fluorides and oxide fluorides using gaseous KrF_2 has also been observed [243].

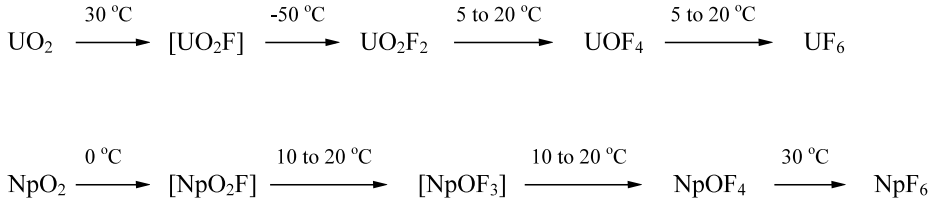

Scheme 5. Sequences and approximate temperature ranges for the fluorination of UO_2 and NpO_2 in anhydrous HF using KrF_2 as the fluorinating agent [236].

Americium trifluoride, AmF_3, is oxidatively fluorinated to AmF_4 in HF by KrF_2 [238]. Americium hexafluoride cannot be synthesized by high-temperature, direct fluorination procedures using elemental fluorine. It is claimed that AmF_4 reacts with KrF_2 at 40–60 °C in HF to form previously unknown AmF_6, which is reported to be a dark brown, crystalline substance having a significant vapor pressure [238]. It has also been noted that AmF_6 has powerful oxidizing properties, and rapidly undergoes reduction to AmF_4 on metallic surfaces. In a subsequent study [243], treatment of AmO_2 and 95% PuO_2/5% AmO_2 mixtures with KrF_2 in anhydrous HF at 50–60 °C failed to provide evidence for AmF_6 formation. No characterization of the reaction products was reported. A prior report claims that AmO_2 is fluorinated to AmF_4 by KrF_2 in HF at 20 °C [238].

The low-temperature fluorinations of actinide metal oxides and oxide fluorides by KrF_2 in anhydrous HF have been a subject of considerable interest. The fluorinations of UO_2 and NpO_2 have been shown to proceed stepwise within the temperature ranges specified in Scheme 5 [238]. Both UO_2 and U_3O_8 are fluorinated to UF_6 at ambient temperature, although the reaction with UO_2 derived from crushed fuel pellets occurs at a reduced rate and provides lower yields of UF_6 [243]. Although $NpOF_4$ has been prepared by the reaction of KrF_2 with NpO_2 in anhydrous HF at 20 °C [239,246], this oxide fluoride has also been prepared by the hydrolysis of NpF_6 in HF [239,247]. The room temperature reaction of NpO_2 with excess KrF_2 in HF at an unspecified temperature is reported to yield NpF_6 [239], although in a subsequent report the reaction occurs at 30 °C (Scheme 5) [238]. While NpO_2F and $NpOF_3$ are speculated to be intermediates in the fluorination of NpO_2 with KrF_2 in anhydrous HF, there is no direct spectroscopic or other evidence for their intermediacy. The oxidation of $NpOF_4$ with KrF_2 in HF at 0 °C [239] and at −60 °C [247] yields NpF_6, Kr, and O_2. In addition, oxidation of $NpOF_4$ with KrF_2 in HF at ca. 0 °C has been reported to yield a new volatile neptunium compound, which is colorless in the vapor state and which decomposes rapidly on the walls of the Teflon reaction vessel to $NpOF_4$ [237]. The species has been tentatively assigned, on basis of the infrared spectrum, to $NpOF_5$, but has not been confirmed.

Acknowledgements

The authors thank the Canada Council for a Killam Research Fellowship (G.J.S.) and the Natural Sciences and Engineering Research Council and the donors of the Petroleum Research Fund administered by the American Chemical Society (ACS-PRF 33594-AC3) for support of the krypton chemistry described in this review which originated at McMaster University. We also thank the Natural Sciences and Engineering Research Council of Canada for a postgraduate scholarship and McMaster University for a Dalley Fellowship (J.F.L.). We are particularly indebted to Dr. Scott A. Kinkead, Los Alamos National Laboratory, who provided us with the drawing of the hot wire reactor depicted in Fig. 2.

References

[1] N. Bartlett, Proc. Chem. Soc. (1962) 218.
[2] P. Laszlo, G.J. Schrobilgen, Angew. Chem. 100 (1988) 495; Angew. Chem. Int. Ed. Engl. 27 (1988) 479.
[3] N. Bartlett, F.O. Sladky, in: J.C. Bailar, Jr, H.J. Emeléus, R. Nyholm, A.F. Trotman-Dickenson (Eds.), Comprehensive Inorganic Chemistry, vol. 1, Pergamon Press, New York, 1973, pp. 242–249.
[4] K. Seppelt, D. Lentz, in: S.J. Lippard (Ed.), Progress in Inorganic Chemistry, Wiley, New York, 1982, pp. 167–202.
[5] H. Selig, J.H. Holloway, in: F.L. Boschke (Ed.), Topics in Current Chemistry, vol. 124, Springer-Verlag, Berlin, 1984, pp. 33–90.
[6] B. Žemva, Croat. Chem. Acta 61 (1988) 163.
[7] G.J. Schrobilgen, in: G.A. Olah, G.K.S. Prakash, R.D. Chambers (Eds.), Synthetic Fluorine Chemistry, Ch. 1, Wiley, New York, 1992, pp. 1–30.
[8] B. Žemva, in: R.B. King (Ed.), Encyclopedia of Inorganic Chemistry, vol. 5, Wiley, Chichester, 1994, pp. 2660–2680.
[9] G.J. Schrobilgen, J.M. Whalen, Kirk–Othmer Encyclopedia of Chemical Technology, Ch. 13, 4th ed., Wiley, New York, 1994, pp. 38–53.
[10] J.H. Holloway, E.G. Hope, Adv. Inorg. Chem. 46 (1998) 51.
[11] M. Gerken, G.J. Schrobilgen, Coord. Chem. Rev. 197 (2000) 335.
[12] A. von Antropoff, Z. Angew. Chem. 37 (1924) 217.

[13] A. von Antropoff, Z. Angew. Chem. 37 (1924) 695.
[14] A. von Antropoff, K. Weil, H. Frauenhof, Naturwissenschaften 20 (1932) 688.
[15] H. Moissan, Bull. Soc. Chim. Fr. 13 (1895) 976.
[16] O. Ruff, W. Menzel, Z. Anorg. Allg. Chem. 213 (1933) 206.
[17] A. von Antropoff, H. Frauenhof, K.H. Krüger, Naturwissenschaften 21 (1933) 315.
[18] L. Pauling, J. Am. Chem. Soc. 55 (1933) 1895.
[19] D.M. Yost, H.H. Kaye, J. Am. Chem. Soc. 55 (1933) 3891.
[20] L. Graham, O. Graudejus, N.K. Jha, N. Bartlett, Coord. Chem. Rev. 197 (2000) 321.
[21] N. Bartlett, N.K. Jha, in: H.H. Hyman (Ed.), Noble Gas Compounds, University Chicago Press, Chicago, IL, 1963, pp. 23–30.
[22] A.G. Streng, A.D. Kirshenbaum, L.V. Streng, A.V. Grosse, in: H.H. Hyman (Ed.), Noble Gas Compounds, University Chicago Press, Chicago, IL, 1963, p. 73.
[23] A.V. Grosse, A.D. Kirshenbaum, A.G. Streng, L.V. Streng, Science 139 (1963) 1047.
[24] F. Schreiner, J.G. Malm, J.C. Hindman, J. Am. Chem. Soc. 87 (1965) 25.
[25] T.H. Brown, P.H. Verdier, J. Chem. Phys. 40 (1964) 2057.
[26] J.J. Turner, G.C. Pimentel, in: H.H. Hyman (Ed.), Noble Gas Compounds, University Chicago Press, Chicago, IL, 1963, p. 101.
[27] J.J. Turner, G.C. Pimentel, Science 140 (1963) 974.
[28] A.G. Streng, A.V. Grosse, Science 143 (1964) 242.
[29] A.N. Murin, V.D. Nefedov, I.S. Kirin, S.A. Grachev, Y.K. Gusev, G.N. Shapkin, Zh. Obschei. Khim. 35 (1965) 2137, J. Gen. Chem. USSR 35 (1965) 2126.
[30] M. Pasternak, T. Sonnino, Phys. Rev. 164 (1967) 384.
[31] W.E. Falconer, J.R. Morton, A.G. Streng, J. Chem. Phys. 41 (1964) 902.
[32] R. Burnham, S.K. Searles, J. Chem. Phys. 67 (1977) 5967.
[33] V.S. Zuev, I.F. Isaev, A.V. Kanaev, L.D. Mikheev, D.B. Stavrovskiĭ, N.G. Shchepetov, Kvantovaya Elektron. 8 (1981) 373; Sov. J. Quantum Electron. 11 (1981) 221.
[34] J.J. Tiee, C.R. Quick, A.H. Hsu, D.E. Hof, Phys. Scr. 41 (1990) 71.
[35] E. Minehara, S. Abe, Nucl. Instrum. Methods Phys. Res. 212 (1983) 533.
[36] B. Frlec, J.H. Holloway, J. Chem. Soc. Chem. Commun. (1973) 370.
[37] J.H. Holloway, G.J. Schrobilgen, J. Chem. Soc. Chem. Commun. (1975) 623.
[38] V.B. Sokolov, V.N. Prusakov, A.V. Ryzhkov, Y.V. Drobyshevskii, S.S. Khoroshev, Dokl. Akad. Nauk SSSR 229 (1976) 884; Dokl. Chem. 229 (1976) 525.
[39] S.R. Gunn, J. Am. Chem. Soc. 88 (1966) 5924.
[40] S.R. Gunn, J. Phys. Chem. 71 (1967) 2934.
[41] H.P.A. Mercier, J.C.P. Sanders, G.J. Schrobilgen, S.S. Tsai, Inorg. Chem. 32 (1993) 386.
[42] J.G. Malm, C.L. Chernick, Inorg. Synth. 8 (1966) 254.
[43] C.L. Chernick, J.G. Malm, Inorg. Synth. 8 (1966) 258.
[44] G.K. Johnson, J.G. Malm, W.N. Hubbard, J. Chem. Thermodyn. 4 (1972) 879.
[45] D.R. MacKenzie, Science 141 (1963) 1171.
[46] D.R. MacKenzie, J. Fajer, Inorg. Chem. 5 (1966) 699.
[47] V.N. Pursakov, V.B. Sokolov, At. Energ. 31 (1971) 259; Sov. At. Energ. 31 (1971) 990.
[48] P.A. Sessa, H.A. McGee Jr, J. Phys. Chem. 73 (1969) 2078.
[49] L.V. Streng, A.G. Streng, Inorg. Chem. 5 (1966) 328.
[50] (a) J. Slivnik, A. Šmalc, K. Lutar, B. Žemva, B. Frlec, J. Fluorine Chem. 5 (1975) 273. (b) A. Šmalc, Yugoslavian patent no. 37501 P 159/75, Jan. 23, 1975.
[51] A. Šmalc, K. Lutar, B. Žemva, Inorg. Synth. 29 (1992) 11.
[52] S.A. Kinkead, J.R. FitzPatrick, J. Foropoulos, Jr, R.J. Kissane, J.D. Purson, ACS Symp. Ser. 555 (1994) 40.
[53] V.N. Bezmel'nitsyn, V.A. Legasov, B.B. Chaivanov, Dokl. Akad. Nauk. SSSR 235 (1977) 96; Dokl. Chem. 235 (1977) 365.
[54] J.F. Lehmann, D.A. Dixon, G.J. Schrobilgen, Inorg. Chem. 40 (2001) 3002.
[55] A.A. Artyukhov, V.A. Legasov, G.N. Makeev, B.M. Smirnov, B.B. Chaivanov, Khim. Vys. Energ. 10 (1976) 512; High Energy Chem. 10 (1976) 450.
[56] C.T. Goetschell, V.A. Campanile, C.D. Wagner, J.N. Wilson, J. Am. Chem. Soc. 91 (1969) 4702.
[57] J. Parker, R.D. Stephens, IEEE J. Quantum Electon. 9 (1973) 643.
[58] A.A. Artyukhov, V.A. Legasov, G.N. Makeev, B.B. Chaivanov, Khim. Vys. Energ. 11 (1977) 89; High Energy Chem. 11 (1977) 70.
[59] G.N. Makeev, V.F. Sinyanskii, B.M. Smirnov, Dokl. Akad. Nauk. SSSR 222 (1975) 151.
[60] A.A. Artyukhov, V.A. Legasov, G.N. Makeev, L.A. Palkina, B.M. Smirnov, B.B. Chaivanov, Khim. Vys. Énerg. 11 (1977) 88; High Energy Chem. 11 (1977) 68.
[61] A.D. Kirshenbaum, A.V. Grosse, J.G. Aston, J. Am. Chem. Soc. 81 (1959) 6398.
[62] S.A. Kinkead, Private communication.
[63] G.J. Schrobilgen, Unpublished results.
[64] B. Frlec, J.H. Holloway, Inorg. Chem. 15 (1976) 1263.
[65] (a) H. Meinert, G. Gnauck, East German patent no. 513032, Nov. 5, 1966; (b) H. Meinert, G. Gnauck, British patent no. 1056657, Jan. 25, 1967; (c) VEB Technische Gase-Werke Berlin, Belgian patent no. 672147, March 1, 1966.
[66] V.N. Prusakov, V.B. Sokolov, USSR Zh. Fiz. Khim. 45 (1971) 2950; Russ. J. Phys. Chem. 45 (1971) 1673.
[67] V.N. Prusakov, V.B. Sokolov, Kinet. Katal. 12 (1971) 33.
[68] K.O. Christe, W.W. Wilson, R.A. Bougon, Inorg. Chem. 25 (1986) 2163.
[69] J.C.P. Sanders, G.J. Schrobilgen, J. Chem. Soc. Chem. Commun. (1989) 1576.
[70] C.R. Brundle, G.R. Jones, J. Chem. Soc. Faraday Trans. 2 68 (1972) 959.
[71] G.M. Bancroft, D.J. Bristow, J.S. Tse, G.J. Schrobilgen, Inorg. Chem. 22 (1983) 2673.
[72] F.W. Kutzler, D.E. Ellis, T.I. Morrison, G.K. Shenoy, P.J. Viccaro, P.A. Montano, E.H. Appelman, L. Stein, M.J. Pellin, D.M. Gruen, Solid State Commun. 46 (1983) 803.
[73] H.H. Claassen, G.L. Goodman, J.G. Malm, F. Schreiner, Chem. Phys. 42 (1965) 1229.
[74] D.R. MacKenzie, Unpublished results.
[75] M. Al-Mukhtar, J.H. Holloway, E.G. Hope, G.J. Schrobilgen, J. Chem. Soc. Dalton Trans. (1991) 2831.
[76] H. Bürger, S. Ma, B.P. Winnewisser, J. Mol. Spectrosc. 164 (1994) 84.
[77] C. Murchison, S. Reichman, D. Anderson, J. Overend, F. Schreiner, J. Am. Chem. Soc. 90 (1968) 5690.
[78] H. Bürger, R. Kuna, S. Ma, J. Breidung, W. Thiel, J. Chem. Phys. 101 (1994) 1.
[79] R.J. Gillespie, G.J. Schrobilgen, Inorg. Chem. 15 (1976) 22.
[80] J.P. Jokisaari, L.P. Ingman, G.J. Schrobilgen, J.C.P. Sanders, Magn. Reson. Chem. 32 (1994) 242.
[81] S.L. Ruby, H. Selig, Phys. Rev. 147 (1966) 348.
[82] J.H. Holloway, G.J. Schrobilgen, S. Bukshpan, W. Hilbrants, H. de Waard, J. Chem. Phys. 66 (1977) 2627.
[83] R.D. Burbank, W.E. Falconer, W.A. Sunder, Science 178 (1972) 1285.
[84] S. Siegel, E. Gebert, J. Am. Chem. Soc. 86 (1964) 3896.
[85] W. Harshberger, R.K. Bohn, S.H. Bauer, J. Am. Chem. Soc. 89 (1967) 6466.

[86] S.A. Kinkead, J.R. FitzPatrick, J. Jr. Foropoulos, R.J. Kissane, J.D. Purson, in: J.S. Thrasher, S.H. Strauss (Eds.), Fluorine Chemistry Toward the 21st Century, Ch. 3, ACS Symposium Series, 555, ACS, Washington, DC, 1994, pp. 40–55.
[87] G.A.D. Collins, D.W.J. Cruickshank, A. Breeze, Chem. Commun. (1970) 884.
[88] G.A.D. Collins, D.W.J. Cruickshank, A. Breeze, J. Chem. Soc. Faraday Trans. 2 70 (1974) 393.
[89] P.S. Bagus, B. Liu, H.F. Schaefer, III, J. Am. Chem. Soc. 94 (1972) 6635.
[90] K. Nakamoto, Infrared and Raman Spectra of Inorganic and Coordination Compounds, 5th ed., Wiley, New York, 1997, p. 162.
[91] R. Minkwitz, R. Broechler, R. Ludwig, Inorg. Chem. 36 (1997) 4280.
[92] K.O. Christe, W.W. Wilson, G.W. Drake, M.A. Petrie, J.A. Boatz, J. Fluorine Chem. 88 (1998) 185.
[93] P. Tsao, C.C. Cobb, H.H. Claassen, J. Chem. Phys. 54 (1971) 5247.
[94] P.A. Agron, G.M. Begun, H.A. Levy, A.A. Mason, C.G. Jones, D.F. Smith, Science 139 (1963) 842.
[95] S. Reichman, J. Overend, J. Chem. Phys. 47 (1967) 3690.
[96] A.E. Smolyar, O.P. Charkin, N.M. Klimenko, Zh. Strukt. Khim. 15 (1974) 993; J. Struc. Chem. 15 (1974) 885.
[97] G.J. Schrobilgen, J. Chem. Soc. Chem. Commun. (1988) 863.
[98] G.J. Schrobilgen, J. Chem. Soc. Chem. Commun. (1988) 1506.
[99] J.H. Holloway, G.J. Schrobilgen, Inorg. Chem. 20 (1981) 3363.
[100] R.E. Rundle, J. Am. Chem. Soc. 85 (1963) 112.
[101] R.M. Noyes, J. Am. Chem. Soc. 85 (1963) 2202.
[102] R.J. Gillespie, A. Netzer, G.J. Schrobilgen, Inorg. Chem. 13 (1974) 1455.
[103] W.L. Faust, L.Y. Chow Chiu, Phys. Rev. 129 (1963) 1214.
[104] G.J. Perlow, M.R. Perlow, J. Chem. Phys. 48 (1968) 955.
[105] D.A. Dixon, A.J. Arduengo, III, W.B. Farnham, Inorg. Chem. 28 (1989) 4589.
[106] V.S. Arutyunov, V.N. Prusakov, V.B. Sokolov, A.M. Chaikin, Kinet. Katal. 18 (1977) 221; Kinet. Catal. 18 (1977) 181.
[107] J.H. Holloway, J.G. Knowles, J. Chem. Soc. A (1969) 756.
[108] J.C. Fuggle, D.A. Tong, D.W.A. Sharp, J.M. Winfield, J.H. Holloway, J. Chem. Soc. Dalton Trans. (1974) 205.
[109] J. Burgess, B. Frlec, J.H. Holloway, J. Chem. Soc. Dalton Trans. (1974) 1740.
[110] B. Frlec, J.H. Holloway, J. Chem. Soc. Dalton Trans. (1975) 535.
[111] B. Frlec, J.H. Holloway, J. Inorg. Nucl. Chem. Suppl. (1976) 167.
[112] J. Fawcett, B. Frlec, J.H. Holloway, J. Fluorine Chem. 8 (1976) 505.
[113] V.A. Legasov, B.B. Chaivanov, Zh. Fiz. Khim. 45 (1971) 593; Russ. J. Phys. Chem. 45 (1971) 325.
[114] R.J. Gillespie, B. Landa, Inorg. Chem. 12 (1973) 1383.
[115] A.J. Edwards, J.H. Holloway, R.D. Peacock, Proc. Chem. Soc. (1963) 275.
[116] A.J. Edwards, J.H. Holloway, R.D. Peacock, in: H.H. Hyman (Ed.), Noble-Gas Compounds, University Chicago Press, Chicago, IL, 1963, pp. 71–72.
[117] F.O. Sladky, P.A. Bulliner, N. Bartlett, J. Chem. Soc. A (1969) 2179.
[118] N. Bartlett, F.O. Sladky, J. Am. Chem. Soc. 90 (1968) 5316.
[119] L. Stein, J. Fluorine Chem. 20 (1982) 65.
[120] V.M. McRae, R.D. Peacock, D.R. Russell, J. Chem. Soc. Chem. Commun. (1969) 62.
[121] J. Burgess, C.J.W. Fraser, V.M. McRae, R.D. Peacock, D.R. Russell, J. Inorg. Nucl. Chem. Suppl. (1976) 183.
[122] H. de Waard, S. Bukshpan, G.J. Schrobilgen, J.H. Holloway, D. Martin, J. Chem. Phys. 70 (1979) 3247.
[123] V.A. Legasov, V.N. Prusakov, B.B. Chaivanov, Zh. Fiz. Khim. 44 (1970) 2629; Russ. J. Phys. Chem. 44 (1970) 1496.
[124] L. Stein, Nature (London) 243 (1973) 30.
[125] O.D. Maslov, V.A. Legasov, V.N. Prusakov, B.B. Chaivanov, Zh. Fiz. Khim. 41 (1967) 1832; Russ. J. Phys. Chem. 41 (1967) 984.
[126] G.S. Baronov, N.P. Egorov, A.N. Sopikov, B.B. Chaivanov, Zh. Fiz. Khim. 46 (1972) 18; Russ. J. Phys. Chem. 46 (1972) 10.
[127] B.B. Chaivanov, Zh. Fiz. Khim. 46 (1972) 23; Russ. J. Phys. Chem. 46 (1972) 13.
[128] R.J. Gillespie, D. Martin, G.J. Schrobilgen, J. Chem. Soc. Dalton Trans. (1980) 1898.
[129] B. Žemva, J. Slivnik, J. Inorg. Nucl. Chem. 33 (1971) 3952.
[130] B. Žemva, J. Slivnik, J. Inorg. Nucl. Chem. Suppl. (1976) 173.
[131] V.N. Prusakov, V.B. Sokolov, B.B. Chaivanov, Zh. Prikl. Spektrosk. 17 (1972) 114.
[132] N. Bartlett, M. Gennis, D.D. Gibler, B.K. Morrell, A. Zalkin, Inorg. Chem. 12 (1973) 1717.
[133] J. Binenboym, H. Selig, J. Shamir, J. Inorg. Nucl. Chem. 30 (1968) 2863.
[134] A. Zalkin, D.L. Ward, R.N. Biagioni, D.H. Templeton, N. Bartlett, Inorg. Chem. 17 (1978) 1318.
[135] K.O. Christe, R.D. Wilson, Inorg. Nucl. Chem. Lett. 9 (1973) 845.
[136] N. Bartlett, B. Žemva, L. Graham, J. Fluorine Chem. 7 (1976) 301.
[137] N. Bartlett, B.G. DeBoer, F.J. Hollander, F.O. Sladky, D.H. Templeton, A. Zalkin, Inorg. Chem. 13 (1974) 780.
[138] F.O. Sladky, P.A. Bulliner, N. Bartlett, B.G. DeBoer, A. Zalkin, J. Chem. Soc. Chem. Commun. (1968) 1048.
[139] B.A. Fir, M. Gerken, B.E. Pointner, H.P.A. Mercier, D.A. Dixon, G.J. Schrobilgen, J. Fluorine Chem. 105 (2000) 159.
[140] V.B. Sokolov, Y.V. Drobyshevskii, V.N. Prusakov, A.V. Ryzhkov, S.S. Khoroshev, Dokl. Akad. Nauk SSSR 229 (1976) 641; Dokl. Chem. 229 (1976) 503.
[141] H. Selig, R.D. Peacock, J. Am. Chem. Soc. 86 (1964) 3895.
[142] R.J. Gillespie, G.J. Schrobilgen, J. Chem. Soc. Chem. Commun. (1974) 90.
[143] D.E. McKee, C.J. Adams, A. Zalkin, N. Bartlett, J. Chem. Soc. Chem. Commun. (1973) 26.
[144] B. Žemva, J. Slivnik, A. Šmalc, J. Fluorine Chem. 6 (1975) 191.
[145] V.B. Sokolov, V.G. Tsinoev, A.V. Ryzhkov, Teor. Eksp. Khim. 16 (1980) 345.
[146] R.J. Gillespie, G.J. Schrobilgen, Inorg. Chem. 13 (1974) 1230.
[147] B. Frlec, J.H. Holloway, J. Chem. Soc. Chem. Commun. (1974) 89.
[148] V.D. Klimov, V.A. Legasov, S.S. Khoroshev, Zh. Fiz. Khim. 52 (1978) 1790; Russ. J. Phys. Chem. 52 (1978) 1037.
[149] J.F. Lehmann, G.J. Schrobilgen, J. Fluorine Chem., in press.
[150] T. Sakurai, A. Takahashi, J. Nucl. Sci. Technol. 18 (1981) 239.
[151] R. Bougon, W.W. Wilson, K.O. Christe, Inorg. Chem. 24 (1985) 2286.
[152] T. Schroer, K.O. Christe, Inorg. Chem. 40 (2001) 2415.
[153] K.O. Christe, W.W. Wilson, R.D. Wilson, Inorg. Chem. 23 (1984) 2058.
[154] K. Lutar, A. Jesih, B. Žemva, Polyhedron 7 (1988) 1217.
[155] V.D. Klimov, V.N. Prusakov, V.B. Sokolov, Dokl. Akad. Nauk SSSR 217 (1974) 1077; Dokl. Chem. 217 (1974) 549.
[156] H. Elliott, H.D.B. Jenkins, J.F. Lehmann, G.J. Schrobilgen, Inorg. Chem., in preparation.
[157] K.O. Christe, D.A. Dixon, D.K. Lemore, W.W. Wilson, J.A. Sheehy, J.A. Boatz, J. Fluorine Chem. 101 (2000) 151.
[158] G.J. Schrobilgen, J.H. Holloway, P. Granger, C. Brevard, Inorg. Chem. 17 (1978) 980.
[159] R.J. Gillespie, G.J. Schrobilgen, Inorg. Chem. 13 (1974) 2370.

[160] R.J. Gillespie, G.J. Schrobilgen, Inorg. Chem. 13 (1974) 765.
[161] A. Bondi, J. Phys. Chem. 68 (1964) 441.
[162] L. Pauling, The Nature of the Chemical Bond, 3rd ed., Cornell University Press, Ithaca, NY, 1960, p. 260.
[163] D.A. Dixon, G.J. Schrobilgen, Unpublished results, also see Ref. [139].
[164] J.H. Holloway, G.J. Schrobilgen, P. Taylor, J. Chem. Soc. Chem. Commun. (1975) 40.
[165] J.H. Holloway, G.J. Schrobilgen, Inorg. Chem. 19 (1980) 2632.
[166] P.A. Tucker, P.A. Taylor, J.H. Holloway, D.R. Russell, Acta Crystallogr. Sect. B 31 (1975) 906.
[167] A.A.A. Emara, G.J. Schrobilgen, J. Chem. Soc. Chem. Commun. (1987) 1644.
[168] A.A.A. Emara, G.J. Schrobilgen, Inorg. Chem. 31 (1992) 1323.
[169] A.A.A. Emara, G.J. Schrobilgen, J. Chem. Soc. Chem. Commun. (1988) 257.
[170] C. Eickes, B.A. Fir, K. Koppe, H.P.A. Mercier, G.J. Schrobilgen, R.J. Suontamo, Inorg. Chem., in preparation.
[171] I.H. Hillier, M.A. Vincent, J. Chem. Soc. Chem. Commun. (1989) 30.
[172] W. Koch, J. Chem. Soc. Chem. Commun. (1989) 215.
[173] M.W. Wong, L. Radom, J. Chem. Soc. Chem. Commun. (1989) 719.
[174] P.J. MacDougall, G.J. Schrobilgen, R.F.W. Bader, Inorg. Chem. 28 (1989) 763.
[175] D.A. Dixon, A.J. Arduengo, III, Inorg. Chem. 29 (1990) 970.
[176] B. Liu, H.F. Schaefer, J. Chem. Phys. 55 (1971) 2369.
[177] M.D. Harmony, V.W. Laurie, R.L. Kuczkowski, R.H. Schwendeman, D.A. Ramsay, F.J. Lovas, W.J. Lafferty, A.G. Maki, J. Phys. Chem. Ref. Data 8 (1979) 619.
[178] J. Koehler, A. Simon, R. Hoppe, J. Less-Common Met. 137 (1988) 333.
[179] B.A. Fir, H.P.A. Mercier, G.J. Schrobilgen, R.J. Suontamo, Inorg. Chem., in preparation.
[180] G. Frenking, W. Koch, C.A. Deakyne, J.F. Liebman, N. Bartlett, J. Am. Chem. Soc. 111 (1989) 31.
[181] V.H. Dibeler, S.K. Liston, J. Chem. Phys. 48 (1968) 4765.
[182] K. Seppelt, Angew. Chem. 94 (1982) 890; Angew. Chem. Int. Ed. Engl. 21 (1982) 877.
[183] E. Jacob, D. Lentz, K. Seppelt, A. Simon, Z. Anorg. Allg. Chem. 472 (1981) 7.
[184] J.K. Hovey, T.B. McMahon, J. Phys. Chem. 91 (1987) 4560.
[185] J. Lundell, L. Khriachtchev, M. Pettersson, M. Räsänen, Fiz. Nizk. Temp. 26 (2000) 923; Low Temp. Phys. 26 (2000) 680.
[186] I. Kuen, F. Howorka, J. Chem. Phys. 70 (1979) 595.
[187] I. Yourshaw, T. Lenzer, G. Reiser, D.M. Neumark, J. Chem. Phys. 109 (1998) 5247.
[188] J.G. Stamper, R.F. Barrow, Trans. Faraday Soc. 54 (1958) 1592.
[189] J.L. Weeks, M.S. Matheson, Inorg. Synth. 8 (1966) 260.
[190] J.H. Holloway, J. Chem. Ed. 43 (1966) 202.
[191] J.F. Liebman, Struct. Chem. 11 (2000) 261.
[192] K.O. Christe, D.A. Dixon, J. Am. Chem. Soc. 114 (1992) 2978.
[193] K.O. Christe, W.W. Wilson, R.D. Wilson, Unpublished results.
[194] J. Berkowitz, W.A. Chupka, Chem. Phys. Lett. 7 (1970) 447.
[195] J.F. Liebman, J. Fluorine Chem. 9 (1977) 147.
[196] E.H. Appelman, Acc. Chem. Res. 6 (1973) 113.
[197] E.H. Appelman, Inorg. Synth. 13 (1972) 1.
[198] E.H. Appelman, M.H. Studier, J. Am. Chem. Soc. 91 (1969) 4561.
[199] F.Q. Roberto, Inorg. Nucl. Chem. Lett. 8 (1972) 737.
[200] K.O. Christe, Inorg. Nucl. Chem. Lett. 8 (1972) 741.
[201] K.O. Christe, Inorg. Chem. 12 (1973) 1580.
[202] K.O. Christe, W. Sawodny, Inorg. Chem. 6 (1967) 1783.
[203] M. Brownstein, H. Selig, Inorg. Chem. 11 (1972) 656.
[204] K.O. Christe, R.D. Wilson, Inorg. Chem. 14 (1975) 694.
[205] J.F. Lehmann, G.J. Schrobilgen, Unpublished results.
[206] K.O. Christe, W.W. Wilson, E.C. Curtis, Inorg. Chem. 22 (1983) 3056.
[207] R.J. Gillespie, P.H. Spekkens, J. Chem. Soc. Dalton Trans. (1977) 1539.
[208] R.J. Gillespie, P.H. Spekkens, Isr. J. Chem. 17 (1978) 11.
[209] A.A. Artyukhov, S.S. Khoroshev, Koord. Khim. 3 (1977) 1478; Sov. J. Coord. Chem. 3 (1977) 1478.
[210] O.V. Boltalina, A.K. Abdul-Sada, R. Taylor, J. Chem. Soc. Perkin Trans. (1995) 981.
[211] K. Lutar, H. Borrmann, B. Žemva, Inorg. Chem. 37 (1998) 3002.
[212] A.J. Edwards; W.E. Falconer, W.A. Sunder, J. Chem. Soc. Dalton Trans. (1974) 541.
[213] E.G. Hope, P.J. Jones, W. Levason, J.S. Ogden, M. Tajik, J.W. Turff, J. Chem. Soc. Dalton Trans. (1985) 529.
[214] N. LeBlond, G.J. Schrobilgen, Chem. Commun. (1996) 2479.
[215] N. LeBlond, H.P.A. Mercier, D.A. Dixon, G.J. Schrobilgen, Inorg. Chem. 39 (2000) 4494.
[216] H.P.A. Mercier, G.J. Schrobilgen, Inorg. Chem. 32 (1993) 145.
[217] G.J. Schrobilgen, J.H. Holloway, D.R. Russell, J. Chem. Soc. Dalton Trans. (1984) 1411.
[218] S.M. Yeh, N. Bartlett, Rev. Chim. Miner. 23 (1986) 676.
[219] J.H. Holloway, G.J. Schrobilgen, Unpublished results.
[220] R. Bougon, J. Fluorine Chem. 53 (1991) 419.
[221] K.O. Christe, R. Bougon, J. Chem. Soc. Chem. Commun. (1992) 1056.
[222] K.O. Christe, D.A. Dixon, H.G. Mack, H. Oberhammer, A. Pagelot, J.C.P. Sanders, G.J. Schrobilgen, J. Am. Chem. Soc. 115 (1993) 11279.
[223] R. Bougon, B. Ban, K. Seppelt, Chem. Ber. 126 (1993) 1331.
[224] W.J. Jr. Casteel, D.A. Dixon, H.P.A. Mercier, G.J. Schrobilgen, Inorg. Chem. 35 (1996) 4310.
[225] M. Gerken, G.J. Schrobilgen, Unpublished results.
[226] L. Meublat, M. Lance, R. Bougon, Can. J. Chem. 67 (1989) 1729.
[227] R. Bougon, W.V. Cicha, J. Isabey, J. Fluorine Chem. 67 (1994) 271.
[228] W.E. Falconer, F.J. Disalvo, J.E. Griffiths, F.A. Stevie, W.A. Sunder, M.J. Vasile, J. Fluorine Chem. 6 (1975) 499.
[229] A. Jesih, K. Lutar, I. Leban, B. Žemva, Inorg. Chem. 28 (1989) 2911.
[230] R. Hoppe, Z. Anorg. Allg. Chem. 292 (1977) 28.
[231] K. Lutar, A. Jesih, B. Žemva, Rev. Chim. Miner. 23 (1986) 565.
[232] R. Bougon, H.T. Bui, M. Lance, H. Abazli, Inorg. Chem. 23 (1984) 3667.
[233] B. Žemva, K. Lutar, A. Jesih, W.J. Casteel, Jr, A.P. Wilkinson, D.E. Cox, R.B. Von Dreele, H. Borrmann, N. Bartlett, J. Am. Chem. Soc. 113 (1991) 4192.
[234] K. Lutar, A. Jesih, I. Leban, B. Žemva, N. Bartlett, Inorg. Chem. 28 (1989) 3467.
[235] V.I. Spitsyn, Y.M. Kiselev, L.I. Martynenko, V.N. Prusakov, V.B. Sokolov, Dokl. Akad. Nauk SSSR 219 (1974) 621; Dokl. Chem. 219 (1974) 818.
[236] Y.M. Kiselev, V.B. Sokolov, Zh. Neorg. Khim. 29 (1984) 857; Russ. J. Inorg. Chem. 29 (1984) 493.
[237] M.F. Beuermann, S. Miličev, K. Lutar, B. Žemva, Eur. J. Solid State Inorg. Chem. 31 (1994) 545.
[238] Y.V. Drobyshevskii, V.N. Prusakov, V.F. Serik, V.B. Sokolov, Radiokhimiya 22 (1980) 591.
[239] Y.V. Drobyshevskii, V.F. Serik, V.B. Sokolov, M.N. Tul'skii, Radiokhimiya 20 (1978) 238; Sov. Radiochem. 20 (1978) 200.
[240] D. Cohen, S. Fried, J.H. Holloway, H. Selig, Unpublished work, 1970.

[241] M. Baluka, S. Yeh, R. Banks, N. Edelstein, Inorg. Nucl. Chem. Lett. 16 (1980) 75.
[242] D. Brown, B. Whittaker, J.A. Berry, J.H. Holloway, J. Less-Common Met. 86 (1982) 75.
[243] L.B. Asprey, P.G. Eller, S.A. Kinkead, Inorg. Chem. 25 (1986) 670.
[244] J.G. Malm, P.G. Eller, L.B. Asprey, J. Am. Chem. Soc. 106 (1984) 2726.
[245] W. Bacher, E. Jacob, Chem. Ztg. 106 (1982) 117.
[246] Y.V. Drobyshevskii, V.F. Serik, V.B. Sokolov, Dokl. Akad. Nauk SSSR 225 (1975) 1079; Dokl. Chem. 225 (1975) 675.
[247] R.D. Peacock, N. Edelstein, J. Inorg. Nucl. Chem. 38 (1976) 771.